UNIVERSITY OF SOUTHAMPTON

FACULTY OF ENGINEERING, SCIENCE AND MATHEMATICS

National Oceanography Centre
School of Ocean and Earth Sciences

A satellite view of the space-time variability of phytoplankton biomass in the Mediterranean Sea

By
Gianluca Volpe

Thesis for the degree of Doctor of Philosophy

August 2010

Graduate School of the
National Oceanography Centre

This PhD dissertation by
Gianluca Volpe
has been produced under the supervision of the following persons:

Supervisors:
Dr. Paolo Cipollini
Prof. Ian S. Robinson

Chair of Advisory Panel:
Dr. Duncan A. Purdie

UNIVERSITY OF SOUTHAMPTON

ABSTRACT

FACULTY OF ENGINEERING, SCIENCE AND MATHEMATICS
NATIONAL OCEANOGRAPHY CENTRE
SCHOOL OF OCEAN AND EARTH SCIENCES
Doctor of Philosophy

A satellite view of the space-time variability of phytoplankton biomass in the Mediterranean Sea

By

Gianluca Volpe

The general thesis objective is to determine, with sufficient accuracy (i.e. using the most reliable datasets and techniques) the phytoplankton space time variability in the Mediterranean Sea (MED) using satellite data (SeaWiFS), at different timescales, and their relationship with the physical environment. A validation exercise was performed over SeaWiFS data in the context of the reliability of both oceanic and atmospheric remote sensing data, and using the most comprehensive *in situ* bio-optical dataset over the MED basin. This exercise led to the development of an ad hoc regional ocean colour algorithm, which has then been implemented as standard algorithm within the operational satellite data processing chain at the Group for Satellite Oceanography (GOS) at the Istituto di Scienze dell'Atmosfera e del Clima of the Italian National Research Council, Rome. Moreover, within this context, the MED basin bio-optical signature has been found to be significantly different than the global ocean, ultimately justifying the adopted approach. The derived product (i.e., chlorophyll concentration, CHL) has then been used in the rest of the thesis to answer relevant questions, such as how the phytoplankton dynamics is influenced by its physical environment, from the water column stratification to the atmospheric input of nutrients, at different space and time scales: from daily to seasonal and interannual, and from hundreds of km to the basin scale. The basin scale interannual variability of phytoplankton has been found to be very sensitive to circulation patterns in both the western and eastern sub-basins. A phytoplankton biomass decrease, at basin scale, is significantly correlated with the long-term reduction of the cyclonic circulation in the eastern basin. Similarly, the transport variability associated with the Algerian Current system has been found to play an important role in affecting the cyclonic circulation of the Ionian Sea, which in turn

determines a phytoplankton decrease on a multi-year time scale in the area. Seasonally, localized to the northwestern MED and in the southern Adriatic Sea, where deep water formation processes are active during autumn-winter, the phytoplankton spring bloom dynamics is found to be significantly correlated to the surface thermal field of the previous season: a time lag of six months identifies the coupling between the preconditioning phase to deep water formation and the spring bloom. A debated and still open question concerns with the role of atmospheric dust in the regulation of the biogeochemistry of oligotrophic gyres, so that one of the challenges of this study was to investigate the impact of the atmospheric nutrient deposition on the phytoplankton dynamics of the basin, i.e. to test the Dust Fertilization Hypothesis (DFH) in a Low Nutrient Low Chlorophyll (LNLC) region. This issue has important scientific and to a non lesser extent technical implications, but the DFH is shown here to play only a minor or even negligible role in the regulation of the phytoplankton dynamics in the MED.

DECLARATION OF AUTHORSHIP

I, **Volpe Gianluca**, declare that the thesis entitled

A SATELLITE VIEW OF THE SPACE-TIME VARIABILITY OF PHYTOPLANKTON BIOMASS IN THE MEDITERRANEAN SEA

and the work presented in the thesis are both my own, and have been generated by me as the result of my own original research. I confirm that:

- this work was done wholly or mainly while in candidature for a research degree at this University;
- where any part of this thesis has previously been submitted for a degree or any other qualification at this University or any other institution, this has been clearly stated;
- where I have consulted the published work of others, this is always clearly attributed;
- where I have quoted from the work of others, the source is always given. With the exception of such quotations, this thesis is entirely my own work;
- I have acknowledged all main sources of help;
- where the thesis is based on work done by myself jointly with others, I have made clear exactly what was done by others and what I have contributed myself;
- parts of this work have been published as:

Volpe, G., R. Santoleri, V. Vellucci, M. Ribera d'Alcala, S. Marullo, and F. D'Ortenzio (2007), The colour of the Mediterranean Sea: Global versus regional bio-optical algorithms evaluation and implication for satellite chlorophyll estimates, *Remote Sensing of Environment*, 107, 625-638.

Volpe, G., V. F. Banzon, R. H. Evans, R. Santoleri, A. J. Mariano, and R. Sciarra (2009), Satellite observations of the impact of dust in a low-nutrient, low-chlorophyll region: Fertilization or artifact?, *Global Biogeochemical Cycles*, 23, GB3007, doi:10.1029/2008GB003216.

Volpe, G., B. Buongiorno Nardelli, P. Cipollini, R. Santoleri, and I. S. Robinson (2009), Seasonal to interannual phytoplankton response to physical processes in the Mediterranean Sea from satellite observations, under review in *Journal of Geophysical Research*.

Signed: 

Date: 12 August 2010

Acknowledgment

I am very thankful to my supervisors Dr. Paolo Cipollini, Prof. Ian S. Robinson and Dr. Debora Iglesias-Rodriguez for their guidance and constant scientific and technical support throughout these years. They taught me how to handle scientific and technical problems.
Thank you to Dr. Duncan Purdie for his supervision.
A special thank you goes to Dr. Rosalia Santoleri who made it effectively possible, for the constant scientific, technical and "logistic" support.
Thank you to my co-authors for their help, assistance and patience for finalizing the works we have made into scientific papers: Viva, Bruno, Cipo (again), Fabrizio, Bob, Arthur, Salvatore, Maurizio, Lia (again), Roberto, Ian (again) and Vincenzo.
Thanks to the 94 Milton Road house mates for letting me stay and providing such enjoyable environment during my "short" and periodic visits to Southampton.
A big thank you goes to my parents for having always believed in me and offered the opportunity to go this far.
Thank you very much to Simone for the patience and "tolerance" while hosting me in Spinaceto.
A true thanks goes to my extended family in Rome, the Group for Satellite Oceanography at CNR for sharing their expertises, and for making of the working environment such a familiar and enjoyable place.
None of this could have ever been possible without the priceless and invaluable presence of Angela who gave me the energy in the toughest moments through her incredible and enthusiastic approach to life in general and to science in particular, with a constant support under all points of view; THANK YOU! And thank you to my little kids for giving me an extra reason for closing this chapter of my life. This thesis is dedicated to Angela, Giulia and Andrea.

Table of Contents

List of Figures

List of Tables

1 Introduction

In recent decades it has become more evident that the planet's temperature is increasing [*IPCC*, 2007]. There is growing evidence that this might be caused by the progressive increase of anthropogenic CO_2 (a greenhouse gas) concentration in the atmosphere [*Cox et al.*, 2000; *IPCC*, 2001; *Sarmiento et al.*, 2004]. The ocean contains the largest pool of carbon on the planet; its concentration of CO_2 is in dynamic equilibrium with that in the atmosphere: an increase in the atmospheric concentration of CO_2 enhances the ocean absorbing capacity. This mechanism is regulated by the physical processes at the sea surface. Other than the pure physical gas exchange at the air-sea interface, the ocean can control the atmospheric CO_2 concentration by means of the so-called biological pump. The biologically mediated carbon assimilation refers to the sinking of organic matter from the surface productive layers to deep waters in the oceans. The major player of the oceanic biological pump is phytoplankton (i.e., the unicellular microscopic algae living in the upper layer of all water bodies across the world) which are able to fix CO_2 into organic material, through the process of photosynthesis. Quantitatively, the oceanic photosynthesis accounts for roughly half the biosphere's net primary production [*Field et al.*, 1998; *Behrenfeld et al.*, 2001], fixing into organic material nearly 40 GT of carbon per year, which are then transferred to higher trophic levels and to the entire marine ecosystem by sinking and/or grazing [*Behrenfeld et al.*, 2006].

The ocean overturning period involves millennial temporal scales [*Broecker*, 1995]; so that, once the organic matter leaves the surface productive layers, it could take centuries to re-enter the food web. This mechanism is therefore capable of sequestering CO_2 from the atmosphere to deep oceanic waters on centennial time scales. The biological pump contributes, therefore, to the uptake of the excess anthropogenic carbon from the atmosphere; if it is reduced, the rate of increase of atmospheric CO_2 could be larger, with presumably positive feedbacks on the planet's temperature [*Cox et al.*, 2000]. Quantifying the carbon flux into the ocean through the marine primary productivity, and understanding the mechanisms that might control it, are of crucial importance for defining the planet's carbon budget and its link to climate change.

The interaction between physical processes and biological production has been long studied and conceptualized since 1953 when *Harald Sverdrup* developed an extensively used, simple model describing the necessary conditions for the occurrence of the phytoplankton spring bloom, in the North Atlantic ocean. Since then, a lot of effort has been made to understand the factors controlling phytoplankton growth, at different space and time scales. Phytoplankton distribution in the ocean is mainly driven by the availability of light and nutrients [*Parsons et al.*, 1983]. These growth-limiting factors depend in turn on physical processes such as general ocean circulation, deep water formation, mixed-layer dynamics, upwelling, and the solar cycle [*Behrenfeld et al.*, 2006]. These factors control the phytoplankton dynamics at different space and time scales; for example, the solar cycle, the mixed layer dynamics and the occurrence at specific sites of dense water formation all have a strong seasonal component. On the other hand, while the solar cycle exerts its influence on large spatial scales, determining the seasonal succession, the dense water formation is peculiar to some specific regions. Similarly, the variability of the mixed layer dynamics can span from local to basin scale. Therefore, even if variability of both the mixed layer dynamics and the formation of dense water does have a strong seasonal component, their spatial scales of variability may vary significantly. Water upwelling from below the surface, carrying a larger nutrient load, may be an almost permanent feature of some ocean regions (e.g., the Peru-Chile current system, the Californian current, the equatorial upwelling system, etc), or may exhibit a seasonal or intermittent nature, due to local atmospheric forcing. A sporadic-type of forcing is given by the aeolian dust deposition, which is known to play an important role in the regulation of the upper ocean biogeochemistry. In HNLC[1] regions dust represents the main source of iron (Fe), a micro-nutrient essential to marine phytoplankton growth [*Martin*, 1990]. Dust has also been shown to be an important source of phosphorus (P) and nitrogen (N), especially for those areas of the world ocean exhibiting a prolonged stratification period, where phytoplankton experience high nutrient limitation, such as the Mediterranean Sea, a typical LNLC region [*Guerzoni et al.*, 1999]. The control by dust, as a source of both micro- and macro-nutrients, over the

[1] High Nutrient Low Chlorophyll (HNLC) are those regions of the world ocean where phytoplankton biomass load is low in relation to the concentration of macro-nutrient (N and P) that ideally can support it. Low Nutrient Low Chlorophyll (LNLC) are regions where both nutrient and biomass concentrations are low.

phytoplankton growth is known as the Dust Fertilization Hypothesis (DFH). The heterogeneity between HNLC and LNLC regions results in a non general consensus about dust's unequivocal role in supporting phytoplankton growth. This is due to the fact that these elements (N, P, Fe) are present in several chemical states, which are not all suitable for being assimilated into the vital processes linked to phytoplankton growth: the so-called bioavailability. The elements' bioavailability is linked to several factors, from the provenance of dust to the way dust reaches the ocean surface, via wet or dry deposition (and hence to the local meteorological conditions), as well as to the physical, chemical and biological state of the upper ocean. Within the last decades, there has been a lot of effort for quantifying the coupling between dust and phytoplankton growth investigating both the small and the large scales of influence: from global satellite analysis [such as that by *Cropp et al.*, 2005], to *in situ* measurements at local scale [*Thingstad et al*., 1998; 2005; *Heussner et al.,* 2003; *Bonnet et al.,* 2005; *Eker-Develi et al.,* 2006; *Ternon et al.*, 2010]. Results differ a lot: first, phytoplankton do not always respond to dust addition, and second, when they do respond, the space and time scales of such a response is not always coherent. This suggests that a new approach should be developed, which takes into account all possible sources of variability that might influence results (dust source, nutrient bioavailability etc.), so that the role of dust can be unequivocally addressed.

The spatial and temporal distribution of phytoplankton is nowadays quite well-understood on a climatological basis, resulting in a well-defined zonation of the world oceans, the so-called bio-provinces [*Longhurst*, 1998]. This knowledge is primarily due to the advent of satellite oceanography that offers a synoptic and systematic view of the ocean surface allowing for global, high frequency temporal sampling. Remote sensing is thus a powerful tool for biological oceanography because it routinely measures the ocean surface at scales that are not possible with standard ship surveys. However, satellite data represents a far-reaching investigation tool only if uncertainties are minimized through careful calibration and validation activity. This is a mandatory step for obtaining an unbiased picture of the phytoplankton space and time distribution. This is particularly important if one considers that phytoplankton variability over time is expected not to exceed a small percentage (for example, 6% as estimated by *Gregg et al*. [2003]). Results of variability analysis can be misinterpreted if the phytoplankton distribution is either under- or overestimated with a small percentage error. In this

context, a 6% decline of phytoplankton productivity across three decades was estimated by *Gregg et al.* [2003] based on a multi-mission satellite dataset: Coastal Zone Colour Scanner (CZCS) for the period 1979-1986 and Sea Wide Field-of-view Sensor (SeaWiFS) for the period 1997-mid 2002. These authors found a good correspondence between the phytoplankton production decrease and the global sea surface temperature (SST) rise of 0.2 °C from the CZCS to SeaWiFS eras. The SST increase is supposed to enhance the upper ocean stratification, thence preventing the nutrient entrainment into the enlightened surface layer [*Behrenfeld et al.*, 2006; *Doney*, 2006]. Moreover, a 25% decrease in the atmospheric iron deposition between the same two time segments was claimed to be co-responsible for this global phytoplankton production decline. This work points at the importance of identifying the relationships between physical and biological processes and the link to climate change. However, there remain uncertainties in the methodology used to blend data from different satellite missions used as input to a primary production model, making the overall significance of these results questionable. In other words, we may question whether this assertion of global production decline is undermined by the uncertainties associated with the input data used to derive the global primary production?

Taking advantage of the unique perspective on the natural environment offered by satellite data, *Wilson and Coles* [2005] investigated the role that sub-surface processes (i.e., mixed layer dynamics) have on the surface phytoplankton dynamics, and found a well-defined zonation of the processes concurring to determine the phytoplankton space-time variability: dynamic uplift causing nutrient entrainment into the euphotic layers in the tropics and seasonal control of nutrients and light at mid- and high-latitudes. However, despite the fact that the phytoplankton biomass space-time distribution has been successfully pictured on a global and climatological basis, there is growing evidence that fluctuations of these patterns are related to climate change. Hence, questions such as how changes in the physical environment do affect the biology of the upper ocean, and thus of the entire marine ecosystem, still seek an answer. More recently, *Behrenfeld and co-authors* [2006], using data only from the SeaWiFS mission (1997-mid 2006) found that mid-latitude regions experienced a significant decrease in the phytoplankton production. Similarly to *Gregg et al.* [2003], *Behrenfeld et al.* [2006] explained the production decline with the observed increase in the upper ocean stratification ultimately due to the global increase in the SST. In the same way, *Barale et al.* [2008], used 6 years (1997-2003) of satellite data to retrieve climatological values

(used as proxy for a general oceanographic climate) and anomalies (used to describe trends and hotspots) of phytoplankton biomass over the Mediterranean Sea (hereafter referred to as MED). According to these authors the general positive trend of SST over the basin in the previous 25 years was responsible for both the general biomass decrease, and the increasing negative trend of the phytoplankton anomalies with respect to the CZCS era. The SST positive trend results in a reduction of the vertical mixing between the upper and lower layers of the water column, in turn revealing an increasing nutrient limitation. The observed interannual to decadal variability in the phytoplankton dynamics was interpreted as a premonitory sign of the profound effects and implications climate change can have on the trophic regime of the Mediterranean basin.

Although these investigations do account for different trophic regimes being able to divide the world ocean into different bio-provinces (subtropical, subpolar, etc), they do not consider, for example, changes in the oceanic circulation (in terms of spatial or temporal shifts) that might have occurred within respective study periods and how these might have impacted the phytoplankton dynamics. An attempt to investigate the temporal evolution of the phytoplankton spatial patterns has recently been performed by *Henson et al.* [2009]. They investigated the timing and magnitude of the North Atlantic phytoplankton bloom in the context of the two different regimes: the subtropical, where phytoplankton is exclusively nutrient limited, and the subpolar, in which photosynthetic organisms experience both light and nutrient limitations [*Follows and Dutkiewicz*, 2001]. *Henson et al.* [2009] found a good correlation in the position and spatial extension of the transition zone between the subpolar and subtropical regions with an extensively used climatic index, the North Atlantic Oscillation Index (NAO). Positive or negative NAO phases result in timing variability and location changing of the transition zone. This space-time variability has been demonstrated to have important consequences for the entire marine food web [*Cushing*, 1975]. *Henson et al.*'s [2009] work points to the importance that decadal climate variability can have on the marine food web, highlighting the importance that fine resolution spatial and temporal sampling may have on the comprehension of global climate change and its impact on the marine ecosystem.

An important aspect that has not been taken into account so far is concerned with the space and time scales of variability of the causes (in this case the increased stratification due to global warming) and how these impact the observed variability in the effect (e.g., phytoplankton production decline). For example, the SST increase leads

to an enhanced stratification of the upper oceanic layer which in turn determines a significant decrease in phytoplankton production [*Doney*, 2006]. What is missing in this concept is the knowledge of the time required by the ocean to become more stratified and of the time scales of the phytoplankton response. *Behrenfeld et al.* [2006] showed how sensitive the marine biology can be with respect to changes in the environment, implicitly suggesting that such coupling might occur on a very short time scale; they used monthly averaged satellite images and found a good correlation at zero temporal lag. This would either mean that both increased SST and production decline are effects due to the same cause, or that the temporal binning (monthly) used to average satellite data is such (e.g., too large) that the time lag between cause and effect is not visible, so that it ultimately results in an instantaneous correlation. On the other hand, it seems reasonable to assume that a time lag would exist between the two distinct processes.

Looking for paradigms whose effectiveness is valid globally is always a great challenge, although it is a result not very easy to achieve, especially if the phenomenon under study (phytoplankton dynamics) can exhibit orders of magnitude variability in space and time due to different factors (for example, sporadic to seasonal to permanent upwelling conditions, seasonal light limitation or iron limitation etc). This uncertainty assumes particular emphasis if the phytoplankton dynamics is investigated in the context of a rapidly changing and not yet well-understood climate dynamics. More clearly, physical processes can modulate the phytoplankton dynamics at different space and time scales, depending on the nature of the processes. An approach able to take account of different space and time scales is given by the use of advanced statistical tools such as the Empirical Orthogonal Functions (EOF) coupled with a correlation analysis. This approach allows the observed signal to be decomposed, so that, in principle, one should be able to spot a causal-dependence relationship between two or more processes and to discern different temporal and spatial scales of influence of one process over the other (i.e., physical processes driving biological variability). However, caution should be adopted in the interpretation of results when the length of data time series is unable to resolve (i.e., much shorter than) the temporal scales involved by climate change, if climate change is a candidate explanation for the observed variability.

In this context, it might first be more useful to investigate the phenomenon within specific areas, or test beds, before then verifying and, if possible, extending the validity of results to other contexts. The optimum would be to investigate the phytoplankton

dynamics in a context whose physical or climatic temporal scales of variability are close to, or at least of the same order of magnitude as, the length of the data time series used to investigate it. Its small geographic extent and consequent shorter scales of variability, coupled with both the local anthropogenic pressure and the complexity and variety of its oceanographic features, make the Mediterranean Sea an excellent test bed for investigating the coupling between physical and biological processes at different temporal and spatial scales. This is the concept that underpins this thesis, in which the Mediterranean Sea is used as a test bed for studying three distinct but related elements of the challenge to measure and understand the causes of variability in ocean phytoplankton biomass.

Satellite ocean colour data represent an essential observational tool which, thanks to the sampling frequency and high spatial resolution, have been successfully used to provide unique and important information on surface phytoplankton distribution. For this reason these data will be extensively used throughout the whole thesis. The next section (1.1) in this introduction will therefore introduce the basic concepts and rationale behind the use of satellite data with particular respect to their use over the MED basin. Section 1.2 then briefly reviews the characteristics and peculiarities of the MED basin, considered as a test bed, along with both scientific and technical open issues. Finally, based on this background knowledge, section 1.3 sets out the specific objectives of the substantive new work presented in the rest of this thesis.

1.1 Measuring phytoplankton biomass from space

It is general knowledge and experience that the colour of sea-water provides information about its properties. Mapping the ocean according to its optical properties can thus provide scientists from different branches of oceanography with useful and otherwise unobtainable information. The remote sensing of the ocean colour uses the visible part of the electromagnetic spectrum (400-700 nm). Although the ocean colour is mostly concerned with the phytoplankton biomass distribution, it also supplies information about the depth at which light extinguishes, which is useful for modelling of the upper ocean thermal structure and for heat budget calculations. Moreover, the ocean colour, especially in coastal waters, can be used to assess the water quality in terms of the phytoplankton pigment concentration and other associated substances such as dissolved organic matter (DOM) and other particulates which in turn describe the healthiness of coastal seas [*Robinson*, 2005]. Recently, ocean colour techniques have

been used to further investigate the temporal and spatial distribution of microbes known as mucilage in the Adriatic Sea [*Berthon et al.*, 2000; *Vescovi et al.*, 2003]. However the efficient exploitation of satellite data requires the availability of quality controlled datasets accompanied by robust statistical analyses of the uncertainties associated with the retrieval procedures, such as those arising from atmospheric correction and bio-optical algorithms. For this reason, the space agencies involved in ocean colour missions have established important projects to collect large databases of *in situ* data for calibration and validation of satellite products [*McClain and Fargion*, 1999; *O'Reilly et al.*, 2000; *Gregg and Casey*, 2004]. These *in situ* data have then been used to develop empirical algorithms for Chl retrieval, used operationally in the satellite data processing chains: OC4v4 for SeaWiFS, OC3 for MODIS and Algal1 for MERIS. These standard algorithms proposed by space agencies to process data acquired by their sensors have a nominal accuracy of ~35% for the Chl retrieval in case 1 waters. In theory, empirical ocean colour algorithms are expected to provide reliable measurements only if the observational conditions match or are close to the sampling conditions. Standard satellite data processing chains do account for a number of variables that can influence the ocean colour data quality: from the sea state to meteorological conditions. Nonetheless, the effectiveness of the empirical algorithms for operational applications is strictly connected to the representativeness of the database used to build them. In other words, it is important for the *in situ* dataset collected for algorithm development to cover the whole range of variability of the parameter under study.

Among ocean colour sensors, an extensive calibration and validation activity has been performed over SeaWiFS data by the SeaWiFS and SIMBIOS Projects. SeaWiFS was launched in 1997, and since then has provided the longest time series of ocean colour data over the world ocean. For this reason, SeaWiFS data will be exploited within this thesis. At global scale, the SeaWiFS algorithms showed uncertainties in the range proposed by the space agencies (< 5% for radiances; < 35% for chlorophyll) [*Gregg and Casey*, 2004; *O'Reilly et al.*, 2000]. However, in the Baltic Sea [*Darecki and Stramski*, 2004], southwestern Atlantic Ocean, Southern Ocean [*Garcia et al.*, 2005] and in Mediterranean Sea [*Gitelson et al.*, 1996; *Bricaud et al.*, 2002; *Claustre et al.*, 2002; *D'Ortenzio et al.*, 2002], standard empirical algorithms perform significantly worse than expected. Therefore, in order to avoid misleading results, a careful analysis for error assessments must be performed before using satellite data for quantifying the

phytoplankton space-time variability. This constitutes the main topic of the next chapter.

1.1.1 Definitions in Ocean Colour Remote Sensing

It is useful to introduce some relevant parameters with which the following discussion will be mostly concerned; these are the *Irradiance*, the *Radiance* and the *Reflectance*. All these parameters may refer either to total quantities integrated over a broad spectral range or to a narrow wavelength band in which the units are multiplied by nm^{-1}.

The *Irradiance*, E, is defined as the amount of radiant energy intercepted by a surface area element. It denotes the light arriving on a surface area and has units of W m^{-2}.

The *Radiance*, L, is the measure of the light leaving a surface per unit solid angle in a given direction. Given that a remote sensor measuring the electromagnetic radiation backscattered from the sea views the ocean surface as an extended light source, L is a parameter of great relevance in ocean colour remote sensing [*Robinson*, 2005]. The radiance has units of W sr^{-1} m^{-2}.

The *Remote Sensing Reflectance* of a water body, Rrs, is defined as the *Radiance* to *Irradiance* ratio, that is the amount of light leaving the surface vertically upwards weighted by the amount of light entering the surface from all directions. The spectral shape of Rrs defines the so-called ocean colour. This colour is indexed by the blue-to-green Rrs ratio (B/G), which, in case 1 waters, is essentially governed by the phytoplankton content and the absorption spectrum of sea water. In particular B/G decreases with increasing phytoplankton content [*Claustre et al.*, 2002]; it is of common knowledge that a blooming water body such as a pond appears green and the B/G is low, while off-shore deep oceanic waters appear blue, and the B/G is high.

An important difference in the remote sensing of the ocean colour refers to case 1 and case 2 waters definitions. These definitions refer to the factors affecting the light behaviour in the sea-water. In particular, case 1 are those waters in which the optical properties (absorption and scattering) of the water covary with the chlorophyll concentration [*Morel and Prieur*, 1977]; in other words all particles and dissolved material affecting the light field in the upper layer of the ocean derive from phytoplankton. The opposite is true for case 2 waters. These are well represented by

coastal waters in which the scattering and absorbing particles have a remarkably terrigenous origin mostly due to river run-off [*McClain et al.*, 1997].

1.1.2 The Light, the Atmosphere and the Sea-Water

From the point of view of the ocean colour remote sensing, the sea is a source of radiant energy. Before it can be detected by a remote sensor, light from the sea surface, after interaction with the water and the particles therein, has to go through the atmosphere. Here, light undergoes a series of absorbing and scattering processes due to the air molecules of the atmosphere (Rayleigh scattering) and aerosols. Moreover, depending on the light wavelength, there can be absorption/scattering due to water vapour and ozone. Thus, the light reaching the sensor is basically made of two components: a water-leaving component and an atmospheric component. Of most interest for biological oceanographers is the component coming from the sea, which conveys information about the constituents of the upper layer of the ocean. Unfortunately, the atmospheric component, which has to be filtered out from the total, constitutes as much as the 80-90% of the whole signal [*Gordon*, 1997]. In ocean colour remote sensing the processing step of removing the atmospheric contribution to retrieve the water-leaving radiance is called *atmospheric correction* [*Gordon*, 1997] and constitutes both a crucial issue in ocean colour (see next section) and an important source of data for atmospheric physicists and chemists.

1.1.2.1 Atmospheric Correction

The atmospheric correction procedure is the first of two steps to retrieve the colour of the ocean from satellite radiometer measurements. Atmospheric correction evaluates the atmospheric contribution to the total radiance received by the sensor. Within the data processing chain, an assumption is currently made: the radiance received by the sensor at the top of the atmosphere, L_T, accounts for the radiance due to Rayleigh molecular scattering, L_R, for the radiance due to aerosols scattering, L_A, and for the water-leaving radiance, L_W:

$$L_T = L_R + L_A + T' L_W \qquad 1.1$$

T', in equation 1.1, stands for the atmospheric diffuse transmittance, i.e. the fraction of light leaving the sea surface that effectively reaches the sensor. The single spectral contributions of L_R, L_A and $T'L_W$ vary considerably within the visible and near-

infrared (NIR) band channels (Figure 1.1). Figure 1.1 highlights the three contributions to the total signal on a spectral basis. Concerning the last generation of satellite sensors such as SeaWiFS and MODIS, two strategies for atmospheric correction procedure can be undertaken: the black pixel assumption [*Gordon and Clark*, 1981] and the dark pixel assumption [*Siegel et al.*, 2000].

In both approaches L_R is easily achievable as the viewing and solar geometry are characterized on a pixel-by-pixel basis [*Gordon and Wang*, 1994] and the pressure field and the Ozone concentration are known from global scale atmospheric models with sufficient accuracy (for example National Centre for Environmental Prediction, NCEP, European Centre for Medium range Weather Forecasting, ECMWF). In contrast, as the atmospheric aerosol concentration and composition are highly variable in space and time, the atmospheric correction procedure challenge is to evaluate L_A. In the black pixel assumption L_A is estimated in the NIR band channels where L_W is considered to be negligibly small (Figure 1.1). Then, by means of radiative transfer models which evaluate the aerosol properties spectral dependence, the contribution of L_A in the visible band channel is computed with a 5% uncertainty [*Gordon and Wang*, 1994]. This enables the evaluation of the $T'L_W$ term in Equation 1.1 as L_T is measured and L_R and L_A are calculated.

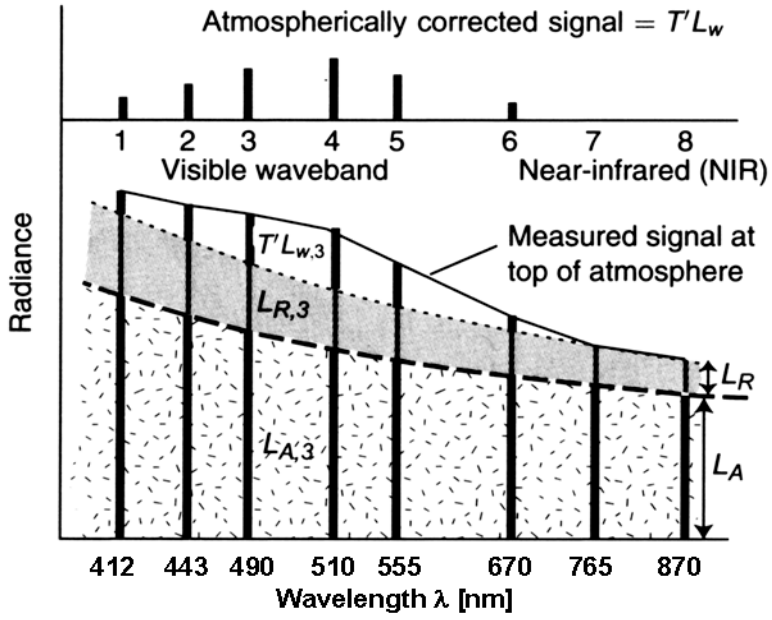

Figure 1.1: Schematic of the principle of multispectral atmospheric correction of ocean colour (adapted from *Robinson* [2005]).

In the dark pixel assumption L_A is considered to be non-zero in the NIR band channels. *Siegel and co-authors* [2000] proposed an iterative procedure which needs a

first guess for chlorophyll (0.2 mg m^{-3}) to estimate Rrs in the NIR band channels and remove it from the Rrs budget; then the application of the atmospheric correction procedure and of the bio-optical algorithm (see below) enables the evaluation of a new chlorophyll value. This process is repeated iteratively until the final chlorophyll value falls within 20% of the last iterate (typically one iteration for open ocean clear waters to three for coastal turbid waters). The dark pixel approach ameliorate the chlorophyll retrieval especially for highly productive waters [*Siegel et al.*, 2000].

1.1.2.2 Bio-Optical Algorithms

Once the atmospheric contribution has been evaluated and subtracted from the total radiance measured by the sensor, the water-leaving radiances at all wavelengths can be used to evaluate the ocean chlorophyll concentration. Ocean colour algorithms relate surface chlorophyll concentration to the blue-to-green reflectance ratio [see *Morel and Maritorena*, 2001; *O'Reilly et al.*, 1998; 2000). In general, the higher the chlorophyll concentration the lower is the B/G ratio. Existing operational global bio-optical algorithms (OC2v4 and OC4v4 for SeaWiFS and OC3 for MODIS) are based on regressions between *in situ* measurements of both water-leaving radiances and chlorophyll [*O'Reilly et al.*, 1998, 2000]. In particular, the OC2v4 algorithm evaluates the chlorophyll concentration by means of a third power relationship between the log-transformed B/G and chlorophyll, while OC4v4 and OC3 functional forms use fourth power relationships between these two same quantities (Table 1.1).

Table 1.1: Functional forms and band ratios of the standard NASA processing bio-optical algorithms for chlorophyll retrieval.

Algorithm	Band Ratio	Functional form
OC4v4	$\mathrm{MBR} = \mathrm{Log}_{10}\left(\mathrm{Max}([R_{555}^{443}, R_{555}^{490}, R_{555}^{510}])\right)$	$\mathrm{Log}_{10}(\mathrm{Chl}) = \sum_{i=0}^{i=4} a_i MBR^i$
OC3	$\mathrm{MBR} = \mathrm{Log}_{10}\left(\mathrm{Max}([R_{550}^{443}, R_{550}^{490}])\right)$	
OC2v4	$\mathrm{BR} = \mathrm{Log}_{10}\left(R_{555}^{490}\right)$	$\mathrm{Log}_{10}(\mathrm{Chl}) = \sum_{i=0}^{i=3} a_i BR^i$

The notation $R_{\lambda 2}^{\lambda 1}$ indicates the λ1 to λ2 Rrs ratio. Both Oc4v4 and OC3 use the maximum band ratio (MBR) as input to the respective forth power polynomial functional forms. OC2v4 uses the band ratio (BR) between Rrs at 490 and 555 nm as input to its third power polynomial functional forms. Term a_i are the coefficient empirically determined for each functional form.

The difference between these algorithms resides in both the functional forms and the choice of the reflectance band ratios and hence, as these algorithms are empirical, of the coefficients. The maximum band ratio (MBR) value is a different approach and has

the potential advantage of maintaining the highest possible signal to noise ratio over a 3 order-of-magnitude range in the chlorophyll concentration [*O'Reilly et al.*, 1998].

1.2 The Mediterranean Sea

In spite of its limited size (~0.6% of the global ocean surface, ~0.3% of the volume), the Mediterranean Sea (MED, Figure 1.2a) is considered one of the most complex marine environments on Earth, because of the variety of physical processes that occur there [*Williams*, 1998]. These processes span from the mesoscale to the basin-scale, and include also deepwater formation. Consequently, the basin has often been considered as a "miniature ocean" or as a "laboratory basin" [*Lacombe et al.*, 1981; *Robinson and Golnaraghi*, 1995] because most of the processes controlling the global ocean general circulation are present here, though with reduced temporal and spatial scales. Thus, in the context of the length of data time series, the impact of a rapidly changing climate on the MED marine ecosystem is expected to be easier to detect than in the global ocean.

1.2.1 Morphology

The MED is a semi-enclosed basin connected to the Atlantic Ocean through the Gibraltar Strait. The basin spans over 4700 km longitude and 1700 km latitude. It is divided into two main sub-basins, the Eastern (EMED) and Western (WMED) Mediterranean by the Strait of Sicily. These two straits (Gibraltar and Sicily) constitute physical constraints for the water mass exchange between the two sub-basins, barely reaching 300 and 500 m depth, respectively (Figure 1.2b). The average depth is 1500 m with a maximum depth of 5150 m in centre of the Ionian Sea. The MED can therefore be considered as a series of deep basins (thousands of meters depth) interconnected between them and with the Atlantic Ocean by shallow sills (hundred of meters depth), with a complex topography and coastline, and entirely surrounded by land. It is bounded by the industrialized European countries to the North, by the African continent to the South, and by Asia Minor countries to the East, thus revealing its fundamental importance also from the socio-economical point of view.

1.2.2Circulation

The basin dynamical circulation can be schematically represented by a three-layer system [*Lacombe and Tchernia*, 1972; *Lacombe et al., 1981*]: the surface layer, which

varies from 50 to 200 m thickness (according to the season and location), the intermediate layer from a depth of roughly 200 to 600 meters, and the deep layer.

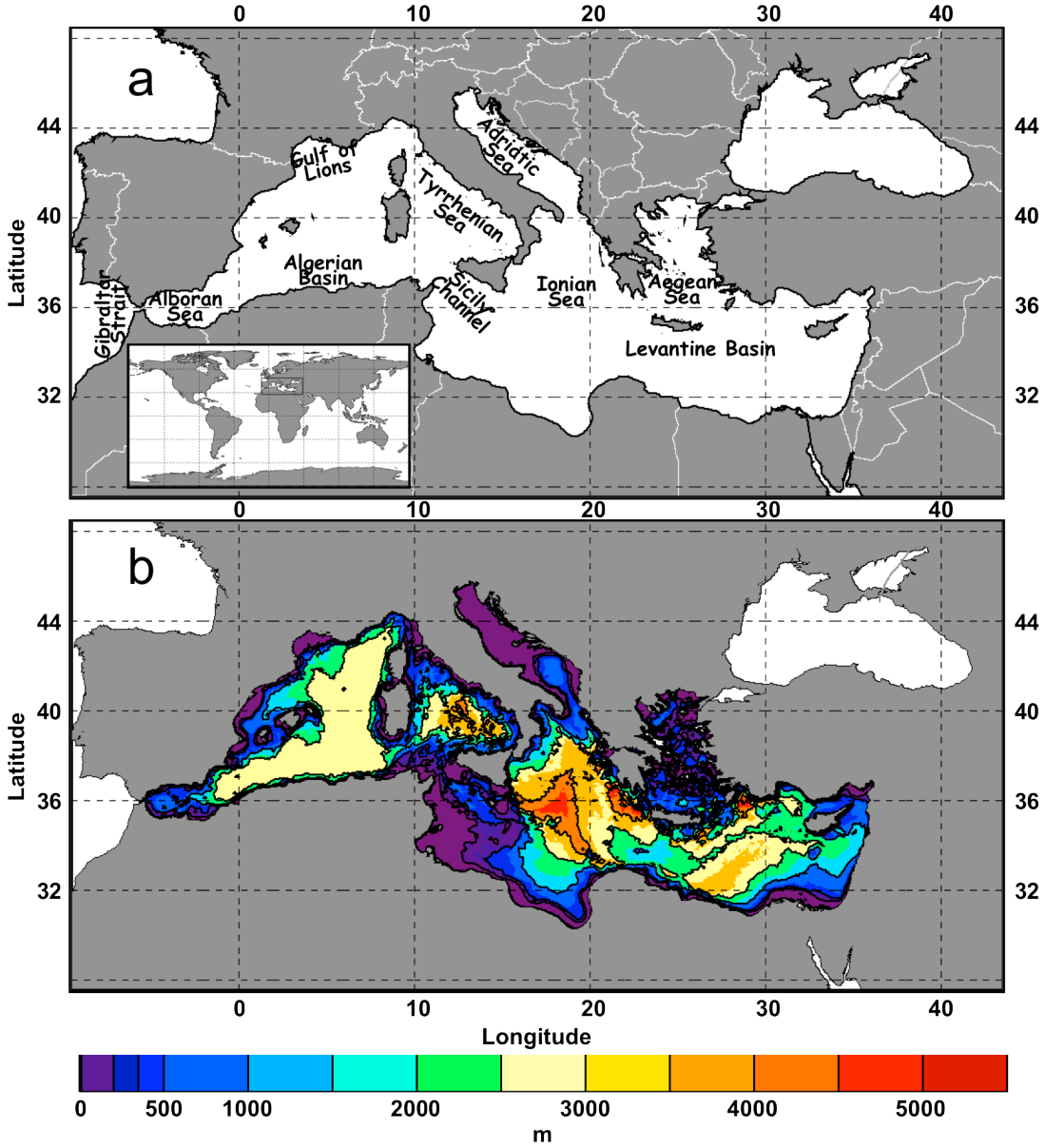

Figure 1.2: a) the Mediterranean Sea with highlighted the names of major sub-basins. b) MED bathymetry; units are in meters.

The water mass exchange between EMED and WMED is limited to the first two layers, as the Sicily Channel is only 500 m deep [*Manzella et al.*, 1988]. Similarly, as the Gibraltar Strait is only 300 m deep, the water mass exchange between MED and the Atlantic Ocean results in importing surface warmer and fresher waters from the Atlantic and exporting intermediate waters [*Astraldi et al.*, 1999, and references therein].

Lascaratos et al. [1999] described the MED circulation as two mutually interacting systems with different space and time scales (Figure 1.3):

- Basin scale circulation

- Sub-basin scale circulation

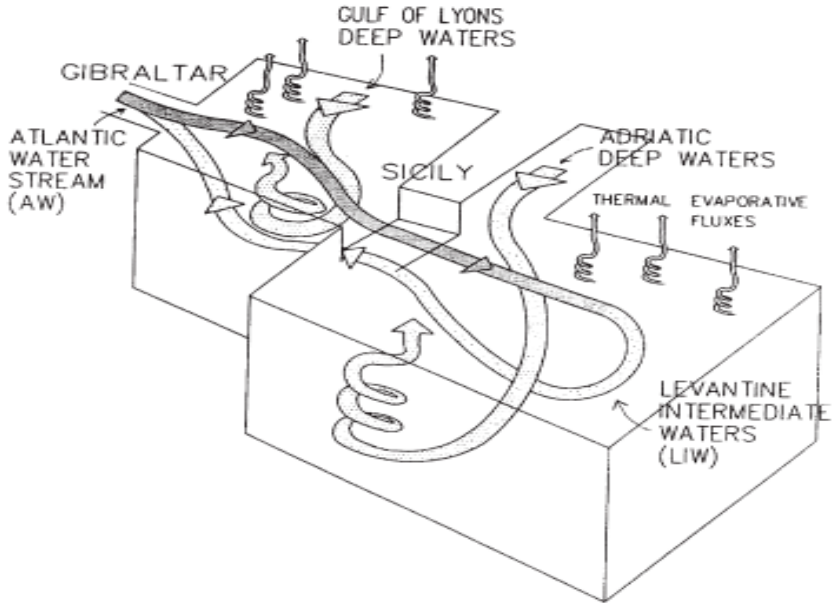

Figure 1.3: Scheme of the Mediterranean Sea general dynamical circulation [from *Lascaratos et al.*, 1999]. Curls indicate evaporation of water due to strong atmospheric forcing.

The basin scale circulation regards the transformation of the Atlantic Water (AW), entering at Gibraltar and moving eastwards to the Levantine basin, into the Levantine Intermediate Water (LIW). This transformation takes place because AW, flowing eastwards, progressively mixes with the surrounding waters becoming saltier and hence deepens to intermediate depth. The thermohaline circulation temporal scale is approximately 100 years [*Roether and Schlitzer*, 1991].

The sub-basin scale circulation is what controls the deep water formation (DWF) within each sub-basin independently of the other. This latter phenomenon takes place at the seasonal timescale. DWF occurs during winter in the Gulf of Lions (WMED) due to strong evaporation induced by the Mistral wind. In the EMED, the location of deep-water formation changed between the 1980s and 1990s. During the 1980s the cell was driven by a deep-water formation source located in the southern Adriatic, while in the 1990s the "engine" of the thermohaline circulation shifted to the southern Aegean/Cretan Sea. This transition had a profound effect on the physical and biochemical processes [*Casotti et al.*, 2003] and property distributions of the entire eastern Mediterranean, with long-term effects spreading to the western basin [*Malanotte-Rizzoli*, 2003].

1.2.3 Biogeochemistry

From the biogeochemical point of view, the MED is considered one of the most oligotrophic seas on Earth [*Crise et al.*, 1999]. Similarly to many open ocean areas, this condition does not allow high biomass levels to be sustained [*McGill*, 1961], with an average yearly phytoplankton biomass load of 0.19 mg m^{-3} [*Santoleri et al.*, 2008]. A significant portion of the world's ocean is oligotrophic (e.g., Sargasso Sea, South Pacific Ocean, the Mediterranean Sea), that is characterized by low nutrients and low chlorophyll (LNLC) [*Howarth,* 1988*; Guerzoni et al.,* 1999*; Bonnet et al.,* 2008]. The oligotrophy of the Mediterranean is mostly due to the import of surface nutrient-depleted waters from the Atlantic Ocean and to the export of nutrient rich intermediate waters. Moreover, the oligotrophy of the basin increases eastwards; probably due to the zonal gradient of the mixed layer depth, which is shallower in the WMED than in EMED [*D'Ortenzio et al.*, 2005]. The shallower depth of the mixed layer results in the WMED water column being more susceptible to the meteorological forcing, leading this sub-basin to have a more pronounced temporal variability. The nutrient availability results in a well defined geographical zonation of the phytoplankton biomass, with a yearly average chlorophyll concentration of 0.05 mg m^{-3} for the oligotrophic Levantine Basin and roughly 0.3 mg m^{-3} for the periodically blooming areas of the northwestern basin [*Santoleri et al.*, 2008]. Moreover, the phytoplankton seasonal cycle is strongly controlled by the trophic regime under which they grow, resulting in a marked space and time variability [*D'Ortenzio and Ribera d'Alcalà*, 2009]. From the temporal point of view, phytoplankton exhibits a subtropical-like seasonal cycle characterized by low surface chlorophyll concentrations and a deep chlorophyll maximum at the nutricline (~40 m in WMED and up to 120 m in EMED [*Crise et al.,* 1999]) in summer when the water column is stratified; on the other hand, winter mixing breaks stratification bringing nutrients up into the euphotic layer finally resulting in a spring bloom [*Santoleri et al.,* 2008]. However, *D'Ortenzio and Ribera d'Alcalà* [2009] more recently showed that there is a clear zonation of the whole basin with regions showing a subtropical-like seasonal cycle, with phytoplankton blooming in early-winter and a North Atlantic-like seasonal cycle with phytoplankton blooming during spring. Moreover, apart from the numerous mesoscale features and the coastal areas contributing to enhance the system biomass load [*Antoine et al.*, 1995; *Santoleri et al.*,

2008], there are the so-defined regions presenting a non-blooming period [*D'Ortenzio and Ribera d'Alcalà*, 2009].

A peculiar characteristic of the Mediterranean basin is the higher N to P ratio (20-27) [*Meybeck*, 1982], as compared to an average value of 16 found in the global ocean [*Redfield et al.*, 1963]. As suggested by *Guerzoni et al.* [1999] this discrepancy may be related to the high N/P ratio found in the atmosphere (~70), pointing to the importance of the nitrogen fixation, the phenomenon through which phytoplankton cells break down and hence assimilate the molecular N into organic N. Moreover, the MED lies adjacent to the Sahara, the world's largest source of aeolian soil dust, and is under a major dust pathway where dust deposition frequently occurs [*Engelstaeter et al.,* 2006]. Thus, the peculiar N to P ratios have been suggested to be due to phosphate removal by mineral dust [*Krom et al.*, 1991; *Herut et al.*, 1999]. The unusual N/P ratio suggests that phosphorus is the Mediterranean Sea limiting factor for phytoplankton growth [*Thingstad et al.*, 1998; 2005]. In this context, a debated and still open question concerns the role of atmospheric dust in the regulation of the biogeochemistry of oligotrophic gyres, i.e., the Dust Fertilization Hypothesis (DFH).

1.3 Thesis objectives and outline

The general thesis objective is to determine the phytoplankton space-time variability in the Mediterranean Sea using SeaWiFS data, at different space and time scales, and its relationship with the physical environment. In the context of validity of results, this work aims to assess the quality of ocean colour data (chlorophyll concentration, Chl) over the Mediterranean Sea with respect to space agencies requirements. This should in principle allow for the phytoplankton space and time variability to be effectively addressed in an unbiased way. In particular, this thesis aims at investigating the cause-effect relationship that might potentially exist between surface phytoplankton biomass and physical processes such as those inducing variations in the thermal stratification of the water column, the surface geostrophic circulation, and the atmospheric deposition of dust. In this respect, the thesis key questions are:

- **What is the phytoplankton space-time variability in the Mediterranean Sea, and what are the space and time scales of influence by physical surface conditions?**
- **Does the Dust Fertilization Hypothesis hold in the Mediterranean?**

- **How accurate is the retrieval of ocean colour products over the basin?** Which, from a technical remote sensing point of view, can be also read as**: by how much and why does the Mediterranean bio-optical regime differ from the global ocean?**

The thesis is thus organized as follows: chapter 2 to 4 are self-standing chapters in the form of scientific articles, in which subjects are introduced, developed, discussed, and from which relevant conclusions are drawn. In detail, chapter 2 deals with the definition and assessment of a new regional Mediterranean Sea algorithm for surface chlorophyll retrieval from SeaWiFS data. The reprocessing of the entire SeaWiFS time series with the new ocean colour algorithm enables the phytoplankton biomass variability to be more confidently addressed in relation to the physical environment (e.g., SST, surface circulation, and atmospheric dust deposition). Since, for its nature, the dust deposition is expected to impact the phytoplankton dynamics on a sporadic temporal basis, it appeared reasonable to treat this issue in a separate chapter (four). In chapter 3 the dependence of phytoplankton dynamics upon variations in the water column stratification and in the surface geostrophic circulation is investigated. Chapter 5 draws the main conclusions.

2 Improved accuracy of phytoplankton retrieval from Mediterranean satellite data: the MedOC4 Algorithm

The contents of this chapter are identical to a paper that has been published in Remote Sensing of Environment: Volpe G., Santoleri R., Vellucci V., Ribera d'Alcalà M., Marullo S., D'Ortenzio F. (2007), The colour of the Mediterranean Sea: Global versus regional bio-optical algorithms evaluation and implication for satellite chlorophyll estimates. Volume 107, Issue 4, 30 April 2007, Pages 625-638.

This paper is made of the contributions by six authors, with the first author leading the whole work by writing the manuscript, assembling data and making the analyses. Rosalia Santoleri provided constant scientific and technical support. Vincenzo Vellucci was in charge of the in situ optical data acquisition and processing. Other authors provided useful comments revising the manuscript and stimulated many fruitful discussions. Other technicians from the Stazione Zoologica "A.Dohrn" Napoli, provided in situ chlorophyll data.

The content of this chapter can be summarised by the following abstract that accompanies the published paper.

In this paper, uncertainties in the retrieval of satellite surface chlorophyll concentrations in the Mediterranean Sea have been evaluated using both regional and global ocean colour algorithms. The rationale for this effort was to define the most suitable ocean colour algorithm for the reprocessing of the entire SeaWiFS archive over the Mediterranean region where standard algorithms were demonstrated to be inappropriate. Using a large dataset of coincident *in situ* chlorophyll and optical measurements, covering most of the trophic regimes of the basin, we validated two existing regional algorithms [*Bricaud et al.,* 2002 and *D'Ortenzio et al.*, 2002] and the global algorithm OC4v4 used for standard NASA SeaWiFS products. The results of

our analysis confirmed that the OC4v4 performs worse than the two existing regional algorithms. Nonetheless, these two regional algorithms do show uncertainties dependent to chlorophyll values. Then, we introduced a better tuned algorithm, the MedOC4. Using an independent set of *in situ* chlorophyll data, we quantified the uncertainties in SeaWiFS chlorophyll estimates using the existing and new regional algorithms. The results confirmed that MedOC4 is the best algorithm matching the requirement of unbiased satellite chlorophyll estimates and improving the percentage of the satellite uncertainty, and that the NASA standard chlorophyll products are affected by an uncertainty of the order of 100 %. Moreover, the analysis suggests that the poor quality of the SeaWiFS chlorophyll in the Mediterranean is not due to the atmospheric correction term but to peculiarities in the optical properties of the water column. Finally the observed discrepancy between the global and the regional bio-optical algorithms has been discussed analysing the differences between the two *in situ* datasets used for tuning the algorithms (SeaBASS versus ours). The main results are that methodological differences in the two datasets cannot play a major role and the inherent bio-optical properties of the basin can explain the observed discrepancy. In particular the oligotrophic water of the Mediterranean Sea is less blue (30 %) and greener (15 %) than the global ocean.

2.1 Introduction

Satellite ocean colour data has been successfully used to provide unique and important information on surface phytoplankton distribution (e.g. chlorophyll), representing an essential element to address marine environmental issues and sustainable management of marine resources. They can provide near real-time, long-term, synoptic, global estimates of key parameters to validate high resolution models and to be assimilated by ecosystem models. Nonetheless, their efficient exploitation requires the production of quality controlled dataset accompanied by robust statistical analyses of the uncertainties associated with the retrieval procedures, e.g. atmospheric correction, bio-optical algorithms.

For this reason, the space agencies involved in ocean colour missions have established important projects to collect vast databases of in situ data for calibration and validation of satellite products [*McClain and Fargion*, 1999; *O'Reilly et al.*, 2000; *Gregg and Casey*, 2004]. These in situ data have been then used to develop the empirical algorithms operationally used in the satellite data processing chains (OC4v4

for SeaWiFS, OC3 for MODIS and Algal1 for MERIS). These standard algorithms proposed by space agencies to process data from their sensors have a nominal accuracy of ~35 % in the retrieval of surface chlorophyll in case 1 waters.

Among ocean colour sensors, an extensive calibration and validation activity has been performed on SeaWiFS data by SeaWiFS and SIMBIOS Projects. At global scale, the SeaWiFS algorithms showed uncertainties in the range proposed by the space agencies (< 5 % for radiances; < 35 % for chlorophyll) [*Gregg and Casey*, 2004; *O'Reilly et al.*, 2000]. However in the Baltic Sea [*Darecki and Stramski*, 2004], Southwestern Atlantic Ocean, Southern Ocean [*Garcia et al.*, 2005] and in Mediterranean Sea, standard empirical algorithms perform generally and sensibly worse.

More specifically in the Mediterranean Sea, *Bricaud et al.* [2002], *Claustre et al.* [2002] and *D'Ortenzio et al.* [2002] demonstrated that the standard NASA algorithms (OC2v4 and OC4v4) lead to a significant overestimation of the SeaWiFS derived chlorophyll concentration (> 70 % for chlorophyll < 0.2 mg m^{-3}). The failure of the SeaWiFS estimates in the Mediterranean Sea was confirmed also by other authors [e.g., *Gregg and Casey*, 2004]. *Claustre et al*. [2002] suggested that the observed bias could be attributed to the presence of Saharan dust in the water column, while *D'Ortenzio et al*. [2002], along with *Gitelson at al.* [1996], proposed as an alternative explanation that the presence of coccoliths, due to the relative abundance of coccolithophores could account, at least partially, for the observed discrepancy.

This observed bias in chlorophyll retrieval can have a strong impact in the use of SeaWiFS global products in primary production models, in validation and tuning of ecosystem modelling and especially in data assimilation systems.

Regional algorithms provide a suitable solution to overcome the above problems [*Gitelson et al*., 1996; *Garcia et al*., 2005, among the others]. *Bricaud et al*. [2002] and *D'Ortenzio et al*. [2002] provided the first attempts for SeaWiFS regional algorithms over the Mediterranean basin. *D'Ortenzio et al*. [2002], using a preliminary Mediterranean bio-optical dataset (45 in- and above-water bio-optical stations), proposed a two band algorithm based on the OC2 NASA functional form (hereafter DORMA). The algorithm was build with in situ chlorophyll concentration ranging between 0.06 and 1.92 mg m^{-3}. Contemporaneously, *Bricaud et al*. [2002] proposed a new regional algorithm for the retrieval of the SeaWiFS chlorophyll concentration in oligotrophic conditions (< 0.4 mg m^{-3}) switching to OC4v4 for values grater than this

threshold (hereafter BRIC). Both algorithms improved the performance of the SeaWiFS pigment retrieval in the Mediterranean Sea. Nonetheless, the statistical robustness of these algorithms is rather weak mainly because in situ data used to retrieve the proposed algorithms did not cover the whole range of Mediterranean trophic conditions. Moreover, these bio-optical regional algorithms, a part of a local validation exercise limited to the Gulf of Lions [*Ouillon and Petrenko*, 2005], have never been validated against an independent *in situ* dataset at basin scale. Finally, their impact on the chlorophyll retrieval with SeaWiFS sensor has never been fully evaluated.

Using a much larger bio-optical dataset we aim at quantifying the uncertainties of the existing regional and global ocean colour algorithms in the Mediterranean waters and at identifying and developing an optimal algorithm for the production of high quality ocean colour datasets for this basin. This work is part of the EU project Marine EnviRonment and Security for the European Area (MERSEA), which aims, besides other objectives, to provide high quality satellite products for data assimilation and validation of global and regional models. The identification of the best suited Mediterranean algorithm for chlorophyll retrieval and its associated uncertainty is an essential step to proceed to the re-processing of the entire SeaWiFS mission. Moreover, this work could also contribute to the definition of a regional ocean colour product for the Mediterranean data assimilation system.

In section 2.2 we present the *in situ* and satellite data and describe the procedure used to build up the matchup datasets. In section 2.3, the quantification of the uncertainties, introduced by regional (DORMA, BRIC) and global (OC4v4) bio-optical algorithms, is analyzed using in situ bio-optical measurements. A new regional algorithm is proposed in section 2.4 while the validation of SeaWiFS chlorophyll estimates obtained using the selected algorithms is presented in section 2.5. Discussion and conclusions are drawn in section 2.6.

2.2 Data and methods

2.2.1 In situ chlorophyll

In situ pigment measurements used in this work consist of 1144 chlorophyll profiles acquired during several cruises performed in the Mediterranean Sea between 1997 and 2004 (Table 2.1). Most of these data were acquired on board R/V Urania of the Italian National Research Council (CNR). During these cruises, standard

oceanographic parameters, such as temperature, salinity and fluorescence were measured using a SBE 911 CTD profiler and a SeaTech fluorometer. Water samples were collected by means of a G.O. Rosette equipped with 24 Niskin Bottles and filtered on board on GF/F filters (low vacuum) and immediately deep-frozen, then chlorophyll concentrations were determined on 90 % acetone extracts within few weeks of the sampling using a SPEX Fluorolog spectrofluorometer with an estimated coefficient of variation for chlorophyll-a concentration of 10 % [*Neveux and Panouse*, 1987].

To increase the depth resolution of pigment data, fluorescence profiles were converted to chlorophyll values after fitting them with bottle data. Conversion factors were obtained with linear regression analysis on log-transformed data [*Campbell*, 1995]. The fluorescence-chlorophyll calibration was performed for each cruise to take account of the intercruise variability of fluorometer sensor response. The uncertainty of the fluorescence-derived chlorophyll, in terms of absolute percentage difference (APD, see Appendix in section 2.7 for the definition of the statistical parameters), was estimated to be on average 20 %.

Additional data were extracted from DYFAMED station time series dataset [*Marty et al.*, 1995] and from SeaWiFS Bio-optical Archive and Storage System (SeaBASS) bio-optical archive (PROSOPE cruise in the Mediterranean Sea; *Hooker et al*., [1994]). These additional data are available on the web (http://www.obs-vlfr.fr/jgofs2/sodyf/home.htm for DYFAMED and http://www.obs-vlfr.fr/cd_rom_dmtt/pr_main.htm for PROSOPE).

To minimize the effect due to non-uniform chlorophyll profiles [*Stramska and Stramski*, 2005], the mean chlorophyll concentration within the penetration depth and weighted for the attenuation coefficient of light, C_M (see Appendix in section 2.7 for formula), was used as a proxy for the Optical Weighted Pigment Concentration [*Clark*, 1997; *D'Ortenzio et al.*, 2002]. It is important to underline that, chlorophyll values range from 0.003 to 7.06 mg m^{-3}, covering almost the whole range of possible values typical of the Mediterranean Sea.

2.2.2 In situ optical measurements

The optical dataset used in this work includes both in-water (106 stations) and above-water measurements (938 data points) (Table 2.1, Figure 2.1a). In water downwelling irradiance (E_d) and upwelling radiance (L_u) profiles were acquired using a Satlantic SPMR (SeaWiFS Profiling Multichannel Radiometer), following the standard

SeaWiFS protocols [*Mueller and Austin*, 1995; *Mueller*, 2000; *Mueller and Fargion*, 2002].

Out of the 106 SPMR measurements, 16 bio-optical stations were obtained by the SeaBASS archive [*Hooker et al.*, 1994]. These data were collected in the Mediterranean Sea during the PROSOPE cruise [*Claustre et al.*, 2002] (see Figure 2.1a for stations location).

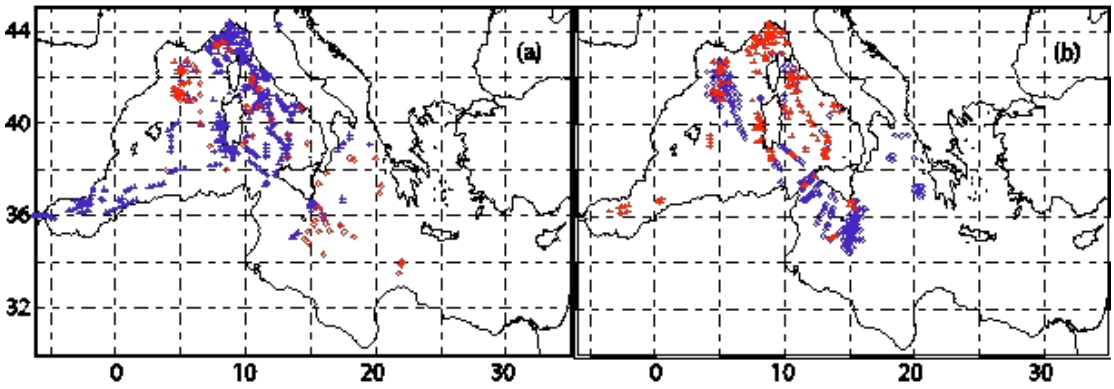

Figure 2.1: (a) Map of *in situ* optical stations. Crosses indicate above-water measurements and diamonds indicate in-water measurements. Points corresponding to co-located chlorophyll *a* measurements are coloured in red. (b) Map of satellite matchup data points. Blue diamonds indicate SeaWiFS-chlorophyll matchups, red crosses indicate SeaWiFS Rrs and *in situ* SIMBADA measurements matchups.

Above-water measurements were acquired with a SIMBADA radiometer during 20 cruises covering all Mediterranean seasonal conditions (Table 2.1). These data were then processed at LOA (Laboratoire d'Optique Atmospherique) of the University of Lille [*Fougnie et al.*, 1998]. Chlorophyll profiles were acquired concurrently with all in-water optical casts, and with 49 SIMBADA stations.

As for the latter, *Hooker and Morel* [2003] describe the difficulty of achieving a reliable above-water measurement of the water leaving radiance with a ± 5 % uncertainty, required for ocean colour algorithm calibration and validation activity, and conclude that the space agencies requirements are unlikely to be achievable by means of this approach. This is an important issue since our above water dataset is much lager then the in-water one. Therefore we compared the above-water dataset with the available in-water measurements in order to assess consistency between the two measurements within our dataset. As long as input parameters for the above-mentioned bio-optical algorithms are Rrs ratios, we will hereafter concern with band ratios:

$$R_{555}^{\lambda} = \frac{Rrs(\lambda)}{Rrs(555)} \qquad 2.1$$

Table 2.1: List of in situ cruises in the Mediterranean Sea from 1997 to 2005.

Cruise	Period	Zone	# of Chl Profiles			Chl range [mg m^{-3}]		# of Satlantic	# of SIMBADA		
			A	B	C	MIN	MAX		D	E	F
MATER 3	Oct 97	Sardinia Channel	76		6	0.034	0.061				
MATER 4	Apr-May 98	Sardinia-Sicily	57		38	0.025	0.073				
MATER 5	Oct-98	Sicily Channel	57		7	0.047	0.085				
EMTEC 99	Apr-May 99	Ionian Sea	126	18	43	0.039	0.095	18			
MATER 6	May 99	Sardinia-Sicily	100		58	0.003	0.094				
PROSOPE	Sep-Oct 99	Western Basin Ionian Sea	16	16		0.020	0.078	16			
SYMPLEX	Oct-Nov 99	Sicily Channel Ionian Sea	221	12	75	0.039	0.122	12			
NORBAL 1	Mar-Apr 00	Gulf of Lions	81		35	0.078	2.289				
MASSFLUX	Oct 01	Tyrrhenian Sea Sicily Channel							64	28	
NORBAL 2	Dec 01	Gulf of Lions Tyrrhenian Sea	65	27	27	0.088	0.268	12	44	16	15
MIPOT	Mar 02	Ionian Sea							23	2	
MEDGOOS 1	May 02	Sardinia(Coastal)							61	24	
M5ODAS	Jun-Jul 02	Ligurian Sea							50	33	
NAPOLI	Jul 02	Ligurian Sea							12	12	
NORBAL 3	Sep-Oct 02	Gulf of Lions	39	7	18	0.115	0.481	7			
LIGURE 1	Oct 02	Corsica(Coastal)							2		
MEDGOOS 5	Nov 02	Sardinia(Coastal)							6		
NORBAL 4	Mar 03	Gulf of Lions	115	43	51	0.297	7.061	16	82	65	27
MEDGOOS 6	Apr 03	Sardinia(Coastal)							25	14	
NORBAL 5	Apr 03	Gulf of Lions	40	11	13	0.420	2.096	4	18	17	7
LIPRO 1	Apr-May 03	Ligurian Sea							37	26	
LIGURE 2	Sep 03	Ligurian Sea							76	51	
MEDGOOS 7	Jan 04	Sicily Channel Sardinia(Coastal)							21	4	
MEDGOOS 8	May 04	Tyrrhenian Sea							96	51	
ALT 1	Aug 04	Tyrrhenian Sea	85	11	43	0.030	0.090	11	95	54	
MFSTEP 1	Sep 04	Ligurian Sea							69	26	
MEDGOOS 9	Oct 04	Western Basin							132	43	
MFSTEP 2	Apr 05	Ligurian Sea Tyrrhenian Sea							22		
DAPHNEII	May 05	North Adriatic							3		
DINA*	Mar-Aug 01	Tyrrhenian Sea	11	10	1	0.079	0.316	10			
DYFAMED*	Feb-98 Nov-02	Liguro-Provencal	55		25	0.042	2.366				
All cruises	1997-2005	Mediterranean	1144	155	440	0.003	7.061	106	938	466	49

Total Number of Chlorophyll profiles acquired in each cruise is reported in column A. Column B indicates the number of chlorophyll profiles constituting the *in situ* bio-optical dataset. Column C indicates the number of *in situ*-SeaWiFS chlorophyll matchups. Chlorophyll ranges (C_M) measured during each cruise are given in the 7th and 8th columns. The 9th column provides the number of stations in which corresponding in-water optical profiles (Satlantic) and chlorophyll samples were carried out. In column D the total number of above-water measurements (SIMBADA) acquired in each cruise is listed. The number of *in situ* Rrs-SeaWiFS matchups is displayed in Column E, while the number of SIMBADA station in which also *in situ* Chlorophyll measurements were acquired is shown in Column F. Symbol * indicates permanent stations. DYFAMED row give information about the number of stations acquired from the DYFAMED web site. DINA is a permanent station located 18 nautical miles offshore the Gulf of Naples (Southern Italy) where "Stazione Zoologica di Napoli *A. Dohrn"* collect data regularly.

with λ equal to 443, 490 and 510 nm, and MBR (Maximum Band Ratio):

$$MBR = MAX\left(R_{555}^{443}, R_{555}^{490}, R_{555}^{510}\right) \qquad 2.2$$

The maximum band ratio (MBR) has the potential advantage of maintaining the highest possible satellite sensor signal-to-noise ratio over a 3-orders-of-magnitude range in chlorophyll concentration [*O'Reilly et al.*, 1998].

Figure 2.2 shows the scatterplot of R_{555}^{λ} and MBR as measured by Satlantic SPMR and SIMBADA instruments in the space-time co-located available stations. Measurements from the two radiometers show a sensibly high agreement with RMS of 0.2, BIAS of 0.02, a relative bias (RPD) of 1.67 % and an APD of 7.38 % (see Appendix in section 2.7 for the definition of the statistical parameters). Therefore our SIMBADA and SPMR measurements can be mutually interchanged and constitute the bio-optical dataset analyzed in this paper for the purpose of algorithms' evaluation.

The remaining above water optical data were used to evaluate the efficiency of the atmospheric correction procedure to retrieve remote sensing reflectances. The chlorophyll profiles collected without optical measurements were used instead to build up a match-up data set for the validation of SeaWiFS derived chlorophyll.

2.2.3 Satellite data

High-Resolution Picture Transmission (HRPT) SeaWiFS Level-1A data, acquired by the receiving station HROM at ISAC in correspondence of all *in situ* measurement stations (chlorophyll a and/or Rrs, Table 2.1), have been used for satellite data validation. SeaWiFS Level-1A passes were processed up to Level-2 with the SeaWiFS Data Analysis System (SeaDAS) software package version 4.8 available from NASA website (www.seadas.gsfc.nasa.gov). Each Level-2 product includes:

- Chlorophyll *a*
- Rrs at 412, 443, 490, 510, 555, 670, 765 and 865 nm
- SeaDAS Level-2 flags (l2_flags)

Siegel's atmospheric correction algorithm was applied to Level-1A raw data [*Siegel et al.*, 2000], which is based on a first guess of chlorophyll concentration to compute water-leaving radiances. Since we selected three bio-optical algorithms (BRIC, DORMA and OC4v4) for our analysis, each Level-1A SeaWiFS pass was processed up to Level-2 two times. In fact, DORMA Level-2 products were obtained directly from SeaDAS after a modification of the code that includes the DORMA

regional algorithm as a further option of the SeaDAS code. On the contrary, following *Bricaud et al*. [2002] the BRIC chlorophyll maps were obtained applying the BRIC algorithm to Rrs produced by the OC4v4 processing.

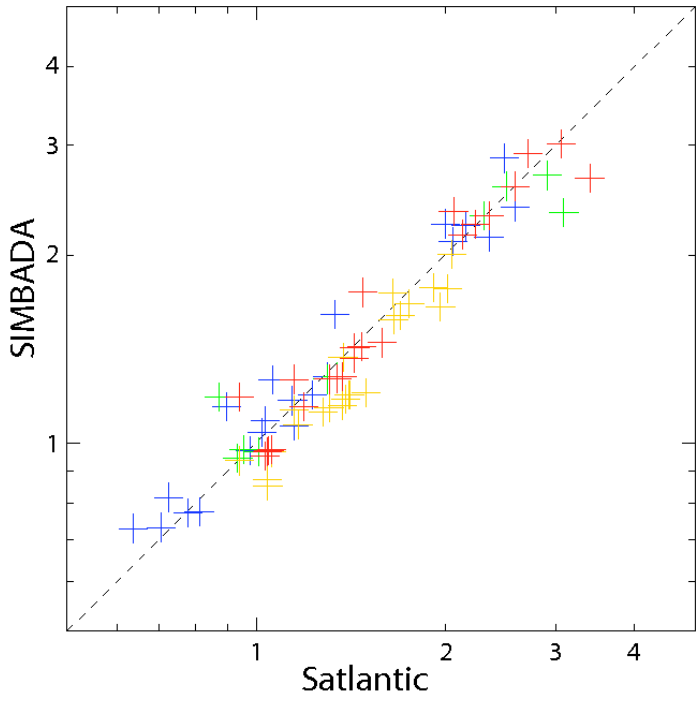

Figure 2.2: Scatter plot of SIMBADA versus Satlantic Rrs ratios. R_{555}^{443} **in blue,** R_{555}^{490} **in green,** R_{555}^{510} **in orange and MBR red.**

Finally all Level-2 products and chlorophyll maps were remapped at 1 km spatial resolution at Nadir on an equirectangular grid covering the Mediterranean Basin and the Black Sea.

Two matchup files have been generated (Figure 2.1b): one between SeaWiFS-derived chlorophyll and C_M, the other between SeaWiFS-derived Rrs's and SIMBADA measurements. Satellite data were averaged on a 3x3 full resolution pixel box centred on the location of the *in situ* measurements, and only boxes with all pixels passing all the l2_flag tests were retained for the analysis. Temporal criteria for coincidence was within the same day for chlorophyll [*Gregg and Casey*, 2004] and within four hours for Rrs's [*McClain et al.*, 1995]. The rationale for discriminating the two parameter matchup time windows is that the chlorophyll field temporal variability is believed to be slower than the Rrs one which depends, beside other factor, also by the cloudiness of the area whose variability is quite fast. The criteria employed reduced the matching observations to 440 (chlorophyll) and to 466 (Rrs).

2.3 Algorithms validation: *in situ* analysis

We applied the three selected algorithms to our *in situ* optical dataset to estimate chlorophyll concentrations, which were then compared with *in situ* chlorophylls (C_M). The derived scatter plot (Figure 2.3a) confirms that the global NASA algorithm overestimates *in situ* concentrations at low chlorophyll values (< 0.4 mg m^{-3}) while regional algorithms are more efficient in reproducing C_M concentrations for this chlorophyll range (Figure 2.3b-c). In particular, BRIC behaves well for chlorophyll values < 0.1 mg m^{-3} but overestimates C_M in the 0.1-0.4 mg m^{-3} range. On the other hand, DORMA reproduces well low chlorophyll concentrations even if it is less efficient for chlorophyll values > 1 mg m^{-3}.

Along with the major patterns displayed in Figure 2.3, we divided the dataset into two clusters with the C_M threshold value of 0.4 mg m^{-3}. The two subsets reflect the main trophic regimes of the Mediterranean open waters: oligotrophic and meso-eutrophic [*Antoine et al.*, 1995].

The statistical parameters (see Appendix in section 2.7 for definitions) are reported in Table 2.2 which includes also results for the whole dataset.

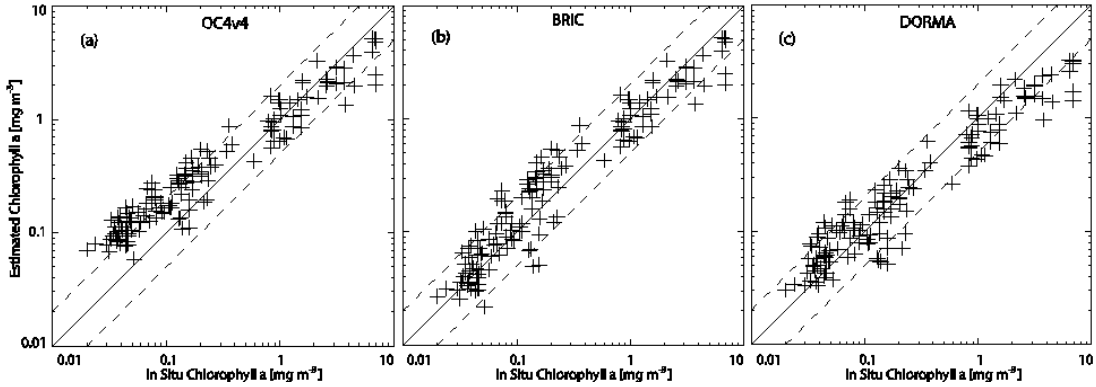

Figure 2.3: Scatter plot of algorithm derived chlorophyll concentration from in situ optical data versus in situ chlorophyll (CM). (a) The estimated chlorophyll is obtained using OC4v4 algorithm. (b) The estimated chlorophyll is obtained using BRIC algorithm. (c) The estimated chlorophyll is obtained using DORMA algorithm. The 1:1 (continuous line) 1:2 (bottom dashed line) and the 2:1 (top dashed line) lines are also plotted.

For the whole dataset (Table 2.2a) all algorithms display a similar r^2. RMS ranges from 0.75 mg m^{-3} (BRIC and OC4v4) to 1.04 mg m^{-3} (DORMA), whereas BIAS indicates that all the algorithms underestimate *in situ* values by an amount ranging from -0.12 and -0.16 mg m^{-3} (OC4v4 and BRIC) to -0.36 mg m^{-3} (DORMA). On the other hand, the analyses of the RPD and APD (i.e. statistical parameters accounting for the absolute value of the variable) indicate an opposite trend. APD values range from 43 %

and 47 % (DORMA and BRIC) to 92 % (OC4v4) and RPD from 8 % and 25 % (DORMA and BRIC) to 78 % (OC4v4).

Note that the evaluation of statistical parameters, such as RMS and BIAS, provide results in complete discordance with those evaluated accounting for the absolute values of the variable (i.e. RPD and APD), which reflects the non normal distribution of chlorophyll around its mean value, spanning over three order of magnitude. In this case the mentioned discordance is due to the fact that differences between measured and estimated chlorophylls at low values are negligible as compared to that at high values.

For $C_M < 0.40$ mg m^{-3} (Table 2.2b), r^2 coefficients do not significantly vary for OC4v4 and BRIC (0.73 and 0.74), while DORMA presents a r^2 coefficient of 0.64. RMS range from 0.06 mg m^{-3}, for DORMA, to 0.13 mg m^{-3}, for OC4v4. The comparison between *in situ* measurements and DORMA-derived chlorophyll reveals a BIAS of 0.02 mg m^{-3}, while the comparison with BRIC- and OC4v4-derived observations yields 0.06 and 0.1 mg m^{-3}, respectively. Since chlorophyll range in this case is narrower than previous scenario's, APD and RPD values are consistent with the RMS and the BIAS statistical parameters. In more details, APD decreases from OC4v4 (122 %) to BRIC (56 %) and DORMA (45 %). Similarly, RPD improves from OC4v4 (120 %) to BRIC (42 %) and to DORMA (29 %) indicating that the regional algorithms are more effective in reproducing *in situ* chlorophyll for this range of concentrations.

Table 2.2: Validation of the selected bio-optical chlorophyll algorithms in the Mediterranean Sea.

(a)	**$0.01 < C_M < 10.0$ mg m^{-3}**			**N=155**	
Algorithms	r^2	RMS	BIAS	APD	RPD
OC4v4	0.85	0.75	-0.12	92	78
BRIC	0.85	0.75	-0.16	47	25
DORMA	0.83	1.04	-0.36	43	8
(b)	**$0.01 < C_M < 0.40$ mg m^{-3}**			**N=105**	
Algorithms	r^2	RMS	BIAS	APD	RPD
OC4v4	0.74	0.13	0.10	122	120
BRIC	0.73	0.11	0.06	56	42
DORMA	0.64	0.06	0.02	45	29
(c)	**$0.40 < C_M < 10.0$ mg m^{-3}**			**N=50**	
Algorithms	r^2	RMS	BIAS	APD	RPD
OC4v4	0.71	1.31	-0.60	29	-11
BRIC	0.71	1.31	-0.60	29	-11
DORMA	0.68	1.83	-1.16	40	-36

Correlation coefficient (r^2), Root Mean Square (RMS), Mean Bias Error (BIAS), Relative Percentage Difference (RPD) and Absolute Percentage Different (APD) between *in situ* Chlorophyll (C_M) and the algorithms-derived chlorophyll *a* using *in situ* Rrs. The statistical parameters are shown for different C_M ranges.

For C_M > 0.40 mg m^{-3} (Table 2.2c), the OC4v4 and BRIC statistics obviously coincide. OC4v4 performs better than DORMA for all the statistical parameters.

DORMA is then the most suitable algorithm for C_M values < 0.4 mg m^{-3}, whereas it is worse than OC4v4 for C_M > 0.4 mg m^{-3}. It is worth reminding that DORMA was built with only few points exceeding 0.4 mg m^{-3} (only 3 > 1 mg m^{-3}), and this could explain the weak performances of DORMA in the third scenario, where most of the dataset is composed with values > 1 mg m^{-3}. Similarly, BRIC does behave well in oligotrophic condition and might probably improve by varying the band ratio instead of using only the R_{555}^{443}.

2.4 Bio-optical algorithm tuning: the MedOC4

In the previous section, we confirmed that the global algorithm, OC4v4, exhibits uncertainty levels in the chlorophyll estimation, which are incompatible with the expected requirements of the ocean colour mission (chlorophyll uncertainty < 35 %) when applied to the Mediterranean Sea. On the other hand, regional algorithms have been demonstrated to perform better in retrieving chlorophyll concentrations in oligotrophic condition. However, BRIC requires the a priori knowledge of the chlorophyll field as obtained from the OC4v4 and then it is implicitly affected by the intrinsic uncertainty on OC4v4. Moreover the systematic use of R_{555}^{443} instead of MBR leads to another unidentified source of error. Similarly, DORMA algorithm gives good performance for low chlorophyll concentrations but underestimates it at high values.

The analysis of the largest *in situ* bio-optical dataset ever used for the Mediterranean area, indicates then the need and implicitly suggests the means for developing a new regional algorithm of the Mediterranean Sea. Although no data are available from the Levantine basin, the present dataset covers the main Mediterranean trophic regimes (0.03 to ~7 mg m^{-3}), whereas DORMA and BRIC were developed using datasets covering limited range of bio-optical conditions. Therefore, our bio-optical dataset (Figure 2.4a) has been used to derive a set of coefficients for a new regional algorithm based on the OC4 functional form, namely MedOC4.

The coefficients were estimated through a fourth power polynomial regression fit between log-transformed *in situ* MBR and C_M:

$$Chl_{MedOC4} = 10^{(0.4424 - 3.686R + 1.076R^2 + 1.684R^3 - 1.437R^4)} \quad (3)$$

where $R = \log_{10}(MBR)$.

In Figure 2.4b, the comparison between the new MedOC4 algorithm and C_M shows that the functional form fits well the observed values. The data points are uniformly distributed around the line of best agreement, with a percent difference that rarely exceeds the 1:2 and 2:1 lines. The RMS is obviously zero and APD is the 30 %.

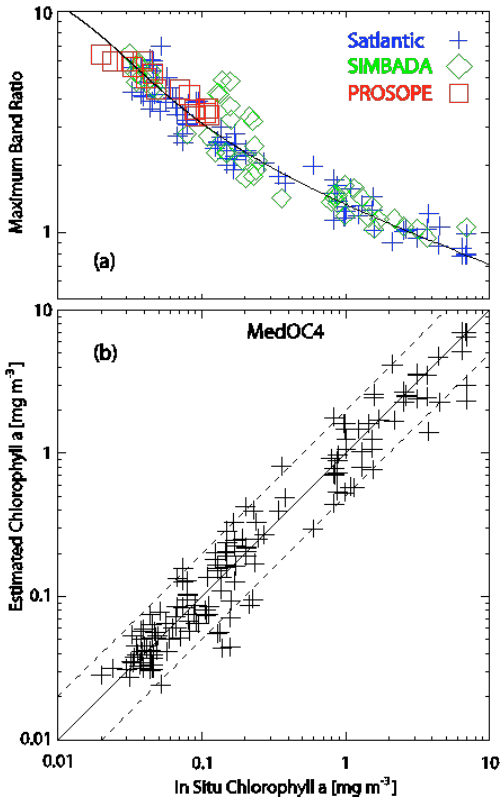

Figure 2.4: (a) Relation between in situ MBR and CM used to derive the new coefficients for the MedOC4 algorithm. Different optical data sources are highlighted with different colours. MedOC4 functional form is superimposed. (b) MedOC4-derived chlorophyll versus C_M. The 1:1 (continuous line) 1:2 (bottom dashed line) and the 2:1 (top dashed line) lines are also plotted.

A final comparison of all algorithms has been carried out by analysing the RPD values in five different chlorophyll ranges (Figure 2.5). They have been chosen to maintain a roughly constant number of points in all intervals. The graph displays RPD trends versus chlorophyll concentration. In particular, OC4v4's RPD improves as chlorophyll increases, whereas BRIC's RPD exhibits a bell shaped curve, with the maximum in correspondence of 0.05-1 mg m^{-3} chlorophyll range. For these ranges, the use of R_{555}^{443} instead of the maximum band ratio, is likely to cause the observed peak in the RPD. Similarly, DORMA performs better when the maximum band ratio coincides with R_{555}^{490} (0.1-1 mg m^{-3}), diverting from the zero RPD line for values lower than 0.1 mg m^{-3} and larger than 1 mg m^{-3}. Compared to the two previous regional algorithms,

the MedOC4 is definitively closer to zero RPD for all the considered chlorophyll ranges (RPD ranges between 5 and 11 %).

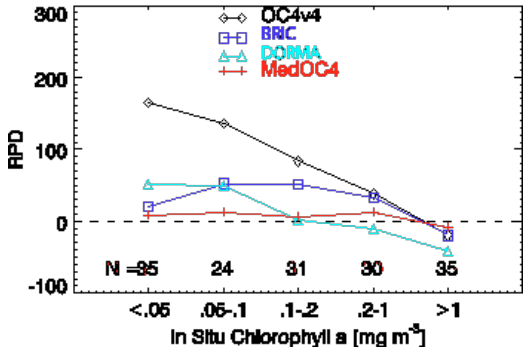

Figure 2.5: Relative Percentage Difference (RPD) for all the four examined algorithms as a function of in situ chlorophyll in five different ranges. Numbers within the plot indicate the number of data points used to retrieve RPD.

2.5 Validation of SeaWiFS Chlorophyll

To quantify the uncertainties on the satellite oceanic products, we compared SeaWiFS remotely sensed Rrs ratio (i.e., input for the ocean colour algorithms) and chlorophyll (output) with corresponding *in* situ measurements.

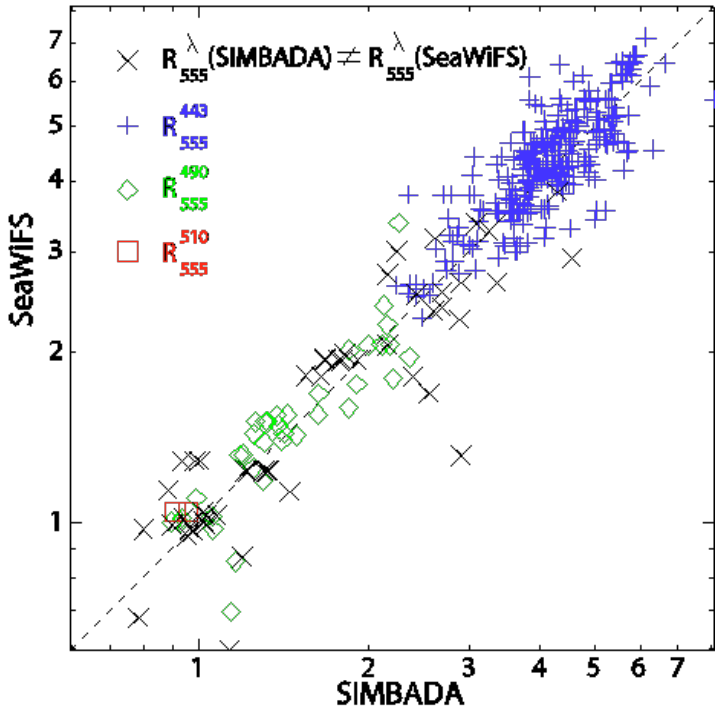

Figure 2.6: Scatter plot of space-time co-located MBRs from SIMBADA and SeaWiFS. Different symbols represent to different band ratio selections: blue crosses refer to R_{555}^{443}, green diamonds refer to R_{555}^{490} and red squares refer to R_{555}^{510}. Black "x" refer to points where MBRs selected by SIMBADA are different from the ones selected by SeaWiFS.

The scatterplot of SIMBADA versus SeaWiFS MBRs for 466 co-located measurements (Figure 2.6) shows a good agreement between the two independent

datasets, which is also confirmed by the statistics in Table 2.3. Moreover, different colours in Figure 2.6 represent the different band ratios used to compute the MBR: no evident bias is appreciable as a function of the different band ratios.

The correlation coefficients decrease as wavelength in the blue spectrum increases. Conversely, RMS values improve with wavelength. This is due to the increasing distance between the extrapolated blue bands and the NIR region during the atmospheric correction procedure. APD values appear independent of the wavelength and stable around ~10 %. However, MBR, by minimizing the signal-to-noise ratio, yields the highest r^2 (0.85) and the lowest BIAS (0.06) and RPD (2 %) values. This result agrees with previous comparison of satellite radiometric products and *in situ* measurements in the Mediterranean Sea [*Zibordi et al.*, 2006]. It is worth noting that the derivative of the chlorophyll concentration with respect to MBR is higher for low values of MBR. Therefore the observed uncertainty on MBR could eventually affect the chlorophyll estimates only at high chlorophyll concentrations.

Table 2.3: Correlation coefficient (r^2), Root Mean Square (RMS), Mean Bias Error (BIAS), Relative Percentage Difference (RPD), Absolute Percentage Different (APD) for 466 co-located measurements between SIMBADA and SeaWiFS radiometers.

R_{555}^{λ}	r^2	RMS	BIAS	APD	RPD
λ=443	0.85	0.59	0.06	14	3
λ=490	0.76	0.48	0.12	12	4
λ=510	0.70	0.28	0.17	14	10
MBR	0.85	0.58	0.06	12	2

Statistics refer to $R_{555}^{\lambda} = \frac{Rrs(\lambda)}{Rrs(555)}$ ratio (with λ= 443, 490 and 510 respectively) and to the Maximum of Band Ratio (MBR, see Equation 2.2). MBR coincides with the single band ratios as 79% (R_{555}^{443}), 20% (R_{555}^{490}) and 1%(R_{555}^{510}) of the 466 matchup points.

To verify the impact of the regional algorithms in the production of Level-3 data with respect to the standard global products, the three selected algorithms and the new MedOC4 were used to retrieve chlorophyll concentrations from SeaWiFS data and subsequently compared with the *in situ* co-located chlorophyll measurements. It is important to underline that the matchup dataset used in this section is independent from the one used in section 2.3 and section 2.4 (Table 2.1).

Scatterplots between C_M and SeaWiFS matchups (Figure 2.7) show that all the regional algorithms improve the SeaWiFS chlorophyll estimates and confirm the results obtained in the previous algorithms validation section: the global OC4v4 algorithm significantly overestimates the chlorophyll in oligotrophic conditions whereas the regional ones do not display significant bias. For higher chlorophyll concentrations,

satellite-derived values appear more scattered around the line of best agreement than the corresponding ones derived from *in situ* radiances (Figure 2.3 and Figure 2.4b) and less correlated to *in situ* measurements (Table 2.4c).

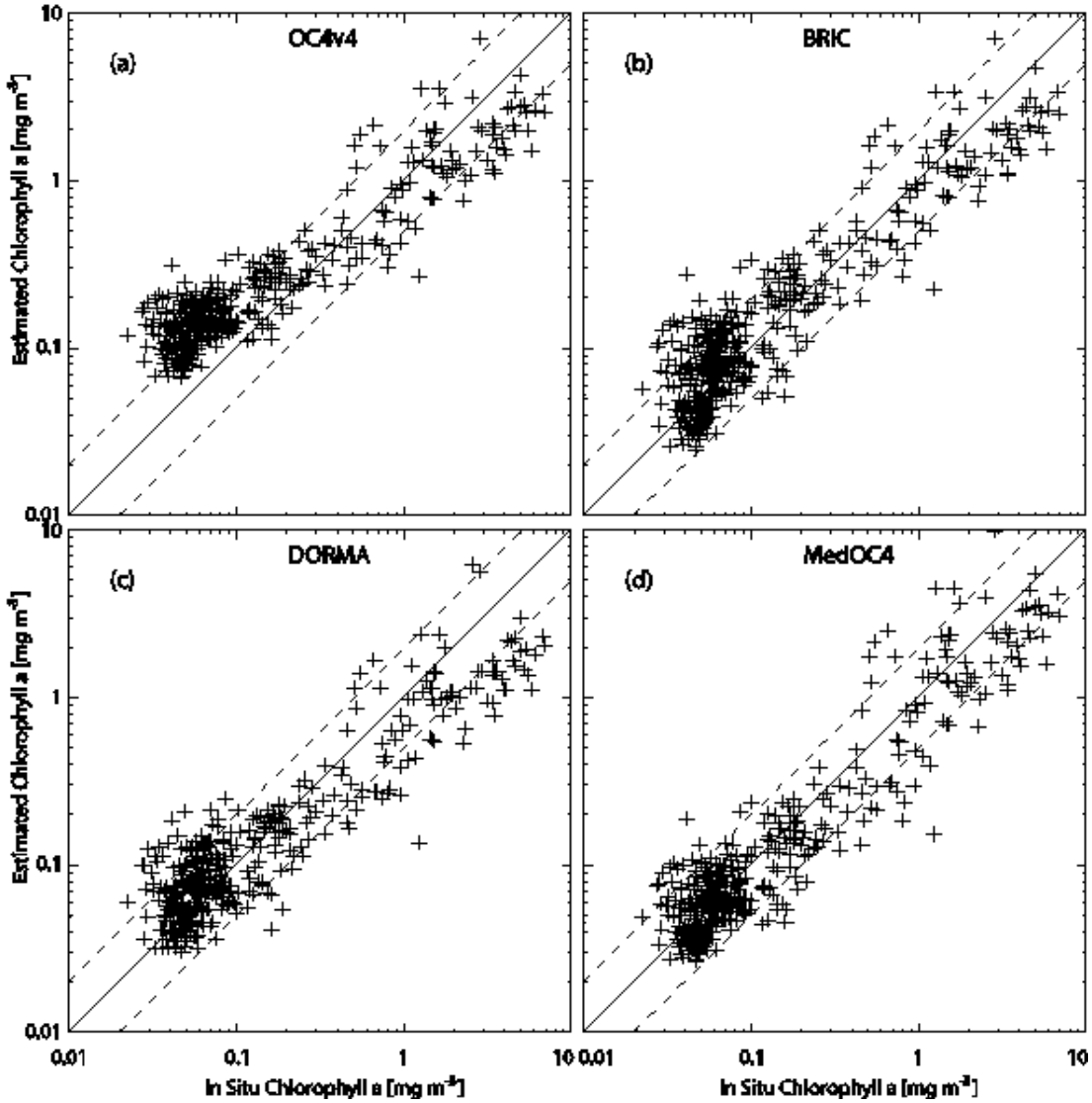

Figure 2.7: Validation of SeaWiFS chlorophyll a estimates against concurrent *in situ* chlorophyll *a* data (C_M). (a) SeaWiFS estimates are obtained applying the OC4v4 algorithm. (b) SeaWiFS estimates are obtained applying the BRIC algorithm. (c) SeaWiFS estimates are obtained applying the DORMA algorithm. (d) SeaWiFS estimated are obtained applying the MedOC4 algorithm. The 1:1 (continuous line) 1:2 (bottom dashed line) and the 2:1 (top dashed line) lines are also plotted.

The analysis of the statistical parameters shows that the overall algorithms' performance is slightly decreased, as compared to results from purely *in situ* data (Rrs and C_M). For consistency with sections 2.3, the statistical analysis has been performed for the whole dataset and the two subsets defined in section 2.3 (Table 2.4).

For the whole dataset r^2, RMS and BIAS are of the same order of magnitude for all algorithms, and show a general C_M underestimation (negative BIAS); on the other

hand APD and RPD decrease from OC4v4 (117 % and 103 %) to MedOC4 (40 % and 3 %).

Table 2.4: Validation of the SeaWiFS Level 3 products produced using the selected regional/global bio-optical chlorophyll algorithms in the satellite data processing chain.

(a) **$0.01 < C_M < 10.0$ mg m^{-3} N=440**

Algorithms	r^2	RMS	BIAS	APD	RPD
OC4v4	0.66	0.72	-0.08	117	103
BRIC	0.66	0.72	-0.13	54	27
DORMA	0.57	0.84	-0.21	48	15
MedOC4	0.62	0.73	-0.11	40	3

(b) **$0.01 < C_M < 0.40$ mg m^{-3} N=348**

Algorithms	r^2	RMS	BIAS	APD	RPD
OC4v4	0.54	0.09	0.08	134	133
BRIC	0.56	0.06	0.02	55	38
DORMA	0.49	0.05	0.01	46	28
MedOC4	0.55	0.04	0.00	35	6

(c) **$0.40 < C_M < 10.0$ mg m^{-3} N=92**

Algorithms	r^2	RMS	BIAS	APD	RPD
OC4v4	0.33	1.56	-0.68	50	-10
BRIC	0.33	1.57	-0.71	50	-12
DORMA	0.24	1.83	-1.04	55	-33
MedOC4	0.31	1.59	-0.49	58	-6

Correlation coefficient (r^2), Root Mean Square (RMS), Mean Bias Error (BIAS), Relative Percentage Difference (RPD), Absolute Percentage Different (APD) for the 440 collocated in situ Chlorophyll (C_M) and SeaWiFS matchups. The statistical parameters are shown for different C_M ranges.

For C_M < 0.40 mg m^{-3}, the correlation coefficient significantly decreases for all algorithms (ranging between 0.49 to 0.56); RMS values show that all algorithms perform at the same way while BIAS significantly decreases from OC4v4 (0.08) to MedOC4 (zero). APD and RPD indicate an increase in algorithms' performance from OC4v4 (134 % and 133 %) to MedOC4 (35 % and 6 %).

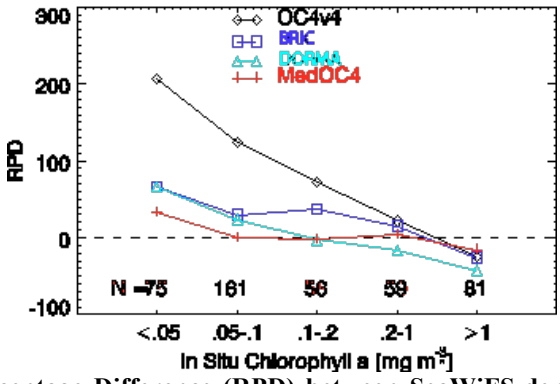

Figure 2.8: Relative Percentage Difference (RPD) between SeaWiFS-derived chlorophyll and co-located in situ C_M for all the four algorithms and for five chlorophyll ranges. Numbers within the plot indicate the number of data points used to retrieve RPD.

For C_M > 0.40 mg m^{-3} the correlation coefficient drops to 0.2-0.3; RMS is sensibly high (1.6-1.8 mg m^{-3}) for all algorithms while BIAS ranges from -0.49

(MedOC4) to -1.04 mg m^{-3} (DORMA). APD and RPD show that there is no significant difference among all algorithms.

The plot of the RPD as a function of chlorophyll range concentrations (Figure 2.8) shows that for $C_M < 0.05$ mg m^{-3} there is a general decrease in algorithms' performance. Moreover, the OC4v4 exhibits an increasing performance towards higher chlorophyll values. BRIC and DORMA performances are similar to that in Figure 2.5. On the other hand, MedOC4 significantly improves the SeaWiFS chlorophyll retrieval in the Mediterranean Sea being very close to zero bias conditions in almost all ranges of C_M.

2.6 Discussion and Conclusions

In this paper, uncertainties in the retrieval of satellite surface chlorophyll concentrations have been evaluated using both regional and global ocean colour algorithms. The rationale for this effort was to define the most suitable ocean colour algorithm for the reprocessing of the entire SeaWiFS archive over the Mediterranean region where standard algorithms were demonstrated to be inappropriate. Using a large dataset of coincident *in situ* chlorophyll and optical measurements, covering most of the trophic regimes of the basin, we validated two existing regional algorithms and tuned a new algorithm for the basin.

The results of our analysis confirmed that the OC4v4 standard algorithm performs worse than the two existing regional algorithms (BRIC and DORMA), at least during the time interval of our dataset (1997-2004). Nonetheless, these two regional algorithms do show uncertainties dependent to chlorophyll values. In fact, these algorithms were based on possibly under-representative datasets. In particular the high chlorophyll values used to calibrate BRIC were all from the Alboran Sea, whose dynamics is quite peculiar and strongly connected with the inflowing Atlantic Ocean [*Astraldi et al.*, 1999], while DORMA did not include values beyond 1.9 mg m^{-3} in its dataset. Due to the more extensive integrated dataset in our hands we introduced a better tuned algorithm, the MedOC4, having the same functional form than OC4v4 but an overall performance significantly better than all the tested ones.

We then analyzed the performance of all the algorithms when used to retrieve chlorophyll concentration from SeaWiFS using an independent set of *in situ* data. The results of this analysis confirmed that MedOC4 is the best algorithm matching the requirement of unbiased satellite chlorophyll estimates and improving the accuracy of the satellite estimate. Moreover, we found that the difference between the chlorophyll

concentrations based on bio-optical *in situ* measurements and those derived from satellite display, on average, a very small difference (Figure 2.5 and Figure 2.8). This suggests that the poor performance of the standard algorithm is not due to the atmospheric correction term, as one might have been hypothesized due to the peculiar aerosol of the region [*D'Ortenzio et al*., 2002; *Claustre et al*., 2002]. This conclusion is also supported by the analysis we conducted on the SIMBADA-SeaWiFS matchup dataset to test the accuracy of the satellite band ratios over the Mediterranean Sea.

The observed discrepancy between the global and the regional bio-optical algorithms might depend on methodological differences between the datasets used to derive the algorithms coefficients, or on differences among the inherent bio-optical properties of the two domains.

The OC4v4 algorithm was built on a later version of the SeaBAM bio-optical archive which is prevalently composed of above-water radiance measurements (88 %, Figure 2.9). On the other hand, the bio-optical dataset used to develop the MedOC4 is mainly based on in-water radiance measurements (67 %). A recent study by *Hooker and Morel* [2003] showed that above-water measurements could account up to 4-8 % RPD for the blue-to-green ratios. The comparison of the two MBRs do show a difference (~65 % in the chlorophyll range 0.01-0.05 mg m^{-3} and ~37 % for chlorophyll at 0.2 mg m^{-3}) which is an order of magnitude grater than what found by *Hooker and Morel* [2003].

A second methodological difference between the datasets is the utilization of mostly surface chlorophyll concentration (SeaBAM) instead of the optically weighted chlorophyll concentration (MedOC4).

Recently, *Stramska and Stramski* [2005] demonstrated that a deep chlorophyll maximum (DCM) close to the surface can affect the radiant field by a non-negligible amount. This can quantitatively explain the failure of standard algorithms (OC4v4) on a regional basis, as long as the use of the surface chlorophyll value, as in the OC4v4, assumes a homogeneous distribution of the pigment for the first optical depth. The extent of the uncertainty depends mostly on the depth of the DCM, but also on its amplitude.

Therefore we selected among our profiles those with a DCM within the first optical depth. Only 10 % of the profiles fell within this category. Afterwards we modelled our profiles with the *Stramska and Stramski* [2005] approach, defining a series of coupled values (chlorophyll at surface – DCM depth), and concluded that only

1 to 2 % of them had a chlorophyll value at surface and a DCM depth such to significantly affect the Rrs(λ). This implies that the influence of the DCM on the surface radiant field is negligible in the Mediterranean Sea.

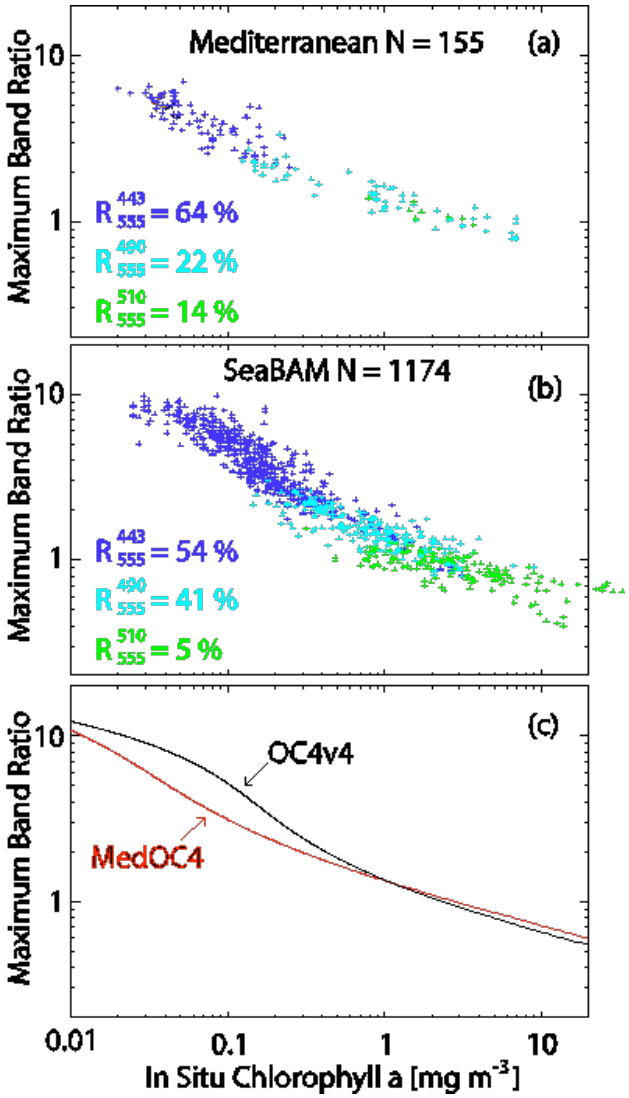

Figure 2.9: Intercomparison between Mediterranean and global (SeaBAM) in situ bio-optical measurements. (a) Relationship between in situ MBR and CM for the Mediterranean dataset (this work, Table 2.2) (b) Relationship between in situ MBR and CM for the global SeaBAM dataset. Blue crosses indicate that MBR corresponds to R_{555}^{443}; light blue crosses indicate that MBR corresponds to R_{555}^{490}; green crosses indicate that MBR corresponds to R_{555}^{510}. The percent number of times in which the three R_{555}^{λ} correspond to MBR are also superimposed. (c) The two best lines fitting the Mediterranean and SeaBAM datasets are plotted: MedOC4 (red) and OC4v4 (black). SeaBAM dataset archive is available on the Internet at http://seabass.gsfc.nasa.gov/seabam/pub/maritorena_oreilly_schieber/seabam919.txt web page.

So far it appears that the observed differences are attributable to environmental bio-optical characteristics of the Mediterranean, which ask for further investigations.

We attempted to characterize the spectral pattern of Rrs, for the two datasets (SeaBAM and ours) at different chlorophyll ranges to highlight the differences in the spectral signatures of the basin versus the global ocean.

To this aim, we analyzed the statistical distribution of Rrs's values in the blue (numerator of MBR) and green bands (denominator of MBR), in the two datasets in different chlorophyll ranges (Figure 2.10). Statistical test (t-Student, 99 % significance) were performed on sample data to verify whether the two datasets are significantly different. In fact, the Mediterranean Sea looks relatively "greener" for low chlorophyll values than the global ocean (Figure 2.9) and this can be either due to the fact that the Mediterranean Sea is less blue and/or effectively greener. The opposite is true for higher chlorophyll values in which the global ocean appears slightly greener than the Mediterranean Sea.

Histograms in Figure 2.10 show that in the 0.01-0.05 mg m^{-3} chlorophyll range the Mediterranean Sea is both less blue and greener than the global ocean. The amount of such a shift has been quantified in ~30 % RPD for the blue bands and ~15 % RPD for the green bands. In the second range, this shift is even more evident: the Rrs in the blue bands measured in the Mediterranean is ~35 % lower than that of the global ocean and the Rrs in the green is ~18 % higher than that measured in the global ocean. In the 0.1-0.2 mg m^{-3} chlorophyll range the different Rrs ratio is due to a blue shift of approximately 32 % while the green bands are not significantly different. The blue and the green in the 0.2-1 mg m^{-3} range are not significantly different. In the last of the considered ranges, even if the two fitting lines appear to be very close to each other (Figure 2.9c), the datasets are significantly different. The Mediterranean is 23 % bluer and 35 % RPD less green than the global ocean.

It is important to underline that the upgraded version of former SeaBAM dataset has been used also to develop the ocean colour algorithms for MODIS Aqua and Terra as well as for MERIS. So it is likely that chlorophyll estimates in the Mediterranean Sea with remote sensors other than SeaWiFS, will be biased as well. The presence of a bias in the chlorophyll estimates is quite problematic when satellite products are used in primary production models, in validation and tuning of ecosystem modelling and especially in data assimilation systems where an error in satellite estimate can worsening rather than improving the model performance. Therefore, the re-analysis of SeaWiFS dataset using the MedOC4 regional algorithm planned in MERSEA is

mandatory before the possible use of satellite data in Mediterranean assimilation system.

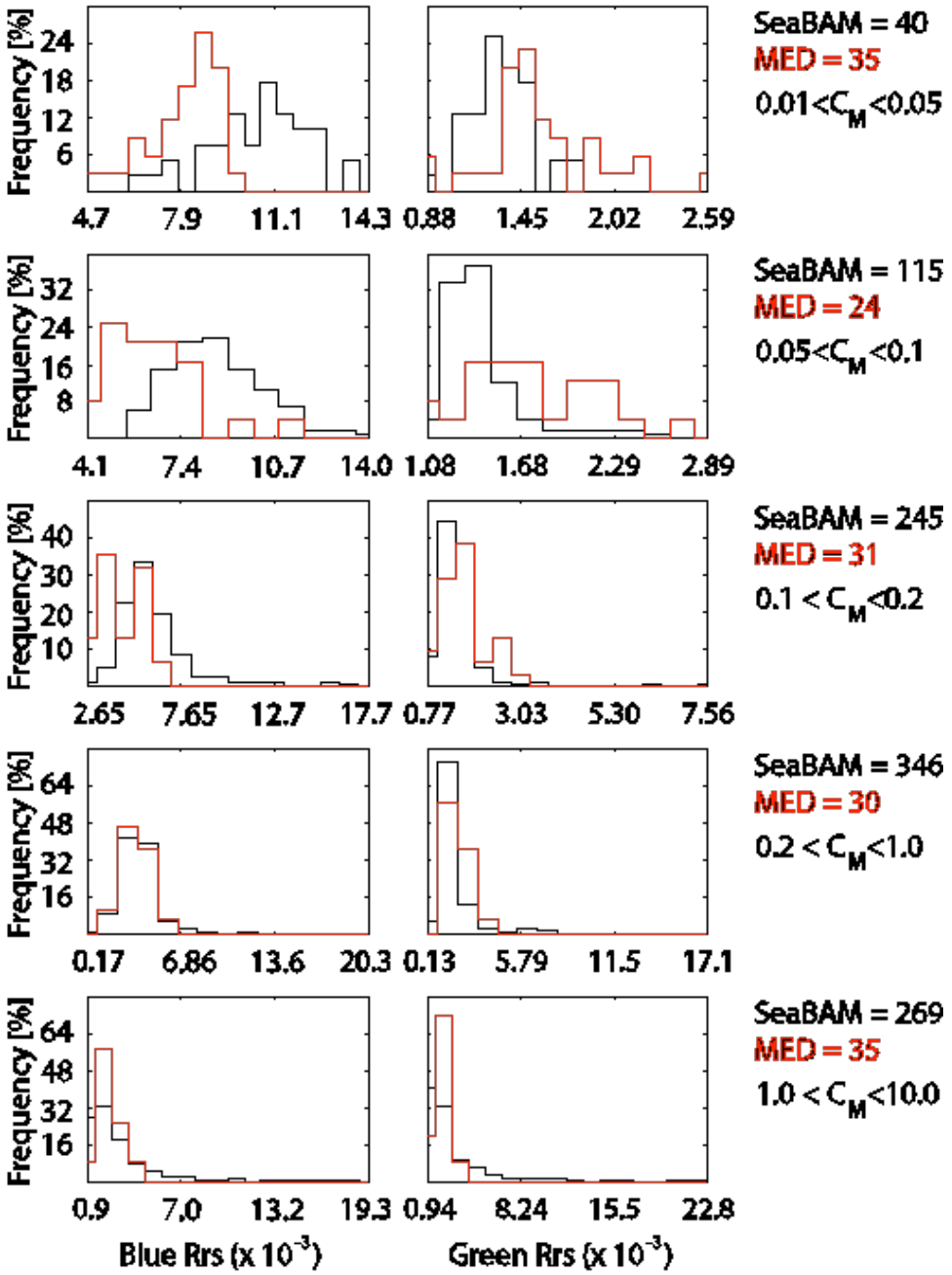

Figure 2.10: Normalized Frequency histograms of the Rrs for the Mediterranean (red) and SeaBAM global datasets (black) for five different chlorophyll ranges. Left panels indicate the maximum value among Rrs(443), Rrs(490) and Rrs(510) (i.e., the numerator of MBR). Right panels indicate Rrs(555) (i.e., the denominator). Chlorophyll a ranges are indicated on the right hand side of each row along with the number of points used for each of the two datasets.

Why then the Mediterranean Sea displays a different colour than the global ocean? Our dataset cannot basically answer this question. Though, some insight can come from two recent studies by *Alvain et al*. [2005; 2006]. They, using the GeP&CO [*Dandonneau et al.*, 2004] dataset which is an upgraded version of the SeaBAM, generated two independent sets of classes for HPLC pigment spectra and normalized

water leaving radiances (nL_w^*) and found a one to one correspondence among the two sets. Since each HPLC class corresponded to a phytoplankton association with the dominance of one of the main group, e.g., diatoms, haptophytes, *Synechococcus* Like Cyanobacteria (SLC) and *Prochlorococcus*, the corresponding class of nL_w^* should then result from the presence of the same association *in situ*. In other words a specific colour signature, within the reduced number of classes they were able to discriminate, should result from the dominance of a phytoplankton group, i.e., from the ecological dynamics of the area. Their approach allowed for the derivation of four community specific bio-optical algorithms which are embedded in the NOMAD global bio-optical dataset. Therefore their curves fall outside the peculiar Mediterranean dataset. Nevertheless, we think that their approach is very enlightening and suggests that Mediterranean peculiarity can likely be related to ecological reasons, rather than abiotic environmental components. Among those, the already stressed presence of coccolithophores [*Malinverno et al.*, 2003], the dominance of prokaryots or a high ratio among eterotrophs and autotrophs [*Casotti et al.*, 2003 and references therein] could play a role.

The extent to which a different phytoplankton community structure and distribution could alter the spectral signature of the water column can be assessed with more refined bio-optical measurements, which will be likely acquired in future campaign. This target should be at hand with the new generation of bio-optical sensors.

2.7 Appendix – Definition of statistical parameters

For the purpose of algorithms' validation, five statistical parameters were chosen. These parameters are:

- Correlation coefficient (r^2)
- Root Mean Square (RMS)
- Mean relative percentage difference (RPD)
- Bias
- Mean absolute percentage difference (APD)

The r^2 coefficient from the correlation analysis indicates the covariance between the *in situ* observations (C_M) and algorithms-derived chlorophyll (Alg). C_M is the mean chlorophyll concentration within the penetration depth (Z_{pd}) weighted for the attenuation coefficient of light (k). It is here used as a proxy for the optically weighted pigment [eq. 6 in *Clark*, 1997] and has been computed as:

$$C_M = \frac{\int_0^{z_{pd}} Chl(z)\exp(-2Kz)dz}{\int_0^{z_{pd}} \exp(-2Kz)dz}$$

RMS indicates the spread of data as compared to the best agreement and was computed as:

$$RMS = \sqrt{\frac{\sum_{i=1}^{N}\left(A\lg_i - C_{Mi}\right)^2}{N}}$$

The mean bias error was computed as:

$$BIAS = \frac{1}{N}\sum_{i=1}^{N}\left(A\lg_i - C_{Mi}\right)$$

RPD is the mean percentage difference between Alg and C_M weighted on C_M values; RPD gives an estimate of the uncertainty as a function of the chlorophyll value and can be thought as a relative BIAS; it was computed as:

$$RPD = \frac{1}{N}\sum_{i=1}^{N}\left(\frac{A\lg_i - C_{Mi}}{C_{Mi}}\right)\times 100$$

APD, as RPD, is the difference between the algorithm estimate and the measurement, weighted on the measured chlorophyll value but, differently, it does not give any information about the direction of discrepancy; that is the difference can be either positive or negative and it represents a sort of relative RMS. APD was computed as:

$$APD = \frac{1}{N}\sum_{i=1}^{N}\left|\frac{A\lg_i - C_{Mi}}{C_{Mi}}\right|\times 100$$

These statistical parameters provide information on the performance and uncertainty about the algorithms.

3 Seasonal to interannual phytoplankton response to physical processes in the Mediterranean Sea from satellite observations

The contents of this chapter are identical to a paper that is currently under review by Journal of Geophysical Research-Oceans: Volpe, G., Buongiorno Nardelli B., Cipollini P., Santoleri R., Robinson I.S. (2009), Seasonal to interannual phytoplankton response to physical processes in the Mediterranean Sea from satellite observations.

This paper is made of the contributions by five authors, with the first two authors particularly contributing to the manuscript drawing up. The first author led the whole work by making the analysis and providing the background and rationale of the work. Other authors stimulated discussions and provided useful comments revising the manuscript.

The content of the chapter can be summarised by the following abstract that accompanies the submitted paper.

The relation between physical and biological processes affecting the Mediterranean Sea surface layer was investigated by means of different Empirical Orthogonal Function (EOF) decompositions of remotely sensed chlorophyll-a (CHL), sea surface temperature (SST) and Mediterranean Absolute Dynamic Topography (MADT) weekly time series (1998-2006). As part of the analysis, the Data INterpolating Empirical Orthogonal Functions (DINEOF) technique was applied to CHL images. Results from the single EOFs, along with a cross-correlation analysis, identified physical-biological interactions at both short (weeks to months) and long (years) temporal scales, and from local to basin spatial scales. Phytoplankton biomass abundance and the sea surface thermal stratification show a strong inverse relationship

at seasonal and sub-basin scales. At regional scale, the spring bloom space-time variability is related to the intensity and spatial extent of the deep water formation process and especially to its pre-conditioning phase. At interannual and sub-basin scales, a gradual decline of the phytoplankton biomass in the whole central Mediterranean occurs with a delay of one year relative to the simultaneous decrease of the cyclonic circulation in the eastern basin, and the northward displacement of the Algerian current. Regionally, the phytoplankton biomass and the surface heat content anomalies associated with extreme atmospheric anomalies (such as the cold 1998-1999 winter and the summer 2003 heat wave) show a significant correlation with a ~5-month time lag.

3.1 Introduction

The ocean, covering more than 70% of the earth surface, can modulate the atmospheric CO_2 concentration by means of the so-called biological pump. This mechanism refers to the sinking of organic matter from the surface productive layers to deep waters in the ocean [*Lalli and Parsons*, 1995]. As the ocean overturning period involves millennial temporal scales [*Rahmstorf,* 2006], the organic matter leaving the productive layers could take centuries to re-enter the food web, therefore enhancing the ocean's capability for further absorbing atmospheric CO_2. Quantifying the carbon flux into the ocean through the marine primary productivity, and understanding the mechanisms that might control it, are of crucial importance for defining the planet's carbon budget. The major player of the oceanic primary production is phytoplankton (i.e., the unicellular microscopic algae living in the upper layer of all water bodies across the world) through photosynthesis. The most widely accepted view, so far, is that phytoplankton distribution in the ocean is driven by the availability of light and nutrients [*Parsons et al.*, 1977]. These growth-limiting factors depend in turn on physical processes at different space and time scales: general ocean circulation, deep water formation, mixed-layer dynamics, upwelling, atmospheric dust deposition, and the solar cycle. The control of the biological activity by these physical processes results in a well-defined zonation of the world oceans: the so-called bio-provinces [*Longhurst*, 1998].

Satellite data provide an opportunity for quantifying oceanic biomass and production at fine space-time resolution. Moreover, remote sensing techniques give a synoptic view of some of the environmental variables capable of influencing

phytoplankton production. Remotely sensed data were recently used to investigate the link between upper ocean stratification and phytoplankton productivity [*Behrenfeld et al.*, 2006]. *Behrenfeld* and colleagues [2006] found a strong correlation among the Multivariate ENSO Index (MEI), a stratification index (computed as the difference between surface and 200 m densities), and the net primary production (NPP) in the permanently stratified ocean. They also showed an inverse relationship between monthly NPP and sea surface temperature (SST) anomalies over about 74% of ocean surfaces, giving a simplified, textbook-like, explanation of the mechanisms linking NPP response to SST variations, in terms of enhanced/reduced nutrient availability as a consequence of decreased/increased stratification [*Doney*, 2006].

Recently, *Wilson and Coles* [2005] analyzed the relationships between SST, sea level and chlorophyll (CHL) monthly climatologies on a global scale, and found a well-defined zonation of the processes concurring to determine the phytoplankton space-time variability; dynamic uplift causing nutrient entrainment into the euphotic layers in the tropics and seasonal control of nutrients and light at mid- and high-latitudes, respectively. Similarly, there has been an attempt to characterize the seasonal trophic regimes from ocean colour satellite data, in the Mediterranean Sea, through cluster analysis [*D'Ortenzio and Ribera d'Alcalà*, 2009]. These works introduced a direct and powerful scheme linking the upper ocean dynamics to the mechanisms driving phytoplankton variability on a seasonal basis. On the other hand, simplified schemes are not directly applicable to all timescales, which possibly involve different physical processes (e.g. mesoscale instabilities, dense water formation, etc.) and in particular they may miss their impact on the long-term variability.

A different method is based on the use of statistical techniques for the identification of principal patterns of variability (Empirical Orthogonal Functions, EOF) in SST, sea level and surface CHL data. EOFs capture variability at all time scales, including the long-term variability. Although the EOFs do not always (and not necessarily) identify physical or biological processes, in some cases their map of variability can be related to distinct physical or biological processes, shedding some light on the link between the biological response and the physical forcing. As a result, EOF decomposition has become a standard technique in bio-geophysical sciences, as shown by the growing body of literature that has utilized this technique to analyse the upper ocean physical and biological coupling using satellite data [i.e. *Wilson and*

Adamec, 2001; *Yoder and Kennelly*, 2003; *Lopez-Calderon et al.*, 2006; *Garcia and Garcia*, 2008; *Iida and Saitoh*, 2007; *Katara et al.*, 2008].

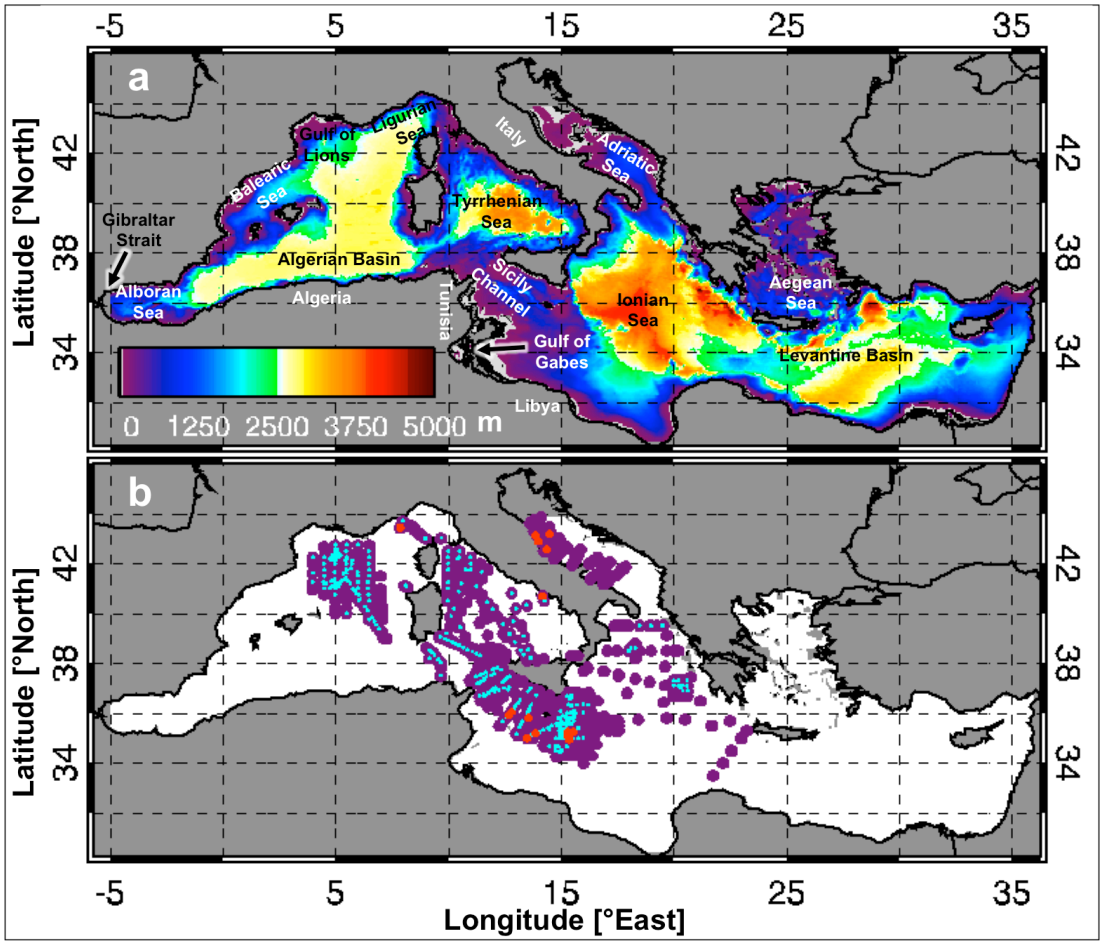

Figure 3.1: a) Mediterranean Sea bathymetry with main sub-basin names are also superimposed; b) Location of the satellite-in situ data matchups when using weekly averages (purple), daily (light blue) and interpolated fields (light blue + purple).

In the present work, the analysis of the co-variability of SST, sea level and CHL is carried out by estimating EOFs for each variable separately. This approach should, in theory, enable the isolation of different physical and biological processes. Similarly, a spatial and temporal correlation analysis can be used in the aim of defining the timing of covariability between physical and biological processes. The temporal extent of the physical-biological coupling may span from the rapid phytoplankton response to nutrient vertical redistribution (through vertical mixing for example), to the delayed response associated with nutrient enhancement (possibly driven by mixing below the nutricline) in association with other environmental factors such as light availability or re-stratification, or to long term modification of water column stratification/heat content, and so on. Here, it is important to notice the distinction between the temporal scales proper of each process, which might be, for example, seasonal or multi-yearly,

and the time lag between two difference processes, which in some cases can be as short as a few days. For instance, two processes with similar annual time scales might be out-of-phase by a month.

We applied the analysis to the Mediterranean Sea (MED), which, for a number of reasons, appears suited for this investigation. First, in spite of its limited size (~0.6% of the global ocean surface, ~0.3% of the volume), the Mediterranean Sea is considered one of the most complex marine environments on Earth, because of the variety of physical processes that occur there [*Williams*, 1998]. These processes span from the mesoscale to the basin-scale, and include also deepwater formation. The Mediterranean Sea is an almost completely closed basin, being connected to the Atlantic Ocean through the narrow Gibraltar strait (14.5 km wide, less than 300 m deep at the sill, Figure 3.1a). The shallow (500 m depth) Sicily Channel divides it into two main sub-basins: the eastern (EMED) and the western basins (WMED). The average depth is 1500 m with a maximum depth of 5150 m in the Ionian Sea.

Consequently, the basin has often been considered a "miniature ocean" or a "laboratory basin" [*Lacombe et al.*, 1981; *Robinson and Golnaraghi*, 1995] because most of the processes controlling the global ocean general circulation are present there, though at reduced temporal and spatial scales. The MED is thus expected to respond more quickly than the global ocean to climatic changes. In that respect, it represents an excellent site to investigate the coupling between physical and biological processes, and to examine, for example, whether global warming reduces phytoplankton growth by enhancing the upper ocean stratification thus limiting the nutrients entrainment to the euphotic layer, as hypothesised by *Behrenfeld et al.* [2006].

The MED oceanic circulation is defined by the complex topography of the basin and can be schematically pictured as a three-layer system: surface, intermediate and deep circulation. An overall cyclonic circulation characterizes the basin scale surface dynamics. The surface Atlantic water (AW) enters at the Gibraltar Strait occupying the top 200 m, approximately. During its eastward flow, the AW progressively mixes with the saltier MED waters. The AW flow is characterized by intense mesoscale activity and creates a series of meanders and gyres such as those associated with the Algerian Current, in the WMED, or with the so-called Atlantic-Ionian Stream or Mid-Mediterranean Jet in the Ionian and Levantine basins, respectively [*Malanotte Rizzoli et al.*, 1997]. Dense water formation processes (DWF) take place in both the eastern and western MED. These phenomena result from the combination of the preconditioning in

the stratification, related to the presence of intense cyclonic gyres, and the severe buoyancy loss due to strong air-sea interaction in specific areas. These areas are the Gulf of Lion – Ligurian Sea, in the WMED, and, in the EMED, the south Adriatic for deep mixing processes and the Rhodes Gyre for formation of Levantine Intermediate Water (LIW). During the 90's, the so-called Eastern Mediterranean Transient moved the DWF location from the EMED to the Aegean Sea, with important consequences for the whole MED circulation. The saltier and warmer deep waters replaced almost 20% of the older deep waters of the basin, and uplifted the deep isopycnals by about 500 m [*Lascaratos et al.*, 1999].

From the biogeochemical point of view, the MED is considered one of the most oligotrophic seas on Earth [*Crise et al.*, 1999], with an average yearly phytoplankton biomass load of 0.19 mg m^{-3} (0.05 and 0.3 mg m^{-3} in the eastern and western basins, respectively) [*Santoleri et al.*, 2008]. The oligotrophic character of the basin can be mainly explained in terms of the water mass exchange at the Gibraltar Strait; the MED exports nutrient rich intermediate waters and imports surface water from the Atlantic Ocean, relatively nutrient-depleted. The order of magnitude difference between the two sub-basins (0.05 versus 0.3 mg m^{-3}) can be attributed to their different trophic regimes, as suggested by *D'Ortenzio and Ribera d'Alcalà* [2009]. They divided the MED into three main regions-of-similarity, or clusters, on the basis of the normalized pixel-by-pixel seasonal cycle, and found a good correspondence with the 10-year average climatology map. This correspondence gives a clear picture of the phytoplankton seasonal variability. In the MED, phytoplankton exhibits both a subtropical-like seasonal cycle, in those areas identified as non-blooming (e.g., the whole EMED and part of the WMED) and a North-Atlantic-like dynamics, though with reduced latitudinal (or temporal, depending on the perspective) range of variability.

In the next section a description of data used and methodologies adopted for the analysis is presented. Section 3.3 deals with the description of the main results achieved along with their interpretation and discussion. Conclusions are drawn in section 3.4.

3.2 Data & Methods

3.2.1 MADT Dataset

The 1998-2006 time series of altimeter data used here is part of the Ssalto/DUACS products, distributed by AVISO (Archiving Validation and

Interpretation of Satellite Oceanographic Data). In order to avoid spurious signals related to uneven data coverage, the Mediterranean Absolute Dynamic Topography (MADT) 'reference' maps were chosen. These are built from only two altimeters at any given time (one occupying a 10-day repeat orbit, TOPEX-POSEIDON or Jason 1, and one in a 35-day repeat, ERS1-2 or ENVISAT), even for periods when a higher number of satellite sensors was available. The spatial resolution of this dataset is thus homogeneous in time, and data are inter-calibrated by referencing all other altimeters (ERS1-2 and ENVISAT) to the TOPEX-POSEIDON or Jason 1 missions, through a global crossover adjustment. Standard corrections have been applied by Ssalto/DUACS [*Le Traon and Ogor*, 1998] to the altimeter data, that were successively merged and interpolated on a weekly basis over a regular 1/8° grid, using an optimal interpolation method that directly corrects residual long wavelength errors [*Ducet et al.*, 2000]. The last step in Ssalto/DUACS Mediterranean product computation is the addition of a mean dynamic topography (MDT) to the sea level anomalies (SLA), as detailed in *Rio et al.* [2007]. *Rio et al.* [2007] estimated the accuracy (RMS error) of the order of 3 cm for the MADT in the Gulf of Lion (roughly 40% of total variance in the area). MADT data were re-sampled on 8-day "week" intervals of which there are 45 in a year of 360 days (the last five days of every year are discarded).

3.2.2 The SST Dataset

The SST dataset used in this work is the optimally interpolated (OISST) re-analysis product described in *Marullo et al.* [2007], extended to include the 2006 measurements. Data cover the Mediterranean area at 1/16° resolution from January 1998 to December 2006. The SST spatial domain was adapted to the MADT dataset where the northern Adriatic Sea is masked out because of its shallowness. The re-analysis is based on Pathfinder SST time series. Comparing OISST data with simultaneous MEDAR/MEDATLAS, MFS-VOS and MEDARGO measurements, *Marullo et al.* [2007] estimated its accuracy in terms of mean bias error (0.04°C) and standard deviation (0.66°C). Their results also indicated that the sensitivity of OISST accuracy to seasonal factors is lower than 0.3°C and, even more importantly, no significant sensor drifts, shifts or responses to anomalous atmospheric events were evidenced. The daily SST time series was averaged into the same 8-day intervals as the MADT time series.

3.2.3 The Chlorophyll Dataset

High-Resolution Picture Transmission (HRPT) SeaWiFS Level-1A data, acquired by the receiving station HROM at Istituto di Scienze dell'Atmosfera e del Clima (Rome, Italy) from January 1998 to December 2006 were processed up to Level-3 with the SeaWiFS Data Analysis System (SeaDAS) software package version 4.8 available from NASA website (seadas.gsfc.nasa.gov). Standard flags and Siegel's atmospheric correction algorithm were applied to Level-1A raw data [*Siegel et al.*, 2000]. The MedOC4 [*Volpe et al.*, 2007] ocean colour algorithm for chlorophyll retrieval in case-1 waters was then applied to the resulting remote sensing reflectances. *Volpe et al.* [2007] have shown that MedOC4 produces more realistic values in the Mediterranean, differing from *in situ* measurements by about 35% (and therefore within the 35% SeaWiFS mission uncertainty target); conversely when OC4v4 is used the uncertainty exceeds 100%.

CHL maps were first remapped at their nominal spatial resolution of 1.1x1.1 km equirectangular grid covering the entire Mediterranean Basin. A spatial scaling to a 1/16° grid map, matching the spatial resolution of the SST OI maps developed in the context of the Mediterranean Forecasting System Towards Environmental Prediction (MFSTEP) project, was performed by averaging the base-10 log-transformed chlorophyll values (LCHL, to differentiate from non-transformed values), to account for chlorophyll lognormal distribution [*Campbell*, 1995]. For consistency among datasets, the spatial domain was then adapted to the MADT dataset, by masking out the North Adriatic Sea. 8-day averages were then computed and used as input to DINEOF analyses for data interpolation (Section 3.2.3.1) and hence to EOF analysis (Section 3.3) for studying the field space-time variability.

3.2.3.1 DINEOF interpolation

The EOF analysis generally requires complete time series of input maps, with no data voids. While respective data providers interpolated SST and MADT time series, LCHL maps have significant data voids due to the presence of persistent cloud cover. Consequently, as a first step before any further analysis, it was necessary to apply an interpolation algorithm to the LCHL time series.

Here, missing data reconstruction was performed iteratively following the Data INterpolating Empirical Orthogonal Functions (DINEOF) method developed by

Beckers and Rixen [2003] and used by *Beckers et al.* [2006]. This technique presents some advantages with respect to more classical approaches (such as optimal interpolation), especially when working on ocean colour data. For example, chlorophyll is characterized by different scales of variability and different background concentrations in the coastal or in the open ocean. However, standard statistical interpolation algorithms are based on the hypothesis of isotropy for the covariance estimation, whose computation would otherwise be quite complicated. This hypothesis of isotropy makes these standard algorithms susceptible to artefact caused by the propagation of coastal signals offshore, especially in the presence of extended cloud cover. The assumption of isotropy is automatically removed when using DINEOF, as this technique explicitly identifies areas that have different sources of space-time variability, through iterative EOF estimation.

In practice, the method works as follows: the time average is removed from valid observations and anomaly data are stored in a matrix **X**. Missing data are then set to zero, which is the equivalent of using, as first guess, the temporal average of each marine pixel (i.e., the climatologic field, Figure 3.2a, was removed from the time series). At the same time, a set of good pixels (usually 1% of the dataset) is set aside to serve as a reference and is replaced by zero within **X**. EOFs are then estimated and the data initially missing are replaced by the reconstructed time series truncated at the first mode. This procedure is repeated iteratively, truncating the time series reconstruction at the i^{th} mode, until convergence is reached. Convergence is specified in terms of the error evaluated in the reconstructed time series with respect to the reference pixels.

In the present work, the same steps as in *Beckers and Rixen* [2003] were followed and it was found that the error continued to decrease up to the 31st iteration. However, the variance explained by the 31^{st} mode was well below the variance explained by noise. In fact, the first mode associated with a random-filled matrix of the same dimensions as **X** explains the same variance as the 20th EOF mode from LCHL. Therefore, this variance level was adopted as the limit to stop the iterations and thus define the number of useful modes. The interpolated dataset and associated EOFs were obtained by reconstructing the time series using this truncated set of modes.

When comparing the spatial patterns obtained from EOF analysis computed over different variables, it is useful to have a measure of their similarity, i.e., to correlate different spatial patterns. In a similar way, the temporal lagged correlation coefficient measures the correlation between amplitudes of different modes of different variables.

This latter parameter may be useful in identifying the time response of one variable to the forcing of the others. All correlation values were tested for significance (99.9% level) through the Student's *t*-test.

3.2.3.2 DINEOF validation

In order to validate the data interpolated with DINEOF, this section presents the results of a matchup exercise between 1304 *in situ* measurements of LCHL (whose location is shown in Figure 3.1b) and both input and output of the DINEOF procedure: 1/16° SeaWiFS weekly averages and resultant interpolated fields. Correlation coefficients, RMS, bias, Relative and Absolute Percentage Differences (RPD and APD, respectively) are discussed (Table 3.1).

Table 3.1: matchup results

Datasets resolution								
Space	Time	r^2	RMS	BIAS	RPD [%]	APD [%]	N	Average # of missing pixels per image
1 km	Daily	0.88	0.22	-0.04	10.61	-12.81	440	40 – 85 %
1/16 °	Weekly	0.82	0.23	-0.04	22.34	-12.96	1287	< 4 %
1/16 °	Weekly (DINEOF)	0.83	0.23	-0.05	8.24	-12.02	1304	0

Statistics of the matchup exercise between 1304 *in situ* measurements of LCHL and the SeaWiFS spatio-temporal averages (second row) and the DINEOF-interpolated field used in the following of this study to address LCHL space-time variability. As means of comparison, SeaWiFS daily 1.1 km fields' performance are shown in the first row, with an average number of missing points strongly varying with the season: large and more frequent gaps occur in winter due to clouds.

As means of comparison, the same statistics have been computed using daily SeaWiFS imagery at their full spatial resolution of 1.1 km. Note that the values in Table 3.1 differ from the one reported in *Volpe et al.* [2007] because here all calculations have been performed on the CHL logarithm, i.e. on LCHL. The DINEOF procedure, as implemented within this study, substitutes the whole field with the newly evaluated LCHL values, thus throwing away the original observations.

Table 3.1 shows that the overall statistics is independent of the spatio-temporal averaging (and hence of the number of the matchup points) and that the DINEOF does not introduce any significant error. It is not surprising then that the APD improves using DINEOF output, even if only slightly. This improvement is due to the DINEOF procedure filtering the noise out. The number of missing data within daily images (and to a lesser extent within weekly fields) varies with the season, with autumn-winter period being the most affected by clouds. As a result the average number of good pixels can vary by a factor of two throughout the year (Table 3.1).

3.2.4Data filtering

The results of the LCHL variability through the EOF analysis applied to weekly time series are described in Section 3.3.2. Some further data filtering was then applied with the purpose of identifying the presence of long-term time scale signals and to investigate the covariance between the phytoplankton biomass and surface conditions at interannual timescales. This data manipulation consisted in the removal of the annual cycle and of the higher frequency signals. The former was achieved by computing the three dataset anomalies with respect to their weekly climatologies. The weekly climatologies were obtained by averaging all the first weeks, all the second weeks, and so on, of the entire time series (1998-2006). However, the EOF results of the anomaly fields (not shown) are strongly dominated by high frequency signals of difficult interpretation. To remove these high frequency signals, we applied a low-pass filter (one year moving average) to the anomalies. The filtering procedure had also the effect of shortening the data time series by one year cutting out the first and the last six months. The filtered anomalies are referred to as F-LCHL, F-SST and F-MADT (where F stands for filtered), and relevant results are described and discussed in Section 3.3.3.

3.3 Results and discussion

The first EOF analysis has been performed over LCHL, SST and MADT anomalies, i.e. after removing their respective climatological averages (1998-2006). Before proceeding to the analysis of the variability (section 3.3.2), it is worthwhile first to describe the averages, and to identify apparent similarities between the different patterns (section 3.3.1).

3.3.1LCHL, SST and MADT average fields

The chlorophyll map exhibits a zonal gradient with the western basin being generally more productive than the eastern one (Figure 3.2a). The exceptionally oligotrophic character of the EMED has been long known [see among others *Antoine et al.*, 1995, *Bosc et al.*, 2004], and might be explained in terms of mixed layer depth (MLD) dynamics. *D'Ortenzio et al.* [2005] show that the MLD is generally deeper in the EMED than in the WMED. The shallower depth of the surface ML makes the WMED water column being more susceptible to the meteorological forcing, so that generally less energy is needed to break the stratification and to bring nutrients up into

the euphotic layer. It is important to remind that this result is based on ocean colour data, which, referring to the first optical depth (on average 15-35 m in the MED open waters) may miss some important features such as the deep chlorophyll maximum (DCM), commonly observed during the stratified period and in most of the EMED.

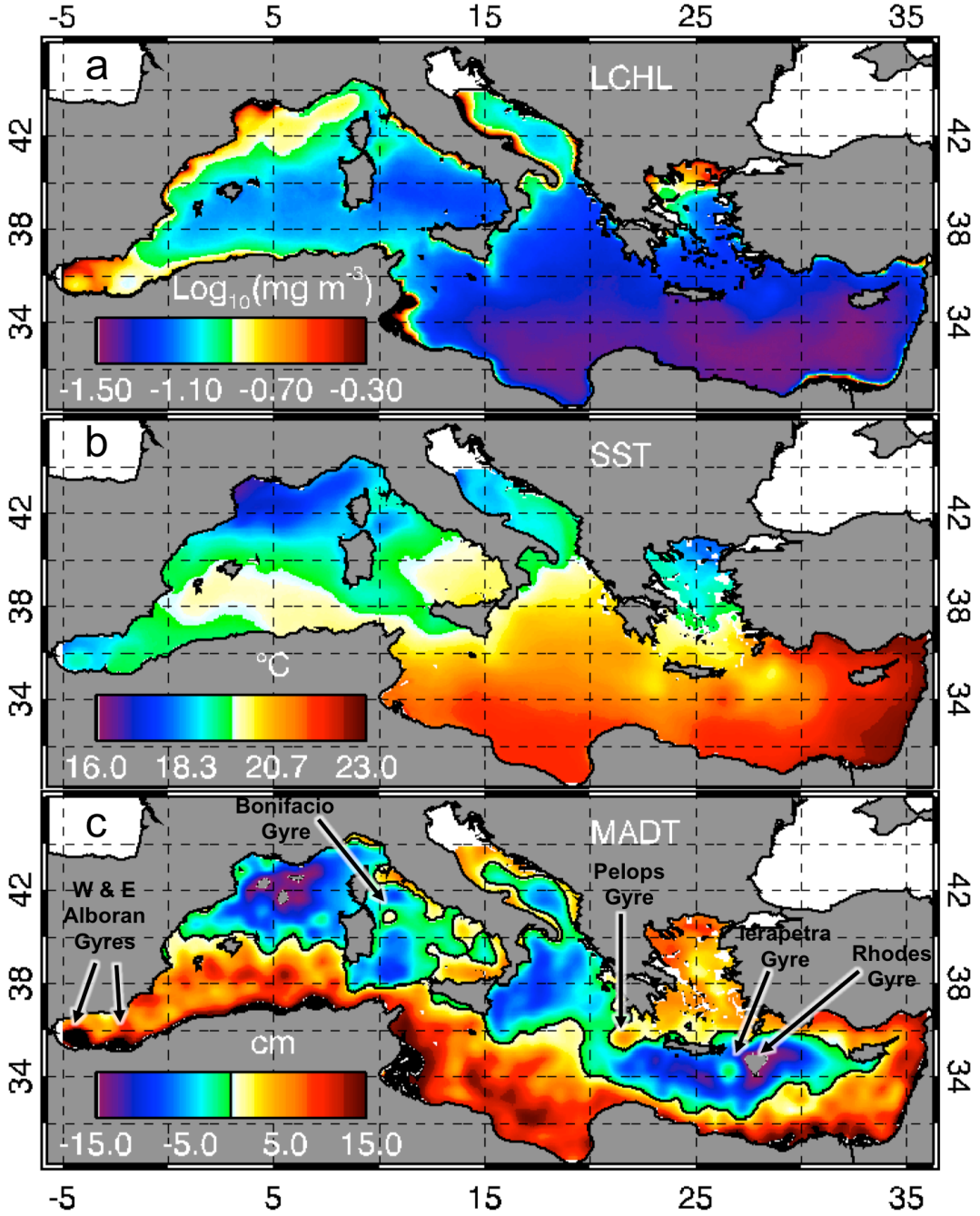

Figure 3.2: field climatologies (1998-2006) for LCHL (a), SST (b) and MADT (c). Zero level contour line is superimposed onto the MADT map. Superimposed on the MADT map is the name of well-known dynamical structures: Bonifacio Gyre, Pelops Gyre, Rhodes and Ierapetra Gyres.

The question remains on whether the difference between the two sub-basins is due to the MLD dynamics or to the intrinsic limits of the satellite observations.

Unfortunately, the *in situ* dataset in our hands is not sufficiently distributed in both space and time to completely address this issue. On the other hand, the SST average map (Figure 3.2b) can suggest a possible first order explanation. There is a strong similarity between the LCHL and SST average patterns at both basin and sub-basin scales (r=-0.64, Figure 3.2a-b), which is consistent with the E-W gradient in MLD. This coupling can be explained in terms of Behrenfeld's hypothesis [*Behrenfeld et al.*, 2006]: lower primary production levels correspond to stronger water column stratification and warmer surface waters, and vice versa.

At sub-basin scale, this inverse correlation is evident in the Alboran Sea, in the Gulf of Lion, along the Italian coasts of the Adriatic Sea, and through the meridional gradient in the whole Levantine Basin, where colder waters correspond to higher biomass concentrations.

Moreover, highly productive areas are found to correspond with well-known and defined dynamical structures (Figure 3.2c): in the WMED, these areas are represented by the cyclonic gyre in the Gulf of Lion (where deep water formation seasonally occurs), all along the Algerian Current from the western Alboran Gyre down to the border between Libya and Tunisia across the southern sector of the Sicily Channel. In the EMED, this coupling appears in relation to the Ierapetra Gyre, though less clearly. There is, however, a poor correlation (r=0.06) between LCHL and MADT average maps. This is because their similarities are associated with phenomena localized in both space and time, whereas the MADT map depicts a general circulation pattern at basin scale.

High values are observed at coastal sites such as the shallow Gulf of Gabes, or corresponding to major outflow areas like the Rhône River in the Gulf of Lion, the Dardanelle Strait in the north Aegean Sea and the Nile River delta. However, these areas can reasonably be classified as Case 2 waters [for a description of water types on the bio-optical perspective, see *Morel and Prier*, 1977], so that particular criticism should be used when interpreting such signals, especially because the implemented algorithm was built and meant for use in Case 1 waters only. The different bio-optical regime (Case 2 waters) relative to the one for which the algorithm is meant for use (Case 1 waters) might result in an overestimation of the actual field.

3.3.2Physical-biological coupling at seasonal time scales

3.3.2.1 The basin scale variability

The first LCHL mode (74% of total variance) represents a large-scale signal with the spatial pattern positive almost everywhere (Figure 3.3a). The main feature in the LCHL pattern is given by an E-W gradient, with most of the variability located in the WMED basin. Thus, the WMED is characterized both by high background productivity (Figure 3.2a) and by higher variability (Figure 3.3a), with respect to the EMED. LCHL EOF temporal amplitude shows maxima generally recurring from mid-January to April and minima from July to September, though in some years (i.e., 1999 and 2004) maxima do start earlier, in December of the previous year (Figure 3.3b). Maxima decrease from winter 1998 to winter 2002/2003, then become stronger in winter 2003/2004 and following years. This annual cycle might reasonably be explained in terms of water stratification. In fact, the amplitude of this mode (Figure 3.3b) turns out (see Table 3.2) to be highly anti-correlated (r=-0.92) to the amplitude of the first mode of SST (Figure 3.3d) at zero time lag: that is, high biomass levels occur during winter when stronger heat loss from the ocean surface is observed (as described by the first SST mode, Figure 3.3c-d). The loss of heat from the surface layer deepens the upper mixed layer, resulting in a stronger nutrient entrainment into the upper mixed layer.

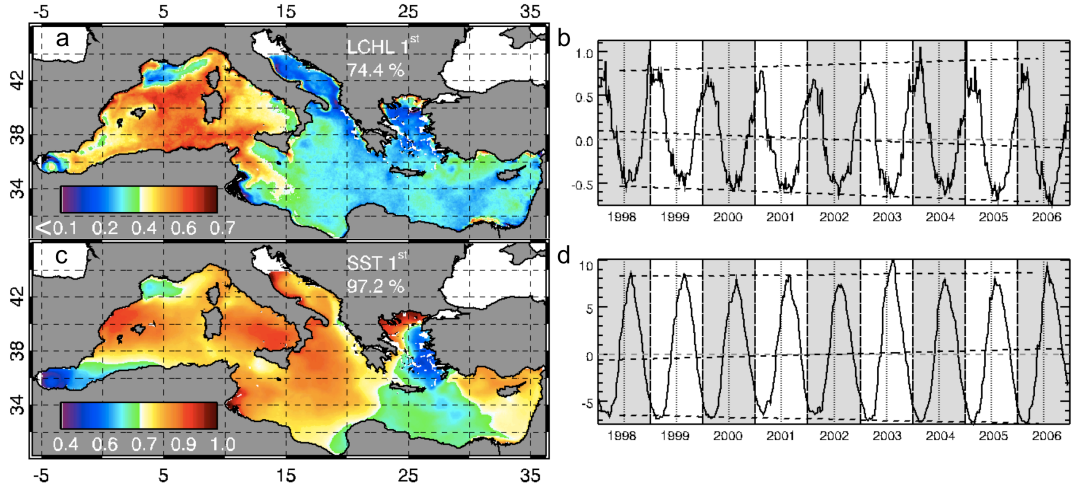

Figure 3.3: first EOF mode computed over LCHL (a-b) and SST (c-d) data time series. Black colour in Figure 3.3a indicates negative values (Gulf of Gabes (Tunisia), and of the Gibraltar inflow to the Alboran Sea). Temporal amplitudes and spatial patterns are normalized on the spatial pattern maximum value for each mode. Units are in Log_{10}(mg m^{-3}) for LCHL and °C for SST. Black and grey dashed lines over temporal amplitude represent trend line (among the maxima, minima and for the whole time series) and zero value, respectively.

However, the SST response to seasonal heating is almost spatially uniform, with a different response only in those areas where recurrent wind regimes play a major role in regulating the seasonal air-sea heat flux (Figure 3.3c): Mistral in the NW MED, and the Etesian in the Aegean Sea and south of Crete [*Zecchetto and De Biaso*, 2008; *Burlando*, 2009]. Another zone where the variability of the seasonal air-sea flux is reduced is the Alboran Sea, which is subject to the inflowing Atlantic waters and to strong and permanent mesoscale dynamics [*Pujol and Larnicol*, 2005]. It is not surprising then to find a poor correlation between LCHL and SST spatial patterns (r=0.24, Table 3.2).

Table 3.2: space-time correlation between different EOF modes of two variables.

Variable 1 (mode #)	Variable 2 (mode #)	Time r	Time lag	Space r
LCHL (1)	SST (1)	-0.92	0	0.24
LCHL (2)	SST (2)	-0.66	5.5 months	0.59
F-LCHL (1)	F-MADT (2)	-0.87	1 year	0.16
F-LCHL (2)	F-SST (1)	0.52	5 months	-0.51

Variable 1 follows variable 2 in the temporal correlation analysis with a time lag as defined in the relevant column. The mode to which the correlation refers is indicated in brackets next to the variable name.

The patch of high LCHL variability extends eastward into the Sicily channel (Figure 3.3a). In this region, the eastward transport of surface Modified Atlantic Waters [MAW, see among others *Manzella et al.*, 1990; *Robinson et al.*, 1999] has already been shown to exhibit a clear annual cycle with maxima in April [*Béranger et al.*, 2005]. We observe from Figure 3.2a-b that the phytoplankton meridional distribution in the Sicily Channel exhibits a similar seasonal variability than the MAW transport across the region [*Béranger et al.*, 2005]. Both variables show a larger seasonal cycle in the southern part of the Channel. One possible interpretation, which needs to be further investigated, is that the space-time variability of the MAW transport, mostly located in the southern part of the Channel for potential vorticity reasons, might be responsible of the larger phytoplankton biomass variability in the southern than in the northern sector of the Channel. The Ligurian Sea – Gulf of Lion area, where a large patch of high average biomass concentration is observed (Figure 3.2a), shows little variations in this mode as compared to the rest of the WMED. Similarly, the dynamics of the western Alboran Gyre, of the Adriatic coastal current and of the shallow Gulf of Gabes is not well represented within this first mode. The space-time variability of these areas is clearly described by the second mode (see next section).

3.3.2.2 The regional scale variability

The second LCHL EOF mode (8% of total variance) identifies some peculiar areas inside the Mediterranean Sea, related to the main open ocean spring blooms (Figure 3.4a). The spatial pattern displays strong maxima in the north western MED, and to a lesser extent in the Bonifacio Gyre (see location in Figure 3.2c), along the eastern coast of Calabrian peninsula (southern Italy), and in the southern Adriatic and Rhodes Gyres (see location in Figure 3.2c). We believe that the similarities between this LCHL mode and the second SST mode (Figure 3.4c-d) are an indicator of the link between the phytoplankton dynamics and mixing/re-stratification seasonal cycle of the water column. This succession is visible from the temporal amplitudes of both SST and LCHL second modes (Figure 3.4b and Figure 3.4d, respectively), and from respective spatial patterns (Figure 3.4a and Figure 3.4c). In fact, the LCHL amplitude exhibits a recurrent feature with a strong negative signal during winter always followed by a marked positive bloom-like pulse during spring. Minima in the LCHL amplitude are an indication of the deep mixing associated with open ocean deep-water formation (DWF). It has already been shown that DWF can be seen in CHL images as an intense minimum at its onset [*Santoleri et al.*, 2003], but this mechanism is also recognized as fundamental for nutrient replenishment in the open ocean surface layers [*Levy et al.*, 1998; 1999]. The space-time variability captured by the SST second mode is clearly related to this phenomenon as shown in Figure 3.4c, where highs in the WMED (i.e. the Ligurian Sea, the Bonifacio Gyre and part of the Gulf of Lion) coincide with the areas where preconditioning to DWF is active in late autumn-beginning of winter [*Stommel*, 1972], and also highlighted by the minima in the corresponding amplitude (Figure 3.4d). In other words, there is a sequence from the phytoplankton biomass dilution coinciding with DWF events to the spring bloom that coincides with the gradual re-stratification of the water column. This is also supported by the significant correlation found between these two modes, both spatially (r=0.59) and temporally (r=-0.66, with 5.5 months lag; Table 3.2). Five and a half months is the time lag between the preconditioning phase of the DWF phenomenon and the re-stratification of the water column following the deep mixing (which coincides with the spring bloom), when phytoplankton can efficiently exploit the nutrients made available into the surface layer [*Levy et al*., 1998; 1999; *Barale et al*., 2008].

This phenomenon exhibits a marked interannual variability, with a minimum in the LCHL amplitude during 1998, spring bloom values (maxima) decreasing from 1999 to 2004 (Figure 3.4b), and exceptional high values during 2005 and 2006. The latter are linked to the unusually intense winter convection during this period both in magnitude [*Font et al.*, 2007] and spatial extent [*Smith et al.*, 2008]. Indeed, in addition to the already well-documented area involved by deep mixing [namely the MEDOC area; *Medoc group*, 1970], Argo floats measurements, collected during 2004-2006, revealed an unusual location for the newly formed deep water, in the Ligurian basin [*Smith et al.*, 2008]. Since the DWF has the effect of enhancing the nutrient content of the upper oceanic layer [*Levy et al.*, 1998; 1999], here we hypothesize this "new" location to act as an additional source of nutrient, thus explaining the exceptional high values in the LCHL amplitude during this "anomalous" period (Figure 3.4b). Similarly, *Font et al.* [2007] found that the 2005 winter convection in the NW Mediterranean was more intense than average [*López-Jurado et al.*, 2005] and extended over an unusually large area [*Salat et al.*, 2006], further supporting the correspondence between the exceptionally high LCHL values and the DWF phenomenon.

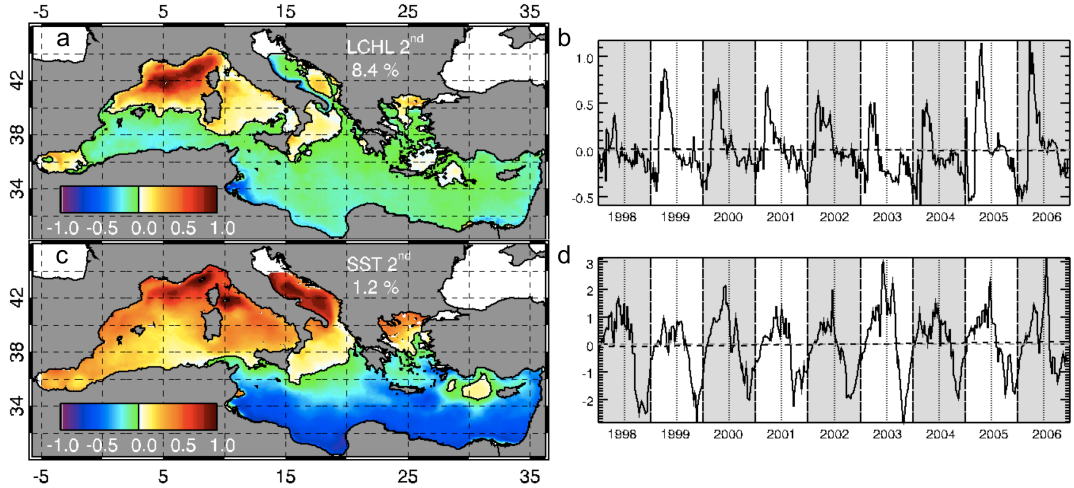

Figure 3.4: second EOF mode computed over LCHL (a-b) and SST (c-d) data. See Figure 3.3 for details.

Figure 3.4a shows that, in the Adriatic Sea, positive LCHL values are associated to the southern Adriatic Gyre where deep mixing generally occurs [*Civitarese and Gacic*, 2001; *Santoleri et al.*, 2008]. Similarly, a positive patch can be seen to correspond to the Rhodes Gyre. An opposition of phase between the Calabrian coast and the rest of the Ionian Sea is visible, and related to the seasonal upwelling of the area [*D'Ortenzio et al.*, 2003].

Another less intense peak is visible, within the LCHL amplitude (Figure 3.4b), during autumn, and is associated to the first response of phytoplankton to seasonal nutrient entrainment in the upper layer after summer stratification. It is common for a temperate system such as the Mediterranean Sea to experience good weather conditions characterized by summer-like atmospheric temperatures soon after the autumn stratification breaking. This results in a weak re-stratification, which enables phytoplankton to exploit the nutrients made available by the autumn stratification breaking. This phenomenon is also known as the St Martin Summer bloom [*Zingone et al.*, 1995].

3.3.3 Physical-biological coupling at interannual time scales

The main result of the EOF analysis described in Section 3.3.2 is the identification of the processes dominating the total LCHL variance along with plausible explanations about the observed variability. There was evidence of a significant interannual variability. Nonetheless, the identification of co-variability between phytoplankton biomass dynamics and the temperature field at interannual timescale has not been possible, so far, despite the good correlation between these two variables at seasonal time scale. We interpret this as due to the strong annual component (i.e., the solar cycle), which definitely dominates the overall signal within both the first two EOF modes. In order to highlight then the presence of longer time scale signals and to investigate the covariance between the phytoplankton biomass and surface conditions at interannual timescales, the annual cycle and higher frequency signals have been filtered out from EOF data input (see Section 3.2.4) to obtain the F-fields. Next sections deal with the description of the phytoplankton biomass (F-LCHL) variability and its relationship with F-SST and F-MADT fields at time scales other than seasonal.

3.3.3.1 The circulation impact

The first EOF mode of F-LCHL (explaining ~37% of total variance) identifies a wide region in the central part of the basin where the strongest signal is observed (Figure 3.5a). This area mainly covers the Ionian and Tyrrhenian Seas, as recognized by the largest absolute values in Figure 3.5a. A patch of opposite sign as compared to the one just mentioned in the central basin is visible in the WMED and in particular in the Balearic Sea; these two regions are in opposition of phase. More in details, the F-LCHL temporal amplitude exhibits interannual variations, with strong relative minima

during winter 1998-1999 and 2003-2004, and intense maxima in late-spring 2001 (Figure 3.5b). When the temporal amplitude shows negative (positive) values the central basin displays a biomass increase (decrease), and the Balearic Sea exhibits a biomass decrease (increase), although the signal is smaller in the latter area (average value no larger than 0.3 with respect to -0.6/-0.7 in the central MED).

The F-LCHL temporal evolution (Figure 3.5b) is highly anti-correlated with the second F-MADT mode (explaining 21% of total variance, Figure 3.5d) with a time lag of roughly one year (r=-0.87, Table 3.2). To better describe the process associated with this F-MADT mode and hence to illustrate the relationship between the two F-modes, the surface topography patterns are introduced (Figure 3.5e and Figure 3.5f).

Let us hypothesize first that the whole F-MADT variability can be explained by this mode only, so that the whole time series can be reconstructed from this pattern of variability, i.e., by multiplying the spatial pattern (Figure 3.5c) by each value of the temporal amplitude (Figure 3.5d). Since the EOF was performed from anomaly fields (Section 3.2.4), the temporal average (Figure 3.2c) is added to each weekly bin of the reconstructed time series. Figure 3.5e and 5.5f show the result concerning two extreme cases: spring 2003 and spring 2006 (see Figure 3.5d). The comparison of these two anomaly maps (Figure 3.5e-f) shows that this mode involves a significant change in the surface circulation as seen by the modification of the surface gradients (i.e., which give an indication of the surface geostrophic velocities) both in the WMED and in the EMED (Figure 3.5e-f). This change describes a northward displacement of the Algerian current up to the Balearic Sea [as already reported through occasional *in situ* observations, e.g. *Pinot et al.*, 2002] and a simultaneous decrease of the surface Atlantic water transport along the northern Tunisian coasts already before entering the Sicily Channel. Considering that the spatial gradient of MADT is proportional to the geostrophic surface velocities, it can be observed that this modified surface transport pattern corresponds to a general reduction of the cyclonic circulation both in the Ionian Sea and in the Levantine basin, since 2003. As a matter of fact, the surface topography maps show a decreased gradient between the Nile River delta and the centre of the Rhodes Gyre (the level difference of 36.65 cm in 2003 (Figure 3.5e) reduces by roughly 20% to 29.04 cm in 2006 (Figure 3.5f)). Similarly, in the Ionian Sea (between 33° N and 37° N along 17.5° E), the 2006 versus the 2003 maps show a 40% decrease (11.84 cm in 2003 (Figure 3.5e) against 6.88 cm in 2006 (Figure 3.5f)).

Even though the temporal correlation between these two modes is extremely high (Table 3.2), we can only propose hypotheses about the process linking the phytoplankton dynamics to the observed dynamical signal. One possible explanation is that the reduced advection of the relatively richer waters of Atlantic origin (in terms of nutrients and biomass) in the Tyrrhenian and Ionian Seas and its increased dispersal into the Balearic Sea results in a progressive decrease of F-LCHL concentration in the central MED, creating the positive patch in the western WMED (Figure 3.5a).

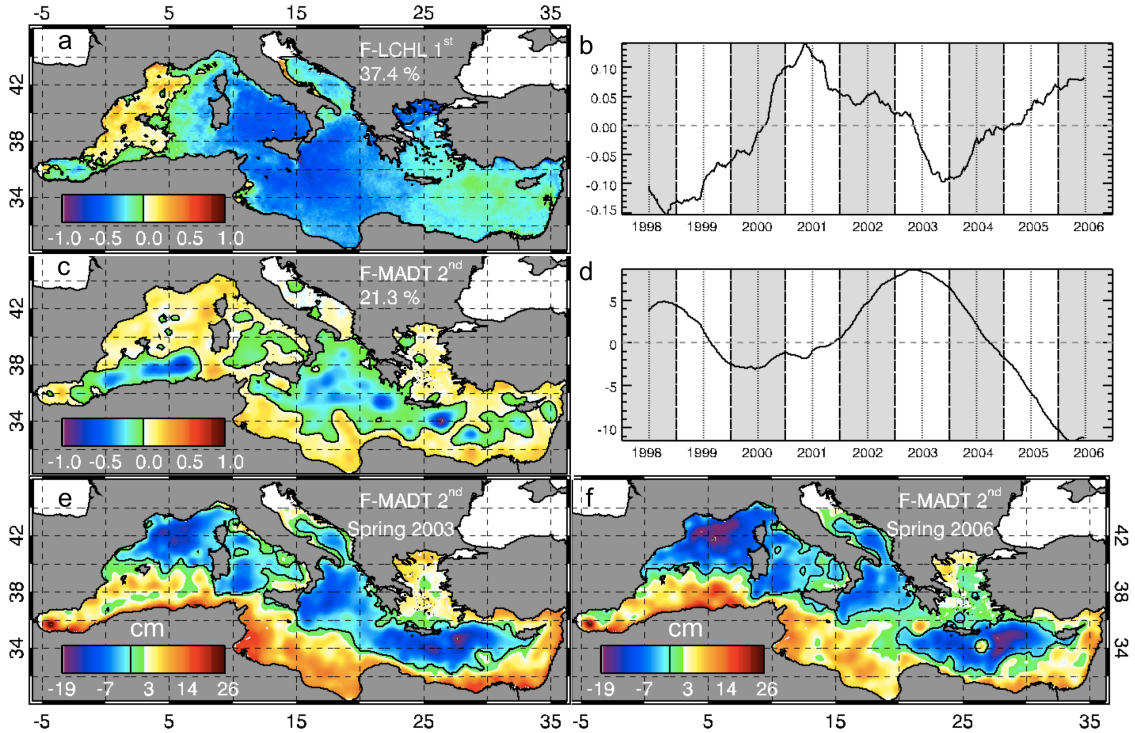

Figure 3.5: first EOF mode computed over F-LCHL (a-b) and second EOF mode computed over MADT (c-d). See Figure 3.3 for details. Anomaly maps are computed as the sum of the field climatology (Figure 3.2c) and the product of the spatial pattern by the relevant amplitude value: spring 2003 (e) and spring 2006 (f).

The timing of the chlorophyll concentration response (1 year) could, in fact, be related to the nutrient consumption within the central basin "resident" surface waters and to the surface waters replenishment time associated with this modified circulation pattern. However, a specific study on the interaction between surface waters renewal times and the phytoplankton dynamics is needed to unequivocally address this issue.

3.3.3.2 The thermal stratification impact

The second F-LCHL mode (22% of total variance) is characterized by large-scale spatial and temporal patterns (Figure 3.6a-b). The region of strongest variability is located west of Corsica and Sardinia islands, extending to most of the central WMED and particularly to the Tyrrhenian Sea (Figure 3.6a). In opposition of phase, there are

the Algerian and Northern currents, and the whole Levantine Basin, though with a less pronounced variability. The temporal component of this mode (Figure 3.6b) is significantly correlated (r=0.52) with the one of the F-SST first mode (which explains 49% of the total variance, Figure 3.6d), with ~5 months lag. Panels in Figure 3.6 suggest that the phytoplankton biomass dynamics, in the region of higher variability, is strongly controlled by the surface layer thermal stratification with a delay of a roughly five months.

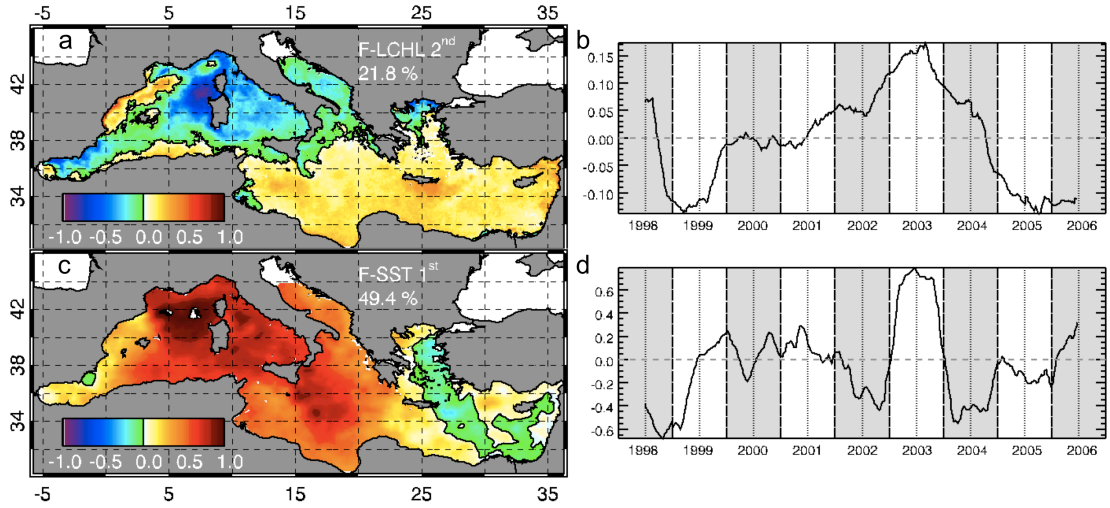

Figure 3.6: second EOF mode computed over F-LCHL (a-b) and first EOF mode computed over F-SST (c-d). See Figure 3.3 for details.

Spatially, this coupling is given by the fact that both maps (Figure 3.6a and Figure 3.6c) show the strongest variability in the central WMED, which is consistent with both Behrenfeld's hypothesis and the significant correlation between the two variables (r=-0.51, Table 3.2). Moreover, both temporal components are characterized by exceptionally low values during winter-spring 1998-1999 and high values during 2003 (Figure 3.6b and Figure 3.6d): i.e., they are in phase. This aspect leads the F-LCHL and F-SST to be anti-correlated, which is consistent with Behrenfeld's hypothesis. More in details, the F-SST mode is clearly dominated by the exceptional heat wave anomaly that affected the European continent in summer 2003 [e.g., *Schär and Jendritzky*, 2004], and the corresponding spatial pattern coherently displays an intense and large-scale signal over the central part of the basin (Figure 3.6c). From the spatial point of view, the heat wave anomaly during 2003 (with F-SST amplitude values larger than 0.6 °C) had the effect of enhancing the difference (0.5 to >1 °C) between the Levantine basin, and the rest of the basin. The significant spatial correlation (r=-0.51) between the second F-LCHL (Figure 3.6a) and the first F-SST (Figure 3.6c) modes highlights the interannual timescale relationship between the phytoplankton biomass

and the surface layer thermal stratification variations. However, the time lag between phytoplankton and SST temporal signals adds some interesting detail to Behrenfeld's model, in which there is no mention of the delay phytoplankton may have in responding to surface thermal variation at interannual time scales. Here, we show that the phytoplankton biomass increase (decrease) follows the decrease (increase) of the water column stratification by roughly five months. This relationship is evident also during the winter-spring 1998-1999 period. As a matter of fact, if the positive heat wave anomaly is associated to a decrease in the phytoplankton biomass, a negative F-SST anomaly, such as the one that occurred during winter 1998-1999, is linked to a stronger positive anomaly in the central WMED. This latter anomaly was already noticed by *Nezlin et al.* [2004], who attributed the unusually large phytoplankton vernal bloom to deeper winter cooling and more intensive winter convection.

3.4 Summary and conclusions

The main scope of this work was to identify physical-biological patterns of covariability that could be linked at different temporal or spatial scales: from seasonal to interannual timescales, and from basin to regional scales. Results from the principal component analysis (EOF) performed over time series (1998-2006) of SeaWiFS chlorophyll concentration (as proxy of the phytoplankton biomass), sea level (as proxy of the surface geostrophic field) and SST (as proxy of the water column thermal stratification) were used as input to a correlation analysis both in space and in time. This approach enabled the relationships between phytoplankton biomass variability and surface physical dynamics to be examined in terms of timing of the covariability, i.e., allowed the estimation of time lags.

In summary, the LCHL surface dynamics is linked to and significantly correlated with both the surface layer thermal stratification and the surface circulation patterns of variability. In particular, the surface phytoplankton biomass abundance is in phase opposition with the thermal stratification of the water column, at seasonal but not at interannual timescale. At seasonal and basin scales, the high correlation between LCHL and SST points at the inverse relationship between phytoplankton concentration and the annual cycle of the water column stratification, consistent with the findings of Behrenfeld et al. [2006] at global scale. However, this relationship characterizes only the areas recently identified as intermittently or non-blooming by D'Ortenzio and

Ribera d'Alcalà [2009]. As for the so-defined blooming areas, which coincide with the Gulf of Lion-Ligurian Sea region, a completely different mechanism links the MED open ocean spring bloom to the DWF processes. This is illustrated by the roughly five months time lag between the local surface cooling and the occurrence of the phytoplankton spring bloom. Firstly, the total amount of nutrients available in the offshore surface waters depends on the deep convection events occurring in late winter [Levy et al., 1998; 1999]. Secondly, the DWF phenomenon is characterized by a fundamental pre-conditioning phase, during which the surface stratification is significantly reduced. This pre-conditioning originates from the combination of more intense sub-basin scale cyclonic circulations and strong buoyancy fluxes associated with severe atmospheric events. However, it is only during the re-stratification phase (about five months later) that the nutrients can be efficiently exploited by phytoplankton. Our analysis shows that the pre-conditioning is the most crucial phase in determining the amount of nutrients in the upper layer and hence the space-temporal extent of the spring bloom.

The physical-biological relationships at longer time scales were investigated isolating those scales by data filtering. The phytoplankton biomass variability was shown to be linked to two distinct interannual signals:

1. to the modified surface circulation pattern consisting in a northward shift and intensity increase of the Algerian current, and concomitantly, to the reduced cyclonic circulation in the whole eastern basin. We hypothesized that this circulation change is responsible of the phytoplankton biomass decline in the whole central basin, via the reduced advection of nutrient richer waters of Atlantic origin into the Tyrrhenian and Ionian Seas, which in turn coincides with a phytoplankton increase in the Balearic Sea.
2. To the surface heat content anomalies during 1998/1999 (anomalously cold winter) and 2003 (summer heat wave). Our own interpretation is that the impact of the surface layer heat content anomalies on the phytoplankton biomass concentration can be explained through the mechanism already proposed by Doney [2006] to predict the ecosystem response to global warming. Our analysis complements Doney's scheme by introducing the time variable, and shows that phytoplankton dynamics and surface conditions may or may not be in phase, depending on both the physical processes that modulate the nutrients

availability in the upper layer and the involved trophic regime. In particular, in the blooming areas [D'Ortenzio and Ribera d'Alcalà, 2009], phytoplankton dynamics and surface stratification are always out of phase, whereas they are in phase in non-blooming regions.

To conclude, even if the EOF decomposition does not necessarily identify processes, in the present study it provides a means of interpretation of the covariability of specific dynamical patterns in the physical and biological fields, at different space and time scales. This results in the suggestion of a number of mechanisms linking the upper ocean dynamics to the ecosystem functioning, that warrant further investigation.

4 Dust and phytoplankton in an LNLC region

The contents of this chapter are identical to a paper that has been published in Global Biogeochemical Cycles: Volpe, G., V. F. Banzon, R. H. Evans, R. Santoleri, A. J. Mariano, and R. Sciarra (2009), Satellite observations of the impact of dust in a low nutrient low chlorophyll region: fertilization or artifact? 23, GB3007, doi:10.1029/2008GB003216

This paper is made of the contributions by six authors. Viva Banzon provided a lot of insights for the manuscript drawing up, along with scientific and technical support for the analysis. The entire analysis was done only by the first author. Roberto Sciarra visually analyzed the entire True Colour dataset and built up the TC catalogue. Other authors provided useful comments especially from the technical point of view; they revised the manuscript and stimulated many fruitful discussions.

The content of this chapter can be summarised by the following abstract that accompanies the published paper.

The coupling between dust aerosols and phytoplankton concentrations in the Mediterranean Sea, a low nutrient low chlorophyll region, is examined at different timescales using SeaWiFS observations (1998-2002). Aerosol optical thickness (AOT) and chlorophyll (CHL) were used as proxies for dust aerosol and phytoplankton biomass, respectively. The AOT data was qualified using quasi-true colour images in order to ascertain the presence of dust. Strong positive correlations were found between AOT and CHL on weekly but not on seasonal timescales. However, weekly analyses cannot distinguish between real phytoplankton response and artefacts due to residual dust in the atmosphere or water. Daily time series of AOT and CHL, for single dust events, and their temporal cross-correlation function were analyzed. Apparent AOT-driven CHL increases principally occurred within 0-2 days and most cross-correlations were significant at zero lag. In contrast, significant negative or positive correlations at

lag greater than 2 days were very few, indicating no compelling evidence that dust enhancement of phytoplankton growth is significant, and that the response at near-zero lags is an artefact of the satellite data processing. Our analysis demonstrates that the dust fertilization does not play a significant role in the sustainment of the phytoplankton dynamics in the Mediterranean Sea.

4.1 Introduction

The dust fertilization hypothesis proposes the existence of a major coupling between ocean phytoplankton production and dust aerosols, and implies an important mechanism for carbon sequestration. Mineral dust originating from desert areas is transported by winds across great distances; dust deposition in nutrient-poor waters may result in blooms that facilitate biomass export to the deep ocean [*Goudie and Middleton,* 2001*; Prospero et al.,* 2002]. A significant portion of the world's ocean is oligotrophic (e.g., Sargasso Sea, South Pacific Ocean, the Mediterranean Sea), that is characterized by low nutrients and low chlorophyll (LNLC) [*Howarth,* 1988*; Guerzoni et al.,* 1999*; Bonnet et al.,* 2008]. For LNLC systems, it has been hypothesized that dust is an important source of macronutrients like phosphorous (P) and nitrogen (N) [*Guerzoni et al.,* 1999*; Migon and Sandroni,* 1999*; Guieu et al.,* 2002*; Markaki et al.,* 2003*; Morales-Baquero et al.,* 2006]. In contrast, in high nutrient low chlorophyll (HNLC) areas, such as the Northwest Pacific Ocean, macronutrients are high but biological production is paradoxically low. Under HNLC conditions, iron (Fe) has been shown to be the limiting micronutrient and dust has been demonstrated to be an important source of iron as proposed by *Martin* [1990]. The importance of dust as a macronutrient source in LNLC systems remains to be demonstrated.

The Mediterranean Sea (MED herein) lies adjacent to the Sahara, the world's largest source of aeolian soil dust, and is under a major dust pathway where dust deposition frequently occurs [*Markaki et al.,* 2003*; Engelstaeter et al.,* 2006]. This makes it an ideal place to examine more closely the dust fertilization hypothesis in the LNLC context (e.g. dust as a source of N and P). The MED is limited to the north by the industrialized European countries, which act as a continuous source of anthropogenic aerosols, and to the south by the Sahara Desert, the primary MED dust source. The most intense dust-producing area is the Lake Chad/Bodélé depression in the interior of the African continent; however, there are other very active sources close to the Mediterranean coastline such as the Libyan Desert and the Northern Algerian

Chotts [*Israelevich et al.,* 2002*; Prospero et al.,* 2002]. In general, Saharan dust events are in the form of episodic pulse-like events, significantly contributing to the atmospheric aerosol characteristics of the basin [*Guerzoni et al.,* 1997]. In summer and fall, atmospheric cyclonic systems develop over the African continent, thereby mobilizing and transporting dust, making it the dominant aerosol over the MED; in winter, the meteorological conditions tend to favor aerosol transport from the north where anthropogenic pollutants are dominant [*Alpert et al.,* 1990; *Israelevich et al.,* 2002].

From an oceanographic point of view, the MED is a mid-latitude semi-enclosed basin, characterized by anti-estuarine circulation which contributes to make it one of the most oligotrophic seas on earth [*Crise et al.,* 1999]. It receives nutrient-depleted surface waters from the Atlantic Ocean through the Gibraltar Straits, and exports relatively nutrient-rich intermediate waters to the Atlantic Ocean [*Bethoux,* 1979; *Sarmiento et al.,* 1988]. The mixed layer is generally deeper in the eastern (EMED) than in western (WMED) sub-basin, contributing to an eastward trend of increasing oligotrophy [*D'Ortenzio et al.,* 2005]. Phytoplankton exhibit a clear seasonal cycle characterized by low surface chlorophyll concentrations and a deep chlorophyll maximum at the nutricline (~40 m in WMED and up to 120 m in EMED [*Crise et al.,* 1999]) in summer when the water column is stratified; in winter, mixing breaks stratification and brings nutrients up into the euphotic layer, resulting in a spring bloom [*Santoleri et al.,* 2008]. High phytoplankton biomass also occurs at coastal sites or in conjunction with high meso-scale activity and at river mouths [*Antoine et al.,* 1996; *Crise et al.,* 1999].

Several studies have focused on the importance of dust to MED biogeochemistry as an additional source of nutrients. *In situ* measurements indicate Fe is relatively abundant in the MED, and the system is macronutrient-limited (N, P or both, depending on season or location) [e.g., *Krom et al.,* 1991; *Guerzoni et al.,* 1999; *Thingstad et al.,* 2005]. The Saharan dust contribution to the North African aerosol nutrient content ranges from 0.02% to 0.07% for inorganic P and 0.2% to 1.5% for inorganic N [*Goudie and Middleton,* 2001]. In the western basin, Saharan dust is estimated to account for ~30-40% of the total atmospheric P flux and is the main source of dissolved Fe [*Guieu et al.,* 2002]. *Guerzoni et al.* [1999] estimated that the impact of atmospheric input of nutrients to the open MED would be negligible during the period of intense primary production because of mixing with deep nutrient-rich waters. On the other hand, during

summer and early fall, stratification of the water column makes the atmospheric input non-negligible and in some cases the dominant source of nutrients, which may trigger small but detectable phytoplankton blooms. On an annual scale, dust is relatively insignificant as a nutrient source for phytoplankton, but can be important at short timescales [*Guerzoni et al.,* 1999; *Eker-Develi et al.,* 2006]. During the EMED stratification periods, atmospheric deposition of dissolved inorganic P could reasonably account for up to 38% of new production [*Markaki et al.,* 2003]. However, a massive experimental P-addition into the ultra-oligotrophic Cyprus Eddy resulted in a decline in phytoplankton biomass and an increase in bacterial production was observed [*Thingstad et al.,* 2005]. Phytoplankton did increase in on-deck incubations that received additional N, leading *Thingstad et al.* [2005] to conclude that P and N were probably co-limiting. *Guerzoni et al.* [1999] estimated that atmospheric N could account for 60% of new production in WMED oligotrophic areas, and less in the EMED. The importance of dust as a source of N was also indicated by microcosm studies on northwestern Mediterranean natural phytoplankton assemblages, i.e., the larger eukaryotic (e.g., diatoms) fraction increased only in treatments with added dust but not in those enriched with a combination of Fe and non-N containing anthropogenic particles [*Bonnet et al.,* 2005]. In particular, *Bonnet et al.* [2005] observed that chlorophyll biomass progressively increased reaching ~50% of the initial value after three days following dust addition. Contrary to the dust fertilization hypothesis, *Krom et al.* [1991] proposed that Fe-rich dust particles could favor absorption of the inorganic P in seawater, thus explaining the unusual N:P ratio (~27) in the eastern Mediterranean which is unfavourable for phytoplankton growth. In the northeast MED, *in situ* measurements at bi-weekly or more frequent intervals showed little or no phytoplankton biomass response following episodic dry and wet deposition events [*Eker-Develi et al.,* 2006]. Within the framework of the EU-funded ADIOS project, a fast response-sampling program off Crete also did not detect any phytoplankton increase following dust events even though dissolved P increased immediately [*Heussner et al.,* 2003]. Variability in these results is not surprising given that each episode represents different conditions (e.g., dust source, deposition, nutrient bioavailability, and the biophysical-chemical state of the upper ocean). Thus, an approach is needed to monitor individual dust events and their biological responses on a more local scale, that takes into account the scales of advection under stratified conditions when upwelling and other

oceanographic processes do not introduce additional nutrients. Furthermore, these individual events can be treated as a population and analyzed in a statistical manner.

The objective of this study is to conduct a systematic investigation of MED dust events and their impact on phytoplankton biomass within expected response times (as suggested in the literature) in order to test the dust fertilization hypothesis in the LNLC context. We aim to examine a large number of events to establish their collective importance to short term variability of MED phytoplankton blooms. Satellite observations, characterized by regular temporal frequency and large spatial coverage for both aerosol and phytoplankton parameters, represent a useful tool to investigate the phytoplankton-dust linkage on various space and time scales, and to establish the reproducibility of the effect. The Sea-viewing Wide Field-of-view Sensor (SeaWiFS) provides estimates of chlorophyll, a widely used proxy for phytoplankton biomass, and aerosol optical thickness at 865 nm (herein, referred to as AOT) as an estimate of the columnar aerosol loading. AOT is estimated as part of the atmospheric correction procedure and can be used as a proxy for dust concentrations during the summer, with some caveats (discussed in section 4.2). For SeaWiFS, AOT represents the best available parameter to represent dust as there is no implemented dust detection algorithm. Moreover, the standard atmospheric correction compensates only for weakly or non-absorbing aerosols, but not for absorbing aerosols such as dust. Thus, there is an inherent error in AOT and chlorophyll estimates where dust aerosols are present but not detected and pixels pass the standard data quality tests. The presence of dust aerosols has been shown to introduce up to a twofold bias in SeaWiFS chlorophyll estimates, due to increased dust absorption in the shorter visible wavelengths, mimicking phytoplankton absorption [*Moulin et al.,* 2001]. Obviously clouds and thick dust can obstruct the satellite view, so no AOT and chlorophyll estimates are possible at the height of the storms. However, data can be obtained for the area immediately adjacent to the dust plumes, and in the preceding and subsequent cloud-free days so that time series of chlorophyll and dust aerosol may be obtained. While analogous atmospheric parameters are available from other instruments such as the Total Ozone Mapping Spectrometer (TOMS), the lower spatial resolution tends to miss smaller plumes that are common in the Mediterranean.

On a global scale, *Cropp et al.* [2005] found a strong positive correlation on weekly AOT and chlorophyll fields derived from SeaWiFS, thereby demonstrating the impact of dust. However, their maps showed high negative correlations in the MED,

which they proposed could be either due to the nature of the dust transport, which is more intermittent and less intense than where the correlation was positive, or due to the influence of anthropogenic-derived aerosols [*Cropp et al.,* 2005]. On the other hand, *Cropp et al.* [2005] showed examples of standard processed images with Saharan dust inducing abnormally high chlorophyll values around dust plume edges. Increased MED chlorophyll concentrations after dust storms had also been reported based on observations from the Coastal Zone Color Scanner, which preceded SeaWiFS [e.g., *Dulac et al.,* 1996]. However, it is not possible to discriminate if the satellite-observed increase in chlorophyll is due to incorrect atmospheric correction (also referred to as the Artifact Hypothesis) rather than a phytoplankton response (also referred to as the Dust Fertilization Hypothesis). This work addresses this issue by a careful analysis of satellite products, and by analyzing the short-term chlorophyll increase after individual dust events in the context of biological response times (on the order of several days) as indicated by previous studies [*Turner et al.*, 1996; *Guerzoni et al.*, 1999; *Bonnet et al.*, 2005; *Eker-Develi et al.*, 2006].

4.2 Data and Methods

4.2.1 Data and Processing

Five years (1998-2002) of SeaWiFS data were analyzed. For good high-resolution 1 km coverage of the Mediterranean Sea, Level 1A data collected by the HRPT receiving station located in Rome, Italy (41.84°N, 12.65°E) were used. The station is managed by the Satellite Oceanography Group of the Rome Institute of Atmospheric Sciences and Climate. Over 4100 passes were processed to Level 2 using SeaDAS v.4.8 [*Baith et al.,* 2001]. Chlorophyll concentrations were computed from Level 2 water leaving radiances, using a validated regional algorithm called MedOC4 that takes into account that the Mediterranean open water is less blue (30%) and greener (15%) than the global ocean [*Volpe et al.,* 2007]. The MedOC4 CHL product used in this study is herein referred to as MCHL to differentiate it from the standard product which uses the OC4v4 algorithm [*O'Reilly et al.,* 2000]. Note that both CHL algorithms are empirical and are based on the blue-to-green band ratio, but the MedOC4 coefficients and function shape are more suited to the particular bio-optical characteristics of the Mediterranean. *Volpe et al.* [2007] have shown that MedOC4 produces more realistic values in the Mediterranean, differing from *in situ* values by

about 35% for CHL<0.4 mg m^{-3} and 40% for CHL>0.4 mg m^{-3}, in contrast to over 100% when OC4v4 is used (relative to the 35% SeaWiFS mission goal). Matchup datasets used to develop CHL algorithms are very carefully screened to exclude less than ideal conditions (e.g., shallow water and dust events [*Mueller and Austin*, 1995; *Mueller*, 2000; *Mueller and Fargion*, 2002]). Thus, in theory, both algorithms retrievals should provide realistic CHL values under clear sky conditions in those areas and time of the year which actually reflect the *in situ* sampling conditions used to build the algorithms. MedOC4 provides more accurate CHL retrievals than OC4v4 because it is optimized for Mediterranean conditions [*Volpe et al.*, 2007]. Moreover, since both chlorophyll algorithms do not include atmospheric correction, both are susceptible to the artefact effect under dust-dominated conditions. While dust correction algorithms [e.g., *Moulin et al.*, 2001] have been developed, they are not widely used since there are unresolved issues such as how to automatically apply them on a pixel-by-pixel basis.

Standard masking criteria for detecting clouds or other contamination factors were applied, i.e., land, cloud, sun glint, atmospheric correction failure, high total radiance, large solar zenith angle (70°), large spacecraft zenith angle (56°), coccolithophores, negative water leaving radiance, and normalized water leaving radiance at 555 nm < 0.15 Wm^{-2} sr^{-1} [*McClain et al.,* 1995]. While AOT is the most simple and readily available aerosol concentration indicator from SeaWiFS, its validity as a proxy for dust concentration needs to be qualified using the corresponding quasi-true colour image (QTC), i.e., a composite of the Rayleigh-removed top-of-the-atmosphere reflectances using the 670, 555 and 443 nm bands, respectively, as described in the next section. Moreover, it should be noted that with standard SeaWiFS processing, products are not computed for a pixel when dust is present if total surface reflectance is high. Thus, QTC data offers a means to document the intense dust events.

The QTC, MCHL and AOT fields were remapped using cylindrical equirectangular projection covering the entire Mediterranean (27.569-48.43 °N; -9.5-43.5 °E). The latter two parameters were binned to make daily 1/16 of degree (ca. 6 km) resolution maps with reduced spatial gaps. Weekly (8-day), monthly, seasonal and annual averages were computed from the daily composites. For seasons, the standard meteorological convention was followed: winter (December to February), spring (March to May), summer (June to August) and fall (September to November).

The correlation (r) between weekly maps of MCHL and AOT was computed at 1/16 degree resolution. Since the spatial scales of the dust plumes in the Mediterranean

Sea are very variable and can include very elongated structures, we chose a resolution higher than 1 degree used by *Cropp et al.* [2005] to better resolve these features. Following *Cropp et al.* [2005], we refer to these weekly averages as "raw" values to differentiate from the "residual" response, which is obtained by subtracting out the preceding value in each time series of MCHL and AOT in order to remove temporal trends. The correlation between the raw parameters was computed, for each sea pixel (63167 grid points), using: 1) all the data (225 pairs of data for each ocean pixel with some gaps due to persistent cloud cover or to missing satellite coverage of the area), and 2) data only from the predominantly dusty period (May to September, explained in next section) of each year (in this case the number of data pairs is 80 with the same constraints due to clouds and satellite area coverage). Correlations were also calculated on the equivalent residual datasets. A Student-T distribution was assumed to calculate the confidence levels of 99.9% at each ocean pixel. Note that this takes into account both the value of the correlation coefficient r and the number of degrees of freedom given by the length of each ocean pixel time series. As a consequence of different cloud-free periods at different locations, the magnitude of the lowest significant r is expected to be higher for case 2 (short time series) than for case 1), mentioned above (and as reported in the caption of Figure 4.4).

4.2.2 Saharan Dust Event Recognition

One of the challenges in this study is how to recognize dust events, e.g., high AOT needs to be combined with the additional information. The effectiveness of proposed automatic dust detection algorithms using ocean color bands have been evaluated by side-by-side visual comparisons with QTC images (e.g., *Nobileau and Antoine,* 2005). For dust identification, the Angstrom exponent produced by the SeaWiFS standard processing cannot be used because the model-retrieved aerosol parameters are not correct in the presence of absorbing aerosols, as explained in detail in several previous works [e.g., *Gordon,* 1997; *Gordon et al.,* 1997]. The use of QTC as a dust surrogate is justified by a comparison with an absorbing aerosol index (AAI; a simplified version of that of *Nobileau and Antoine* [2005]), defined as:

$$\mathrm{AAI} = \frac{\mathrm{Ls}(555)}{\mathrm{Ls}(865)}$$

where Ls(555) and Ls(865) are the Rayleigh-removed total radiances at 555 and 865 nm, respectively. That is, AAI is conceptually analogous to the clear-water epsilon,

ε(555,865), of *Gordon and Clark* [1981]. The principle is that in regions of low chlorophyll concentration, the effect of phytoplankton variability on the optical signature is very small except in the blue, and therefore the AAI is nearly invariant. In contrast, dust absorption increases with decreasing wavelength, and thus dust presence results in a decrease in the AAI relative to the background.

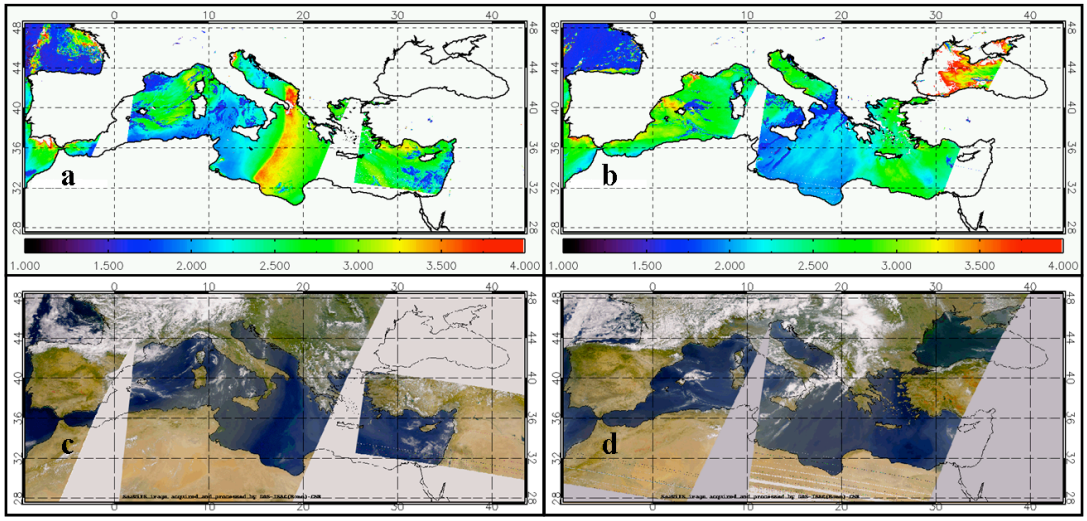

Figure 4.1: Comparison of Absorbing Aerosol Index described in Section 4.2.2 for (a) 6 July 1999 (Julian day 187), and (b) 14 July, 1999 (Julian day 195), and the corresponding true color images: for day 187 (c) and 195 (d).

As illustrated by Figure 4.1a and Figure 4.1b, there is a large low AAI (blue region) coming off Africa corresponding to the QTC brown region in Figure 4.1c and Figure 4.1d, respectively. In contrast, the remainder of the image has higher background AAI (green to red region) due to scattering aerosols, except where clouds are present. Thus, by QTC visual inspection, dust aerosol events are easy to recognize as large-scale atmospheric features with a characteristic brown color and originating from Africa, while haze (pollution) aerosols are white and tend to come from Europe. Consequently, the routinely available AOT and QTC fields can be used to define dust aerosol presence.

A mask of the 18 MED subregions was defined to analyze the entire QTC image inventory (Figure 4.2a). The subdivision takes into account the typical dust trajectories in order to differentiate zones proximal to source areas, and typical oceanographic conditions, such that more quiescent areas (black regions in Figure 4.2a) are separated from more dynamic zones. Note that the quiescent (or low-dynamics) areas are generally oligotrophic areas where chlorophyll values tend to be low and nearly invariant, while the high-dynamical regions (in white) are subject to more vigorous

physical processes that play a major role in the modulation of the biological activity, resulting in a distinct spring bloom and mesotrophic conditions.

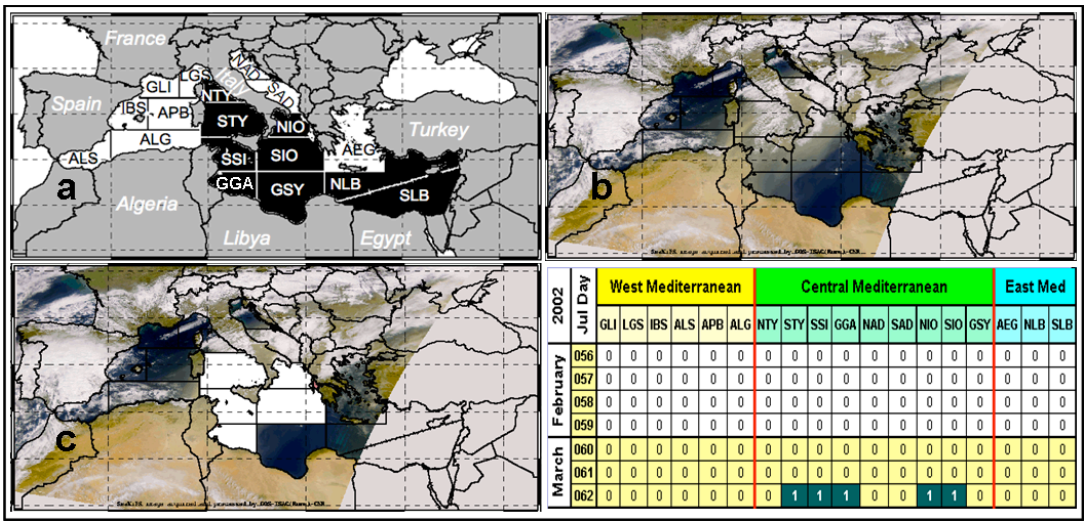

2002 Jul Day	West Mediterranean						Central Mediterranean								East Med		
	GLI	LGS	IBS	ALS	APB	ALG	NTY	STY	SSI	GGA	NAD	SAD	NIO	SIO	GSY	AEG	NLB	SLB
February 056	0	0	0	0	0	0	0	0	0	0	0	0	0	0	0	0	0	0
057	0	0	0	0	0	0	0	0	0	0	0	0	0	0	0	0	0	0
058	0	0	0	0	0	0	0	0	0	0	0	0	0	0	0	0	0	0
059	0	0	0	0	0	0	0	0	0	0	0	0	0	0	0	0	0	0
March 060	0	0	0	0	0	0	0	0	0	0	0	0	0	0	0	0	0	0
061	0	0	0	0	0	0	0	0	0	0	0	0	0	0	0	0	0	0
062	0	0	0	0	0	0	0	1	1	1	0	0	1	1	0	0	0	0

Figure 4.2: Example showing the logical sequence adopted for compiling the dust events catalogue based on QTC visual inspection. (a) Mediterranean Sea subregions in alphabetical order: AEG=Aegean Sea, ALG=Algerian basin, ALS=Alboran Sea, APB=Algero-Provencal Basin, GGA=Gulf of Gabes, GLI=Gulf of Lion, GSY=Gulf of Sidra, NAD=North Adriatic Sea, NIO=North Ionian basin, NLB=North Levantine Basin, NTY=North Tyrrhenian Sea, SAD=South Adriatic Sea, SIO=South Ionian basin, SLB=South Levantine Basin, SSI=Straits of Sicily, STY=South Tyrrhenian Sea. Black (white) sectors indicate low (high) dynamics oceanographic areas. (b) QTC image for 3 March 2002, with the subregional mask overlaid; (c) dust-affected regions in white; (d) dust event catalogue, where "1" indicates the presence of dust in the relevant boxes (Julian day 62, in bottom row).

Photo-interpretation of the QTC images was performed by a trained image analyst in the following manner: first, the single QTC satellite scene was displayed then, the subregion mask was overlaid (Figure 4.2b), permitting dusty areas to be identified (Figure 4.2c, in white). This enabled a catalogue of events for each subregion to be compiled for the each day (example in Figure 4.2). In this analysis, white areas with clouds were not considered dusty even though clouds exhibited continuity with dust features: for example, the SAD region in Figure 4.2c has not been marked as dusty in order to avoid misinterpretation of clouds as dust. For each subdivision, if two images were available, only one occurrence per day was recorded (Figure 4.2). Since our aim was not to obtain the maximum number of possible events in each area, but to identify "true" dust events as unequivocally as possible, a subregion was considered dusty only if more than 50% of the area appeared affected by dust in at least one scene. In this context, box ALG in Figure 4.2c is not marked as dusty because only a small portion of it is covered by dust. Details of the entire catalogue can be found in *Sciarra et al.* [2003]. Over the entire study period, dust was visually detected on 532 days, 405 of which occurred from April to September. However, because in April the water column

is not completely stratified and the spring bloom is still present, the dusty period is defined here as May to September, which had 333 dusty days basinwide. Counting all occurrences over the study period, monthly and seasonal maps were produced.

4.2.3 Single Event Analysis

To differentiate between the Artifact Hypothesis and the Dust Fertilization Hypothesis, the MCHL response time after a dust event was determined by correlating AOT and MCHL daily time series. For this analysis we chose a spatial scale larger than the typical Rossby radius of deformation (order of 10-20 km in summer) and larger than the typical mesoscale circulation features in the MED (order of 150 km) in order to minimize problems due to advection. Since the subregions (Figure 4.2a) take into account characteristic scales of atmospheric and oceanographic processes in the MED, correlations were made on a box-by-box basis. Daily average AOT and MCHL for each box were computed as input for the correlations, while the QTC catalogue provided a reliable record of dust events. This analysis was limited to the dusty period not only because high AOT is more likely indicative of dust presence and intense events are more frequent, but also because during this period horizontal and vertical mixing processes are minimum. For each subregion, only catalogued events that had no other dust occurrences 7 days prior to 14 days following the end of an event were selected, in order not to introduce ambiguous results. The time window associated with each event allowed correlations to be performed over a 14 day-period with a maximum of time lag of 7 days. The expected timescale of a phytoplankton response in the MED has been established to be within the order of a week [*Guerzoni et al.,* 1999; *Bonnet et al.,* 2005; *Eker-Develi et al.,* 2006]. Thus the selected time window should be sufficient to detect any impact. To have confidence in the data, daily subregional averages were used only if at least 20% of the pixels in a box were valid. Moreover, the use of subregional averages had the advantage of minimizing gaps in the time series, and consequently reducing the lagged cross-correlation estimation error. After considering all the abovementioned constraints, 60 independent events were obtained, which is a significant number of replicates for statistical tests since it is much larger than the minimum of 30 independent samples as suggested by early works of *Student* [1908, *the pen name of W. Gosset*]. The QTC, MCHL, and AOT images within the time window for these 60 events were visually re-checked to make sure there were no intervening dust events or mesoscale oceanographic perturbations. The dust-induced phytoplankton

response was analyzed for each of the boxes (Figure 4.2a) that had been classified as dusty in the catalogue.

In order to make the different time series comparable, the MCHL anomaly at each day i, ΔMCHL(i), was computed by subtracting out a pre-event value such that:

$$\Delta MCHL(i) = 100 * \frac{\left(MCHL(i) - \overline{MCHL} \right)}{\overline{MCHL}}$$

where $\overline{MCHL}$ is the average concentration for the 7 days preceding the event, and MCHL(i) is the concentration after the event for day i.

The cross-correlations between AOT and MCHL for time lags between 0 to 7 days were computed for each event. The correlation coefficient (r) between MCHL and AOT was computed and tested for significance using the Student's T-test (using different confidence levels from 90% to 99%, see Sections 4.3.2 and 4.4). All correlation coefficients that were not statistically different from zero were classified as a null outcome. Using only the significant results, the occurrence of positive and negative correlations was then tallied for each lag. To see if there was any difference due to oceanographic regimes, a tally was also made for high- and low-dynamics subregions as defined in Figure 4.2a.

4.3 Results

4.3.1 Seasonal patterns of dust frequency, AOT and MCHL

Seasonal maps of dust event occurrence for the study period (1998-2002) show that Saharan dust events over the MED have a north-south gradient, with highest occurrences along the African coast (Figure 4.3, middle panels). Events were more frequent during the summer than in winter and fall, with activity shifting from the eastern basin in spring to the western basin in summer. In winter, dust frequency is low basinwide.

While occurrences appear high in fall, most of the events actually occur in September (not shown). Among the eighteen subregions, the highest number of dust events occurs in the Algerian basin (ALG), when the wind blowing through the Atlantis chain enhances dust transport. Frequencies are also high in adjacent areas, i.e., Gulf of Syrtis (GSY), Gulf of Gabes (GGA) and Strait of Sicily (SSI). These results are in

general agreement with previous results [*Moulin et al.,* 1998; *Antoine and Nobileau,* 2006].

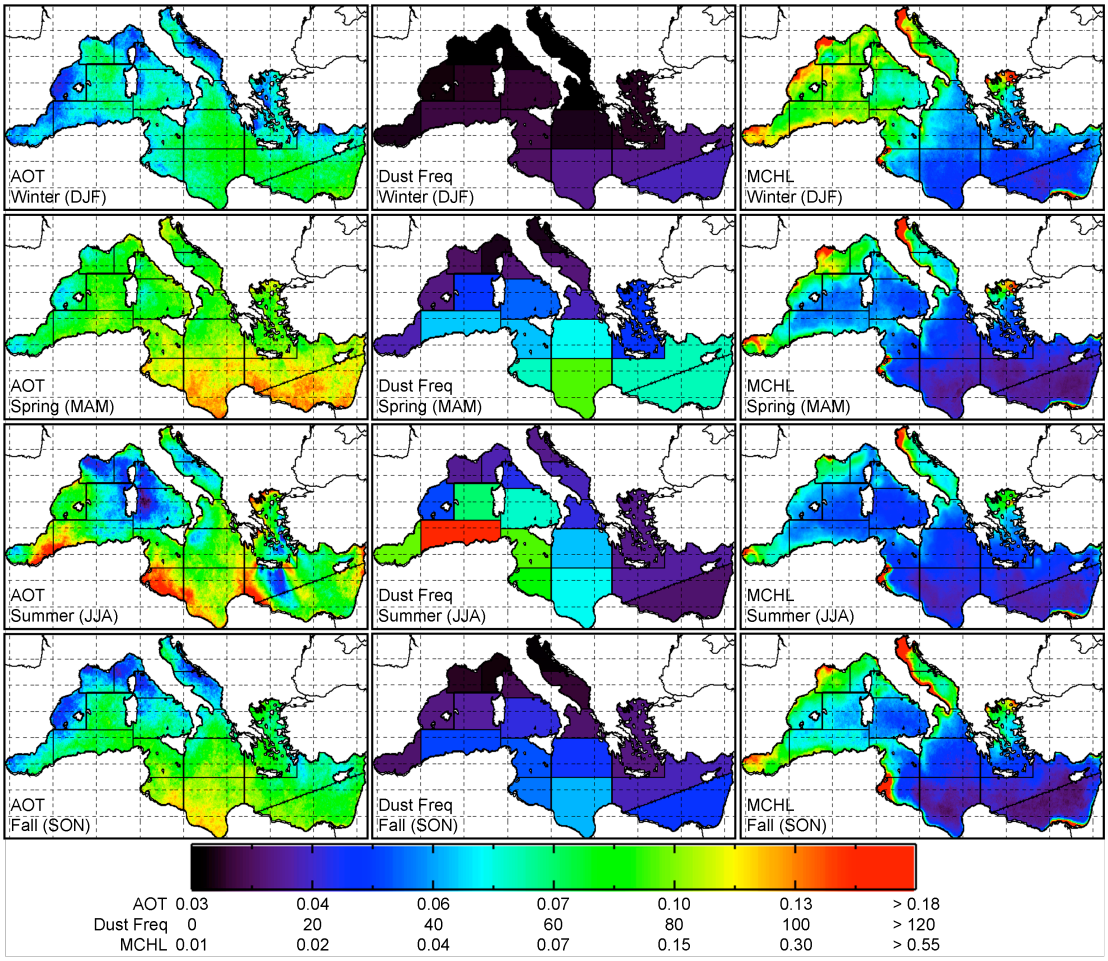

Figure 4.3: Maps of seasonal averages of AOT (left column), total number of dust events in each season (middle column) and MCHL (right column) averaged over the entire study period 1998-2002 for winter (DJF), spring (MAM), summer (JJA) and fall (SON).

The seasonal, basin-scale variability of AOT (Figure 4.3, left column) shows similar spatial and temporal patterns as the QTC-derived frequencies (Figure 4.3, middle column). The lowest AOT values occur in winter, and the highest, in summer. During fall, AOT maxima are located in the central basin. In wintertime, AOT tends to be lower than other seasons, but relatively high values occur in the eastern basin. There is a north-south gradient with the highest AOT along the African coast, proximal to the dust source areas. The seasonal AOT patterns also evoke the dust plume shapes seen in individual images, which are dictated by the predominant meteorological conditions of the season. This pattern also suggests continual deposition occurs as dust travel out to sea. In accordance with the frequency results, the region of maximum AOT shifts seasonally from the central-east to the central-west part of the basin during spring and

summer, respectively. Thus, the seasonal maps of mean AOT are consistent with the location of known large dust events.

However, some dissimilarity is also evident: the biggest difference between AOT and the event frequency maps is that in summer, the maximum frequency occurs only in the Algerian basin box, whereas the AOT field shows several active areas along the African coast. In part, this disparity is a consequence of the size and path of the dust plumes relative to the rectangular subregions. Also, areas where the dust plume is thick is treated by the standard processing as cloud and thus, AOT values are not computed.

Seasonal MCHL maps (Figure 4.3, right column) show high MCHL associated with hydrodynamics that enhances nutrient inputs to the surface layers. As discussed in previous works [*Antoine et al.,* 1995; *Santoleri et al.,* 2008], these patterns are associated with oceanographic processes such as deep convection, upwelling, coastal dynamics or freshwater outflow. The relevant result for this study is that on a seasonal scale, MCHL fields are clearly not temporally or spatially related to those of AOT or dust frequency. The main feature of the MCHL field is the dominant zonal gradient with wintertime maxima, opposite to the dominant meridional gradient with summertime maxima for dust. Moreover, the areas with highest dust concentrations are located along the African coasts, which are the areas with lower chlorophyll concentrations. These observed patterns do not suggest that dust availability is a major factor controlling seasonal phytoplankton variability in the Mediterranean. The next section examines the Saharan dust impact on the biogeochemistry of the Mediterranean open waters on a weekly time scale.

4.3.2 Correlations between weekly MCHL and AOT means

Weekly averages of raw MCHL and AOT, over the entire study period, were negatively (bluish areas) or not correlated at all (i.e., non-significant: $-0.21 \leq r \leq 0.21$; light blue) at most grid points (Figure 4.4a). Our results using 1/16 of degree resolution maps for the Mediterranean mirror those of *Cropp et al.* [2005] where global analyses were computed for the same years as this study at 1 degree resolution, i.e., the increased spatial resolution did not significantly change the cross-correlations. However, the correlations changed significantly using data only from the dustiest months (May to September; Figure 4.4b). A positive r value (up to 0.75) was observed over most of the basin. Zones with non-significant r values ($-0.35 \leq r \leq 0.35$) occur out of the range of dust plumes, near rivers, and/or regions affected by vigorous ocean dynamics. One

particularly large zone of non-significant r is located in the northwestern region, which is rarely traversed by dust plumes (Figure 4.3, middle column). Moreover, this area is affected by the Rhone River, and has a particularly large seasonal upwelling resulting in the largest bloom in the MED (Figure 4.3, right column). Thus without any manipulation to remove seasonal or temporal trends, a strong coupling between atmospheric and oceanic optical products can be observed on a weekly scale if the analysis is focused on the dust-dominated period.

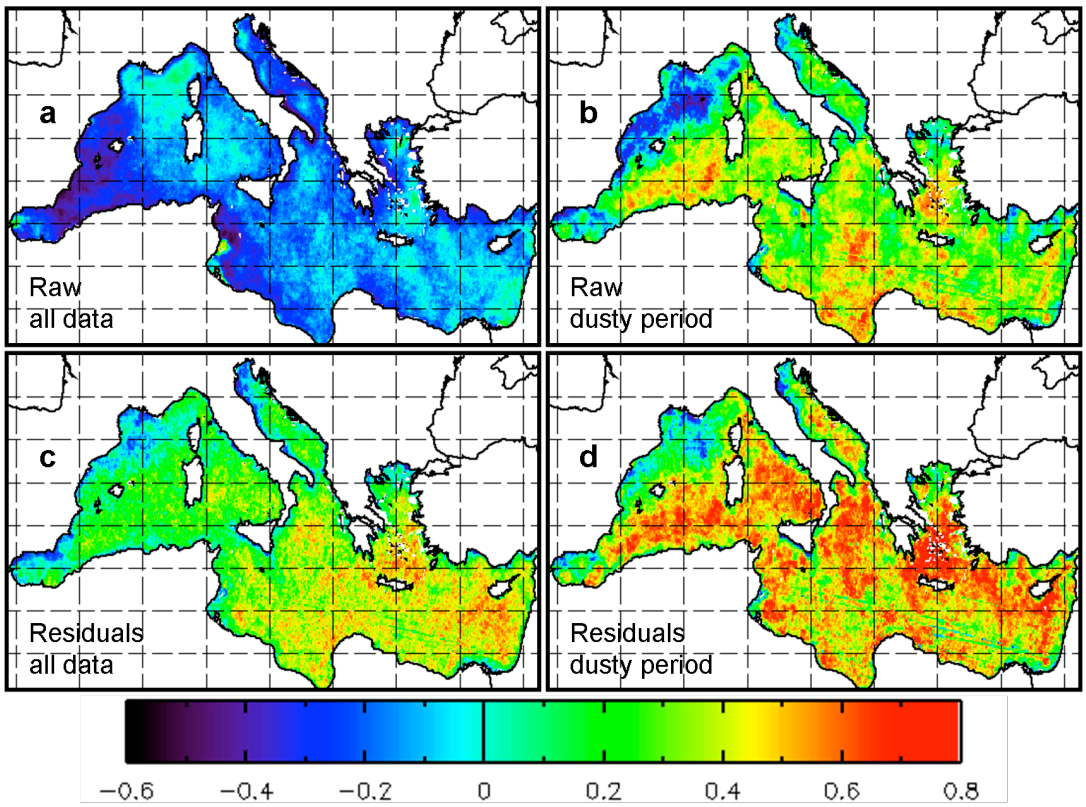

Figure 4.4: Spatial maps of the cross-correlation between weekly (8-days) mean MCHL and AOT using a) raw data for the entire study period (225 pairs of data for each ocean pixel), b) raw data from May to September of every year (80 pairs of data for each ocean pixel), c) residual response for the entire study period (same number of data as a), d) residual response from May to September of every year (same number of data as b). Correlation coefficients with magnitudes greater than a) 0.21 b) 0.35 c) 0.21 and d) 0.36 are statistically different from zero at the 99.9% confidence limit.

Correlation between the residual MCHL and AOT responses produces r values that are generally positive, especially in the eastern basin (Figure 4.4c), as also observed by *Cropp et al.* [2005] in their global analysis at lower spatial resolution. When the analysis was restricted to the dusty period, the strongly positive correlations became higher and more widespread although the spatial pattern was conserved, with non-significant r-values in the northwestern basin and near river mouths (Figure 4.4d). These results underline that the atmosphere-ocean coupling is largest for time periods when dust is the known dominant aerosol. It also indicates that to establish the

phytoplankton-dust linkage, high spatial resolution is not critical even in an environment where phenomena take place at reduced space-time scales such as the Mediterranean.

When the correlation was computed with a 1-week lag in MCHL (not shown), r was not significant for most of the pixels (72 %), while for the remaining significant r values (not exceeding 0.4), the number of positive and negative correlations were approximately the same. The same 1-week lagged analysis on the residuals produced practically no positive correlations. These results underline that the weekly AOT and MCHL are most correlated at zero temporal lag, consistent with *Cropp et al.* [2005].

4.3.3 Daily time series of selected dust events

To investigate the biological response time to dust deposition, we analyzed 60 selected dust events defined in section 4.2.3. Examples of positive and ambiguous responses to a dust event are shown in Figure 4.5. Since the length of the time series is now much shorter than those presented in previous section, a confidence level of 90% is now used to constrain the results. The first example (Figure 4.5a) represents a dust event on July 6, 1999 (day 187) in the northern Adriatic Sea (QTC in Figure 4.1c). An anomalously high MCHL value is associated with a high AOT value on the day of the event (Figure 4.5a1 and Figure 4.5a2). Maximum cross correlation was observed at zero lag between the AOT and MCHL time series (Figure 4.5a3).

Since phytoplankton response (up to 400% the pre-event mean value) on the same day as the dust event is unlikely due to fertilization, this suggests that dust absorption in the atmosphere or water was affecting the MCHL satellite value. The second AOT peak on day 195 does not have the same effect on MCHL because it involves non-absorbing aerosols, as indicated by the normal AAI values in the NAD (Figure 4.1b), in contrast to the lower values occurring on day 187 (Figure 4.1a). This is also apparent in the QTC images of the two days (Figure 4.1c-d). There is hazy air (light-white color) over NAD on day 195, and dust (light-brown color) on day 187. This particular case study also supports the choice of having visually detected the dust events using the QTC imagery, rather than using AOT only.

Figure 4.5b represents the clearest example of a significant phytoplankton increase 6-7 days after a dust event. The duration of this dust event over the Gulf of Lion (GLI) was several days. The day in which dust was last seen on the QTC images (July 6, 2001) is considered as the reference day (lag=0 days). Note that the complete

absence of data on the reference day indicates that, at a minimum, the region was 80% covered by dust.

The AOT levels begin to peak two days prior the reference day and reach a maximum of 0.25, then eventually return to pre-event values, though with greater daily variability. The corresponding MCHL time series has the same range of variability before and after the event for the week after the event, then starts to increase reaching double the initial value (from 0.075 to 0.15 mg m^{-3}) after two weeks.

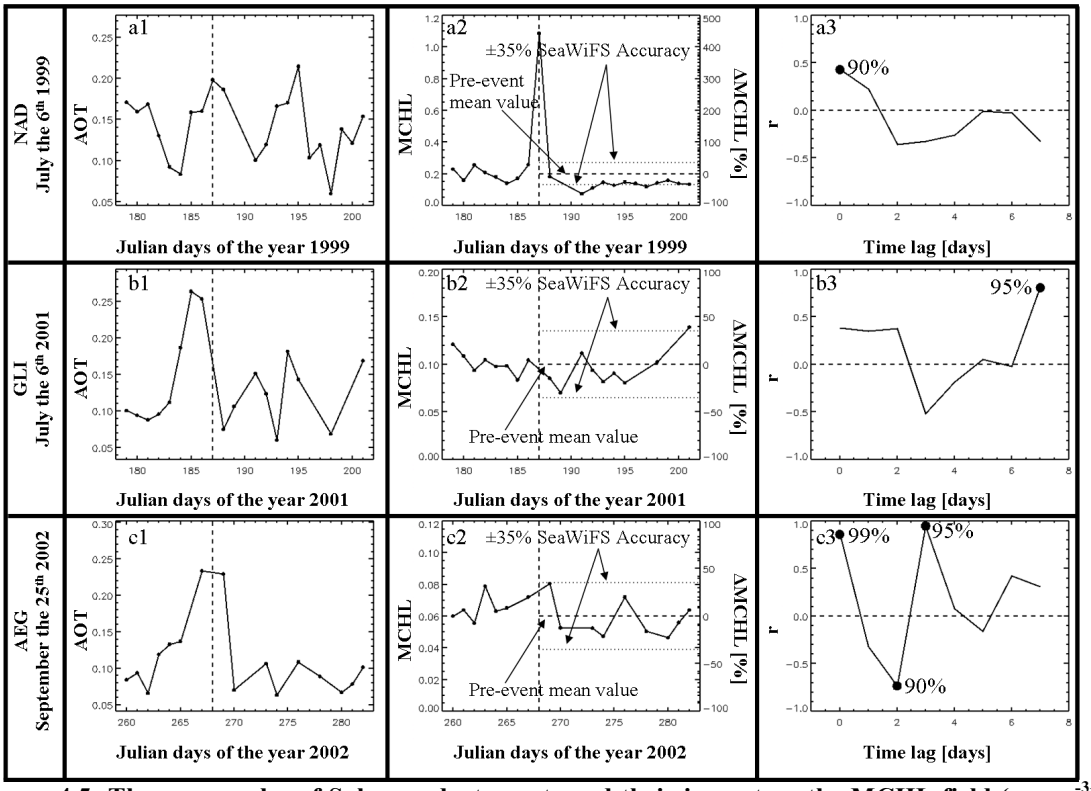

Figure 4.5: Three examples of Saharan dust events and their impact on the MCHL field (mg m^{-3}): (top row) significant MCHL response on the day of the dust event over NAD (6 July 1999: Day 187); (middle row) significant positive MCHL response several days after a dust event in GLI (6 July 2001: Day 187); (bottom row) significant but inconsistent MCHL response with r fluctuating between positive and negative signs in a matter of days in AEG (25 September 2002: Day 268). For each example the AOT time series (left column), MCHL time series (middle column), and the cross-correlation coefficient r between AOT and MCHL is shown as a function of time lag (days). Vertical dashed lines indicate the day of event. Also shown in the middle column is ΔMCHL (in percent on the right axis), the background pre-event MCHL average (dashed horizontal line), with the ±35% MedOC4 accuracy levels (dotted lines). On right panel, points where r is significant are labeled with the corresponding significance level of r. Note that unlabelled points are not significant.

The correlation coefficient r reaches 0.8 (95% level of confidence) at 7 days lag. Examination of the QTC images (not shown) verified that the smaller AOT peaks following the event are due to non-dust aerosols. The cloud patterns suggest a northern aerosol origin, indicating the arrival of mistral winds that can drive nutrient upwelling. Sea surface temperature images (not shown) for this period show a large patch of cold

water, verifying an upwelling occurrence in the GLI. Thus, the increase in MCHL is more likely due to this oceanographic process.

Figure 4.5c shows a dust event over the Aegean Sea on September 25, 2002 with ambiguous response. The AOT time series shows a two-day peak including the day of event with values (~0.23) much higher than previous and subsequent days (~0.07). Even if r shows significant values at 0, 2 and 3 days lag, the variability in the MCHL field is the same before and after the event, and the correlation shifts from a positive to a negative correlation within a 3-day period indicating a non-response.

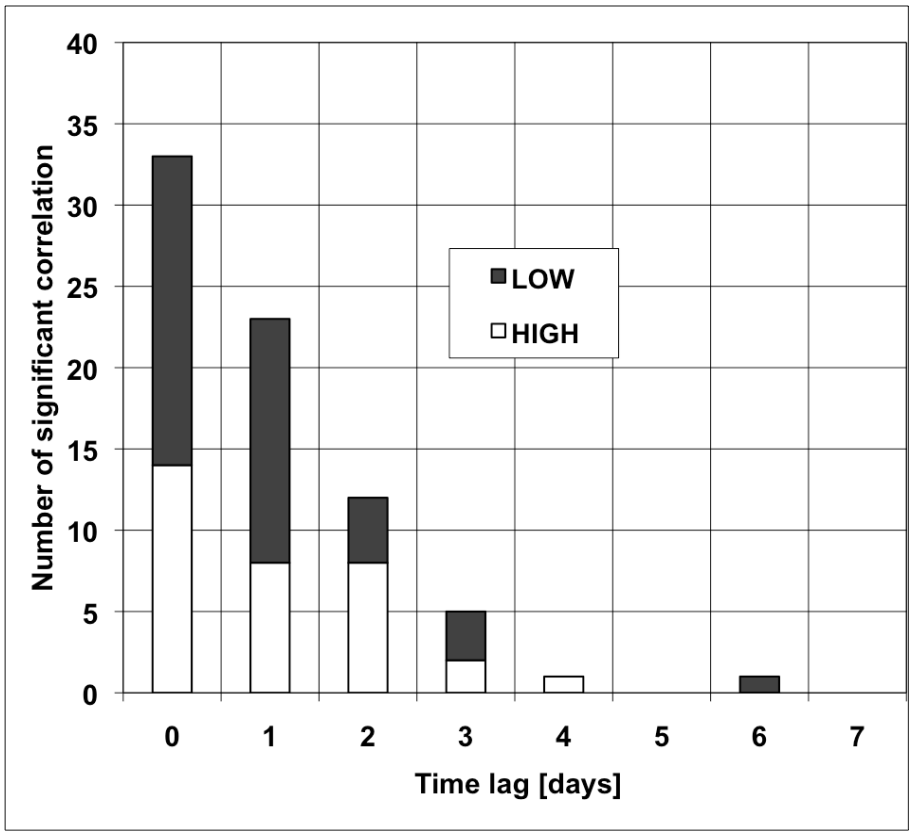

Figure 4.6: Occurrence of the significant positive r (at 95% confidence level, Student T-test) between MCHL and AOT as function of the time lag (days) for all 60 eligible events (see Section 4.2.3). Black (white) bars represent results for low (high) dynamics subregions.

Figure 4.6 summarizes the daily time series results, in terms of occurrence of significant correlation values (using a confidence level of 95%), as function of the time lag (in days), for 1) subregions with high dynamics (39 events; white bars), 2) low dynamics (21 events; black bars), and 3) all subregions (the sum of the two).

It is important to note that only 42% of the analyzed events exhibited a significant non-negligible response. For all areas, the most frequent result is a positive cross-correlation at zero lag (>30 occurrences). The occurrence of the negative correlation values is two or less for each time lag (not shown). Moreover, and even more

importantly, the number of positive correlations quickly decays within two days after the event, which is consistent with the Artifact Hypothesis. At temporal lags greater than two days, the total number of significant correlations is always low (<5). Although one would expect to find the difference between high and low dynamics areas due to the effect of physical processes on nutrient availability, the response of the MCHL field following a Saharan dust event was independent of this subdivision.

4.4 Discussion

In the MED where the phytoplankton community is strongly P- and/or N-limited, and Fe is relatively abundant, it has been suggested that atmospheric inputs of nutrients can have a significant impact on plant growth especially in the oligotrophic interior basin [e.g., *Guerzoni et al.,* 1999]. Several scientific projects have been designed to investigate this idea. The clearest demonstration of a positive response is provided by enrichment incubations where phytoplankton responded to dust additions within several days [*Bonnet et al.,* 2005]. At the other extreme, during a gyre-scale experiment, a massive P-addition (to simulate the enrichment effect of dust) did not result in a detectable chlorophyll increase [*Thingstad et al.,* 2005]. In other cases, weak or no chlorophyll response was observed following dust events [*Heussner et al.,* 2003; *Eker-Develi et al,* 2006].

We estimated whether dust events could result in a chlorophyll response that is detectable by satellite. The AOT levels can provide an order of magnitude estimate of the amount of dust deposited and the subsequent maximum potential MCHL increase. First, the dust load can be computed by dividing AOT by the light extinction cross section, σ [*Moulin et al.*, 1997]. For $\lambda = 550$ nm, σ is estimated to be roughly 0.79 m^2 g^{-1} [*Dulac et al.,* 1996]. This value can be used for the SeaWiFS AOT retrieved at 865 nm because dust absorption is stronger in the blue part of the spectrum, but weak and fairly constant above 500 nm [*Moulin et al.,* 2001]. Consider only 20% of dust load falls as dry deposition [*Guerzoni et al.,* 1999], and is mixed into the top 5 meters of the water column (converting from g m^{-2} to g m^{-3}). Measurements by *Guerzoni et al.* [1999] indicate that only 0.4% of dust is P, of which only 8% is bioavailable. Assuming Redfield stoichiometry to convert grams of P into grams of C (where C= P*(12/31)*106), and C:CHL=50, the expected MCHL (in mg m^{-3}) can be thus estimated by multiplying AOT by 34.14. For example, an AOT of 0.2 could potentially lead to a chlorophyll increase of up to 6.8 mg m^{-3}. Strong dust storms have AOT's higher than

0.2. In contrast to the very oligotrophic concentrations in the Mediterranean, a chlorophyll increase of this magnitude should be easy to detect. Assuming a background chlorophyll concentration of 0.04 mg m^{-3}, doubling to 0.08 mg m^{-3} would require only 1% deposition, all other factors being equal.

Taking advantage of the spatial and temporal resolution offered by frequent satellite observations, *Cropp et al.* [2005] analyzed the multi-year SeaWiFS dataset for correlations between chlorophyll and AOT to examine the Fe-fertilization effect on phytoplankton growth on a global basis. Here, we used SeaWiFS data only on the MED to test whether dust is important as a macronutrient source. We used the satellite data to investigate the phytoplankton-dust link on seasonal and weekly scales, but also to define the phytoplankton response time (in days) to the dust events, individually and as a population. The daily time-series analysis was especially important in order to differentiate between a true phytoplankton response (order of one week) versus a satellite data artifact due to inappropriate atmospheric correction (order 0-2 days).

The satellite view offers only an indication of presence of dust in the atmosphere. In the absence of any large-scale *in situ* measurements over the ocean, it was necessary to assume that deposition occurred and nutrients were bioavailable for each event. This assumption reflects the general knowledge of MED biogeochemistry. Frequent dust deposition occurs all over the MED and is associated with the arrival of African dust plumes [e.g., *Goudie and Middleton,* 2001; *Eker-Develi et al.,* 2006]. Increased dissolved N and P levels have been measured within a day after a dust event and continuing for many days [e. g., *Loye-Pilot and Martin,* 1996; *Heussner et al.,* 2003]. Due to the predominant meteorological conditions in the MED, atmospheric washout of dust particles is much more active in northern sectors [*Moulin et al.,* 1998; *Bergametti et al.,* 1989]. On the other hand, dry deposition is more important in the rest of the basin and can account for up to 80% of total deposition during summer [*Herut et al.,* 1999]. All these considerations indicate that a detectable chlorophyll response should be observable after deposition of a very small amount of dust.

Our AOT and dust event frequency maps match the general spatial pattern of measured dust deposition, as discussed above. On a seasonal basis, our results show that the spatial and temporal patterns of dust occurrence and phytoplankton biomass in the MED are not coupled because the annual chlorophyll cycle is strongly controlled by oceanographic processes. This is not in contradiction with other works since dust-derived nutrients are expected to be important during the stratified conditions (typically

summer). Moreover, as mentioned earlier, the phytoplankton response to such inputs is expected to be on the order of days, and thus would not be manifest on a seasonal scale but could produce episodic blooms [e.g., *Guerzoni et al.,* 1999; *Bonnet et al.,* 2005; *Eker-Develi et al.,* 2006]. The time scale of the phytoplankton response was clearly demonstrated in dust addition experiments by *Bonnet et al.* [2005] with an increase from 0.05 to 0.075 mg m^{-3} in 70 hours.

We found a strong correlation between phytoplankton and dust within a weekly timescale when the analysis is limited to the dusty season (May to September) in contrast to the negative correlations in the MED reported by *Cropp et al.* [2005] when data for the entire year were used. This indicates that the dust-phytoplankton link can be observed only during the stratified season and when Saharan dust is the predominant aerosol over the MED. Use of the residual time series further improved the correlation, but was not as critical as the effect of limiting the analysis to the dusty period.

An analysis based on weekly averages would not be able to distinguish for periods less than a week between immediate artifact and fertilization (several days delay) effects. Our strategy was to examine the behavior of chlorophyll following each summer dust event (indicated by high AOT and dust visible in QTC). Isolated dust events were chosen to clearly separate a fertilization event from a response due to incomplete atmospheric correction. A time window criteria (7 days prior and 14 days following a dust event) was also applied to select single events. As previously mentioned, the literature suggests that in the MED, dust fertilization leads to a response within a week. Thus the choice of 0-7 days lag should be sufficient to observe a fertilization response. The 7 days prior allows us to establish a pre-event baseline value. The analysis was performed using subregional averages that represented oceanographically homogeneous areas, at the expected phytoplankton response scale to dust. In fact, the high-resolution (1/16 degree) weekly correlation map shows homogeneous areas of similar correlation values at scales compatible with the subregions (Figure 4.4d). Additionally, the use of regional averages increases the opportunity to obtain a gapless time series. By applying these criteria, we obtained 60 events that permit a clear discrimination between potential dust fertilization and incomplete atmospheric correction.

From the lagged time series analysis, the most common result (about 60% of the time) was a non-response. These results are in agreement with the findings of the ADIOS project that conducted a year of *in situ* experiments during our study period

[*Heussner et al.,* 2003]. ADIOS results measured Saharan dust deposition, but found no subsequent phytoplankton response. Among the significant cross correlation results, the dominant result was a positive response at 0-2 days lag (Figure 4.6), which supports the artifact hypothesis. We had expected a major impact in low dynamics areas where nutrient-limitation is more important. However, no difference between the low and high-dynamic regimes was found.

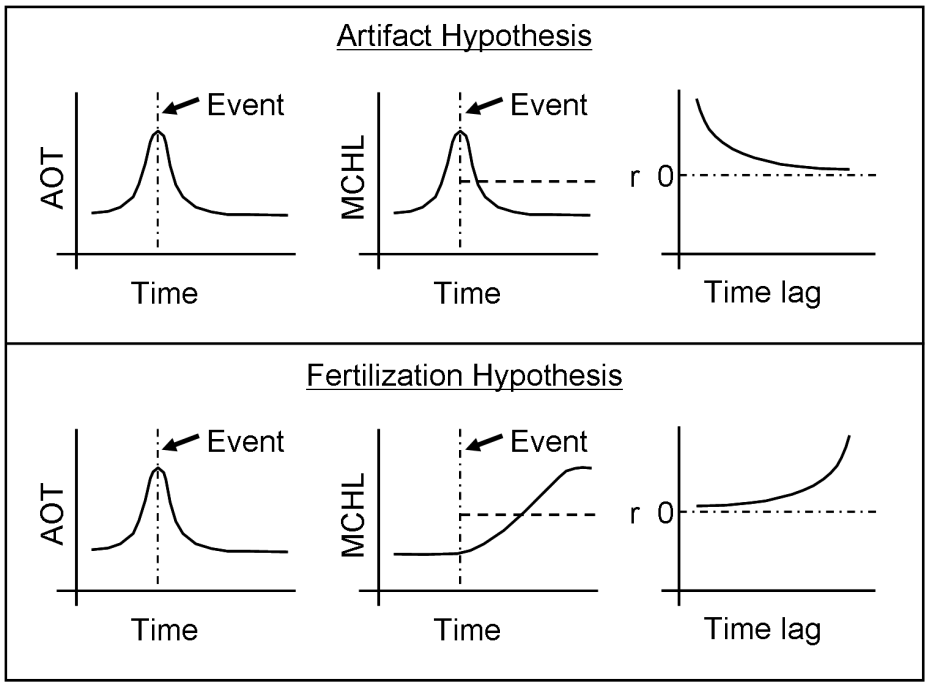

Figure 4.7: Schematics of the expected time series for AOT, CHL and correlation coefficient (r) for the artifact (top panel) and fertilization (bottom panel) hypotheses. Dashed lines in correspondence of the MCHL fields, and starting from the day of event indicate an approximately mean value when averaging over one week time.

We examined the patterns in the individual time series in the context of a schematic diagram (Figure 4.7). The dust event is marked by an increase in AOT and qualified with QTC (Figure 4.7a). Since with the artifact hypothesis, the apparent chlorophyll increase is due to incomplete satellite dust compensation, a chlorophyll increase occurs concurrently with the AOT, with a residual effect that can last up to two days after the dust event (Figure 4.7b). Thus, the highest r occurs at time lag 0 (Figure 4.7c,), and some significant correlations may be detected in the next 2 days due to residual dust presence in the atmosphere or water column that may not be detected by SeaWiFS processing flag tests [*Claustre et al.,* 2002]. In contrast, when fertilization occurs, the chlorophyll response lags the AOT peak (Figure 4.7d, Dust Fertilization) by several days and shows a gradual increase consistent with phytoplankton growth, and the r peaks at the timescale of the chlorophyll response (Figure 4.7e-f).

When we observed a positive dust fertilization response in our time series results, we found that the chlorophyll increase could be ascribed to other oceanographic forcing (e.g., upwelling; section 4.4) or do not exhibit a coherent response (fluctuating up and down at the baseline level; Figure 4.5c). In contrast, the artifact response at ≤2 days lag was a very clear signal, with a peak at 0 days and decreasing correlation for the next two days. These daily results suggest that in dust-impacted regions, the incorporation of chlorophyll data within two days following a dust event will introduce spurious results into weekly averages. That is, the chlorophyll average for the week that includes the dust event will probably have a positive bias.

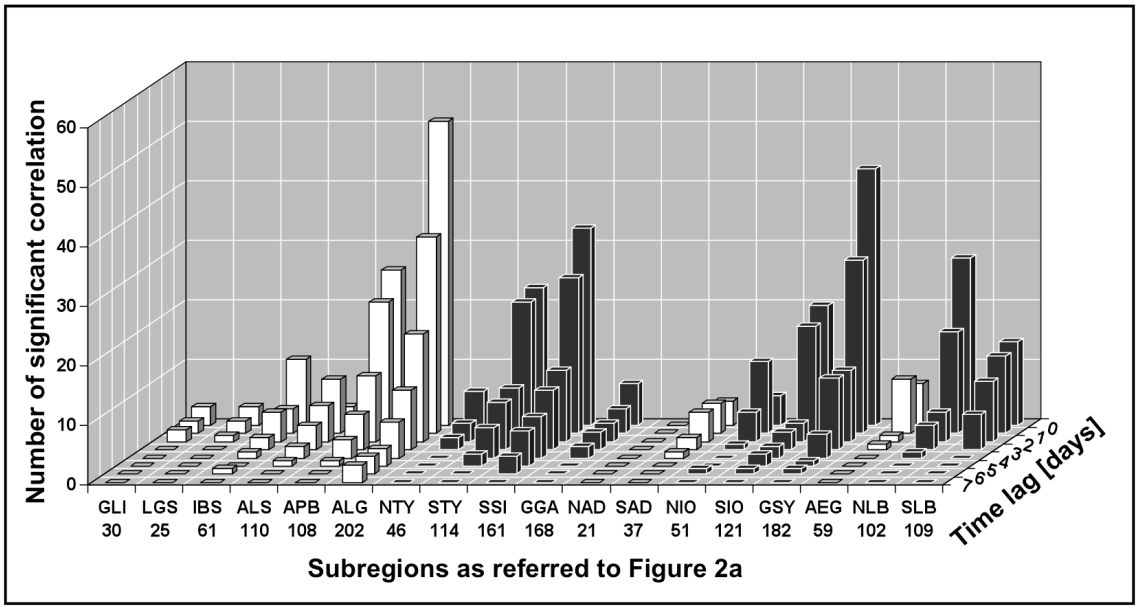

Figure 4.8: Occurrence of the significant positive correlations (at 99% confidence level, Student T-test) between MCHL and AOT as function of both subregions (x-axis) and the time lag (in days; y-axis). The number of events for each subregion is indicated below each label, on the x-axis. Black and white bars represent results for low and high dynamics subregions (as referred to Figure 4.2a).

We applied the selection criteria in anticipation of observing a fertilization effect, but instead we found that the zero temporal lag artifact effect was dominant. To determine the predominance of the artifact effect and whether the fertilization effect was not detected because of cases eliminated by applying the selection criteria, we examined all the dust events independent of whether they met the single events selection criteria. Furthermore, to test whether the confidence level was crucial in the analysis, we computed the occurrence of the significant correlation values as function of the time lag (in days) using different confidence levels (90% to 99%). The results did not change drastically, and are reported relative to the 99% in Figure 4.8. The most important result is that when dust aerosols were present, a maximum correlation at zero temporal lag was observed (Figure 4.8).

The occurrence of significant r mirrors that seen in Figure 4.6. In most of the subregions, independent of the number of respective dust events, we observed a maximum frequency of positive correlations at 0 temporal lag, with a sharp decrease in frequency for the next 2-3 days. This trend is mostly evident for the Algerian basin (ALG), the south Tyrrhenian Sea (STY), the Sicily Channel (SSI), in the Gulf of Sydra (GSY) and in the northern Levantine Basin (NLB). Some subregions such as North Adriatic (NAD), the Gulf of Lions (GLI) and Ligurian Sea (LGS) exhibit a very low number of significant correlation occurrences, probably due to the very limited number of events (not exceeding 30). Thus, to have confidence in a satellite-observed chlorophyll increase in response to dust fertilization, it is necessary to exclude the first 2 days following the dust event. It is obvious that our weekly analysis results are dominated by the artifact effect, particularly because the observed increases in chlorophyll tend to be more than 100% of the background value, dominating the weekly average. Furthermore, if there was any phytoplankton response within 0-2 days after a dust event, it would not be possible to deconvolve it from the aliased signal. However, it would be reasonable to expect that a chlorophyll increase would persist beyond 2 days.

4.5 Conclusions

The dust fertilization hypothesis in an LNLC region was investigated using a multi-year satellite dataset consisting of quasi-true color, aerosol optical thickness (AOT) and chlorophyll (MCHL) fields. A regional empirical algorithm (MedOC4) was used to provide realistic chlorophyll values for the Mediterranean Sea. The AOT observations were qualified by a careful visual inspection of quasi-true color images to validate the presence of dust. Different space and time scales were used to investigate the phytoplankton-dust coupling and the outcome of a population of dust events was examined. Strong coupling between phytoplankton and dust had been detected on a weekly, but not on a seasonal scale. Analysis of daily AOT and MCHL time series allowed us to distinguish between artifact hypothesis (chlorophyll increase within 0-2 days after a dust event (Figure 4.7, Artifact Hypothesis)) and the dust fertilization hypothesis (chlorophyll increase after >3 days (Figure 4.7, Fertilization Hypothesis)). As demonstrated by this analysis, the strong positive correlation found at weekly scales is likely due to atmospheric correction failure in disqualifying dusty pixels close to the dust plumes, and that such biases can easily propagate to averages over longer periods if

dust events are very frequent. Therefore, an important point of this paper is that the present SeaWiFS (and MODIS as well since the same algorithm is used) atmospheric and in-water products should not be used to test a dust fertilization hypothesis without careful consideration of the limitations, i.e., the current atmospheric correction scheme does not include any models that represent Saharan dust aerosols. Thus, it is not surprising that, like OC4v4, MedOC4 is susceptible to bias caused by absorbing aerosol presence. Although dust fertilization has been claimed to play a role in climate by supplying nutrients to surface oceanic waters and therefore stimulating phytoplankton growth, we found that this does not apply to the Mediterranean Sea. Whether our results could be extended to all LNLC regions of the world ocean requires further investigation. In this context, if satellite data are to be used, in order to correctly interpret the results, one should not use standard weekly products. Thus, we have determined that when dust is present, one must exclude data from the initiation of the event to 2 days following the termination of the event. In dust-affected areas, the use of standard weekly products will lead to an incorrect interpretation. Pending routine availability of absorbing aerosol corrected chlorophyll fields, application of SeaWiFS ocean color observation to problems such as observing a dust fertilization event is possible if sufficient care is exercised to exclude contaminated retrievals from the observation time series.

5 Conclusions

This chapter presents and summarizes the main achievements of this thesis. The scientific questions that have been addressed within this study are:

- **What is the phytoplankton space-time variability in the Mediterranean Sea, and what are the space and time scales of influence by physical surface conditions?**
- **Does the Dust Fertilization Hypothesis hold in the Mediterranean?**
- **How accurate is the retrieval of ocean colour products over the basin?** Which, from a technical remote sensing point of view, can be also read as**: by how much and why does the Mediterranean bio-optical regime differ from the global ocean?**

These scientific questions required technical issues to be addressed. One of the key points of this thesis was concerned with the reliability of both atmospheric and oceanic ocean colour products over the MED. In particular, the uncertainties in the retrieval of satellite surface chlorophyll concentrations have been evaluated using both regional and global ocean colour algorithms. In the MED region, where standard algorithms were demonstrated to be inappropriate, there has been the need for defining the most suitable ocean colour algorithm for an accurate, unbiased assessment of the phytoplankton dynamics. Using a large set of coincident *in situ* optical and chlorophyll measurements, covering most of the trophic regimes of the basin, two existing regional algorithms and a global algorithm were validated. In this work, the global product was confirmed to be very sensitive to the geographical distribution of the *in situ* data collected for building up the algorithm. In fact, only a few data were collected in the Mediterranean Sea, so that this basin results poorly represented within the global dataset, and hence the derived algorithm is unable to reproduce accurately the chlorophyll field. On the other hand, the two regional algorithms, if on one side performed better than the global one, on the other showed uncertainties dependent on the chlorophyll value itself. The analysis of the largest *in situ* bio-optical dataset ever used for the Mediterranean area, indicated then the need and implicitly suggested the means for developing a new regional algorithm for the Mediterranean Sea: the

MedOC4. The implementation of this algorithm over SeaWiFS-derived Rrs data confirmed that, among the four, the MedOC4 is the best algorithm matching the requirement of unbiased satellite chlorophyll estimates thus improving the accuracy of the satellite chlorophyll retrieval. This result enabled the MedOC4 to be adopted as standard algorithm in the ocean colour processing chain at the Group for Satellite Oceanography at the Institute of Atmospheric and Climate Science of the Italian National Research Council. The results of this piece of work encouraged for a similar analysis for qualifying the oceanic products of both MODIS and MERIS [as summarized in *Santoleri et al.*, 2008].

Several hypothesis have been tested in order to address the question about the difference between the MED and the global ocean bio-optical signatures; differences that might reflects different methodological approaches in building up the databases from which the algorithms have been derived; or due to differences in the inherent bio-optical properties of the two domains. The formers (i.e., different methodological approaches) have been demonstrated to introduce negligible uncertainties as compared to the order of magnitude difference between the two domains. Therefore, it appears that the Mediterranean is distinguished for its peculiar bio-optical characteristics from the global ocean. The attempt to characterize the two-domain Rrs spectral patterns (SeaBAM, i.e., global, and MED), for different chlorophyll ranges, led to the quantification of such a difference. Thus, on one side, the two datasets do not include the necessary information for actually answering the question as to why the MED and the global ocean exhibit different bio-optical regime. On the other hand, the two datasets, along with the performed analysis, do offer a quantitative estimate of the difference between the two domains, providing a solid baseline and a guidance into the range of variability and applicability for future research.

The reprocessing of nine years of SeaWiFS data (1998-2006) using the new algorithm (MedOC4) allowed for a consistent and uniform dataset to be used for answering the thesis scientific questions. Thus, the investigation of the phytoplankton space-time variability and its dependence on physical processes was possible through the minimization of the satellite ocean colour data uncertainties (from more than ~100% to ~35%). The physical forcings under study were the ocean circulation dynamics and the aeolian dust input of nutrients, along with their space and temporal scales of variability and their contribution in determining the nutrient availability in the upper

layer of the water column. The space-time variability of the ocean circulation dynamics and its effect onto the phytoplankton dynamics has been addressed by investigating the SST (sea surface temperature) and the MADT (Mediterranean absolute dynamics topography) fields. These are the best proxies, measurable at a space and time resolution compatible with the ocean colour sampling, for water column stratification and to a lesser extent of the mixed layer dynamics, and of the surface circulation dynamics, respectively. Similarly, it was demonstrated within this thesis that, under certain conditions, both AOT (aerosol optical thickness) and QTC (quasi true-colour) SeaWiFS-derived products are good proxies for the estimation of the columnar dust load. Thus these products are suited for the estimation of the contribution by the atmospheric dust deposition to the phytoplankton dynamics in the basin. The impact by these potentially physical forcings (e.g., ocean circulation, water column stratification, and the mixed layer dynamics) have been treated separately from the atmospheric dust input for two main reasons; first, because the occurrence of dust events have a sporadic nature [*Guerzoni et al.*, 1997], with one or few of them dominating the total dust fall out by supplying a large fraction (up to 40%) of the annual atmospheric deposition [*Ternon et al.*, 2010]. Second, and strictly connected to the previous point, as ocean colour data essentially refer to the observation of the marine surface being not meant for atmospheric data collection, some caveats have to be used before analysing the entire time series on a statistical basis.

This study demonstrated that, depending on the scales of investigation, the phytoplankton dynamics is subject to a variety of mechanisms forced by different physical processes. So far, it appears that the phytoplankton dynamics is mainly driven by the surface layer thermal stratification at basin and seasonal scales. The inverse relationship between phytoplankton abundance and the SST field finds its rationale in the tight coupling between the SST and the mixed layer depth dynamics at seasonal temporal scale. Intuitively, the SST can be considered as a good proxy of the mixed layer temperature only if one does not consider the short term variability of the uppermost micro-layer of the water column which is more susceptible to the atmospheric forcings (i.e., wind gusts) which are unable to influence through mixing the whole surface mixed layer. In the present analysis the influence of such a small scale of variability was filtered out by considering weekly fields. These fields were also used for investigation of the phytoplankton dynamics on a longer than seasonal time scale.

This latter analysis showed that prolonged, episodic and extreme events such as the particularly cold winter and the summer heat wave, in 1998/1999 and 2003 respectively, also play an important role in determining phytoplankton abundance variability at the scale of sub-basin, determining the above-mentioned inverse relationship, with high phytoplankton concentration in correspondence of cold periods.

An important finding of this work is concerned with the response of phytoplankton to changes in the surface geostrophic circulation. A significant circulation change occurred between 2003 and 2006 in the Algerian basin. Such a change consisted in a northward shift of the eastward flux of the Atlantic-origin water. One of the main implications is that a reduced amount of relatively nutrient-rich water reaches the Tyrrhenian Sea. At the same time, a northward shift of the Mid-Mediterranean Jet occurred in the centre of the Ionian Sea, resulting in an overall decrease of its cyclonic circulation. Within this work, it was hypothesized that such a decrease of the cyclonic circulation might have induced a deepening of the nutricline in the centre of the Ionian Sea, resulting in a decrease of nutrient availability in the area. Phytoplankton dynamics coherently display a long-term decrease in the whole central MED. The phytoplankton long-term variability is out-of-phase by one year with respect to this pattern of circulation variability, shedding light on the coupling between surface circulation and biological response at interannual time scales.

One of the challenges of this study was to assess the effectiveness and feasibility of using ocean colour data for investigating the impact of the atmospheric nutrients deposition on the phytoplankton dynamics of the basin: both technical and scientific issues. The dust fertilization has been claimed to play a role in climate by supplying nutrients to surface oceanic waters, thence stimulating phytoplankton growth. Here, the Dust Fertilization Hypothesis (DFH) in an LNLC region was investigated using five years of SeaWiFS quasi-true colour, aerosol optical thickness (AOT) and chlorophyll (CHL, MedOC4 algorithm) fields. The AOT observations were qualified by a careful visual inspection of quasi-true colour images to validate the presence of dust. Different space and time scales were used to investigate the phytoplankton-dust coupling and the outcome of a population of dust events was examined. Strong coupling between phytoplankton and dust had been detected on a weekly, but not on a seasonal scale indicating that:

1. the ocean interior is the main source of nutrient, even during stratified conditions, when the atmospheric source were thought to play a major role in the regulation of phytoplankton dynamics.
2. The bioavailability of the dust nutrient content remains to be a crucial aspect.
3. The main point, when using ocean colour data, is to distinguish between artefact hypothesis and DFH.

As demonstrated, the strong positive correlation found at weekly scales is likely due to atmospheric correction failure in disqualifying dusty pixels close to the dust plumes, and that such biases can easily propagate to averages over longer periods if dust events are very frequent. Therefore, the present SeaWiFS (and MODIS, since the same atmospheric correction scheme is used) atmospheric and in-water products cannot be used to test a dust fertilization hypothesis without careful consideration of the limitations, i.e., the current atmospheric correction scheme does not include any models that represent Saharan dust aerosols. However, since the analysis was performed on a statistical basis, considering all possible dust events over a five-year period, the important finding of this piece of work is that the DFH does not hold in the MED Sea, at least at the space and time scales that have been considered. The effectiveness of this result might be confuted by an analysis of nutrient budget with a biogeochemical modelling approach, which looks the only way of effectively investigating the fate of such nutrients and how they influence the biogeochemistry of the basin. Whether this result could be extended to all LNLC regions of the world ocean requires further investigation, which have to take account of the limitations highlighted by this study. Finally, as already pointed out the Mediterranean Sea has demonstrated to be an excellent site for testing both the DFH and the physical-biological coupling at different temporal and spatial scales.

6 Bibliography

Alpert, P., B. U. Neeman, and Y. Shay-el (1990), Climatological analysis of Mediterranean cyclones using ECMWF data, Tellus, 42, A, 65-77.

Alvain, S., C. Moulin, Y. Dandonneau, and F. M. Breon (2005), Remote sensing of phytoplankton groups in case 1 waters from global SeaWiFS imagery, Deep-Sea Research Part I-Oceanographic Research Papers, 52, 11, 1989-2004.

Alvain, S., C. Moulin, Y. Dandonneau, H. Loisel, and F. M. Breon (2006), A species-dependent bio-optical model of case I waters for global ocean color processing, Deep-Sea Research Part I-Oceanographic Research Papers, 53, 5, 917-925.

Antoine, D., A. Morel, and J. M. Andre (1995), Algal Pigment Distribution and Primary Production in the Eastern Mediterranean as Derived from Coastal Zone Color Scanner Observations, Journal of Geophysical Research-Oceans, 100, C8, 16193-16209.

Antoine, D., and D. Nobileau (2006), Recent increase of Saharan dust transport over the Mediterranean Sea, as revealed from ocean color satellite (SeaWiFS) observations, JOURNAL OF GEOPHYSICAL RESEARCH-ATMOSPHERES, 111, D12.

Astraldi, M., S. Balopoulos, J. Candela, J. Font, M. Gacic, G. Gasparini, B. Manca, A. Theocharis, and J. Tintoré (1999), The role of Straits and channels in understanding the characteristics of Mediterranean circulation, Progress in Oceanography, 44, 65-108.

Baith, K., R. Lindsay, G. Fu, and C. R. McClain (2001), SeaDAS: Data Analysis System Developed for Ocean Color Satellite Sensors, EOS Transactions, 82, 18, 202.

Barale, V., J. M. Jaquet, and M. Ndiaye (2008), Algal blooming patterns and anomalies in the Mediterranean Sea as derived from the SeaWiFS data set (1998-2003), Remote Sensing Of Environment, 112, 3300-3313.

Beckers, J. M., A. Barth, and A. Alvera-Azcárate (2006), DINEOF reconstruction of clouded images including error maps - application to the Sea-Surface Temperature around Corsican Island, Ocean Science, 2, 183-199.

Beckers, J. M., and M. Rixen (2003), EOF calculations and data filling from incomplete oceanographic datasets, J. Atmos. Oceanic Tech., 20, 12, 1839-1856.

Behrenfeld, M., R. T. O'Malley, D. Siegel, C. McClain, J. L. Sarmiento, G. C. Feldman, A. J. Milligan, P. Falkowski, R. Letelier, and E. Boss (2006), Climate-driven

trends in contemporary ocean productivity, Nature, 444, 752-755, doi:710.1038/nature05317.

Behrenfeld, M. J., J. T. Randerson, C. R. McClain, G. C. Feldman, S. O. Los, C. J. Tucker, P. G. Falkowski, C. B. Field, R. Frouin, W. E. Esaias, D. D. Kolber, and N. H. Pollack (2001), Biospheric primary production during an ENSO transition, Science, 291, 5513, 2594-2597.

Béranger, K., L. Mortier, and M. Crépon (2005), Seasonal variability of water transport through the Straits of Gibraltar, Sicily and Corsica, derived from a high-resolution model of the Mediterranean circulation, Progress in Oceanography, 66, 2-4, 341-364.

Bergametti, G., A.-L. Dutot, P. Buat-Ménard, R. Losno, and E. Remoudaki (1989), Seasonal variability of the elemental composition of atmospheric aerosol particles over the northwestern Mediterranean, Tellus, 41, B, 353-361.

Berthon, J. F., G. Zibordi, and S. B. Hooker (2000), Marine optical measurements of a mucilage event in the northern Adriatic Sea, Limnology and Oceanography, 45, 2, 322-327.

Bethoux, J. P. (1979), Budgets of the Mediterranean Sea. Their dependence on the local climate and on the characteristics of the Atlantic waters, Oceanologica Acta, 2, 157-163.

Bonnet, S., C. Guieu, F. Bruyant, O. Prasil, F. Van Wambeke, P. Raimbault, T. Moutin, C. Grob, M. Y. Gorbunov, J. P. Zehr, S. M. Masquelier, L. Garczarek, and H. Claustre (2008), Nutrient limitation of primary productivity in the Southeast Pacific (BIOSOPE cruise), BIOGEOSCIENCES, 5, 1, 215-225.

Bonnet, S., C. Guieu, J. Chiaverini, J. Ras, and A. Stock (2005), Effect of atmospheric nutrients on the autotrophic communities in a low nutrient, low chlorophyll system, Limnology and Oceanography, 50, 6, 1810-1819.

Bosc, E., A. Bricaud, and D. Antoine (2004), Seasonal and interannual variability in algal biomass and primary production in the Mediterranean Sea, as derived from 4 years of SeaWiFS observations, Global Biogeochemical Cycles, 18, 1.

Bricaud, A., E. Bosc, and D. Antoine (2002), Algal biomass and sea surface temperature in the Mediterranean Basin - Intercomparison of data from various satellite sensors, and implications for primary production estimates, Remote Sensing of Environment, 81, 2-3, 163-178.

Broecker, W. (1995), Chaotic Climate, Scientific American, November, 62-68.

Buongiorno Nardelli, B., O. Cavalieri, M.-H. Rio, and R. Santoleri (2006), Subsurface geostrophic velocities inference from altimeter data: application to the Sicily Channel (Mediterranean Sea), JOURNAL OF GEOPHYSICAL RESEARCH, 111, C04007, doi:10.1029/2005JC003191.

Buongiorno Nardelli, B., and R. Santoleri (2004), Reconstructing synthetic profiles from surface data, J. Atmos. Oceanic Tech., 21, 4, 693-703.

Buongiorno Nardelli, B., and R. Santoleri (2005), Methods for the reconstruction of vertical profiles from surface data: multivariate analyses, residual GEM and variable temporal signals in the North Pacific Ocean, J. Atmos. Oceanic Tech., 22, 11, 1763-1782.

Buongiorno Nardelli, B., S. Sparnocchia, and R. Santoleri (2001), Small mesoscale features at a meandering upper ocean front in the western Ionian Sea (Mediterranean Sea): vertical motion and potential vorticity analysis, Journal of Physical Oceanography, 31, 8, 2227-2250.

Burlando, M. (2009), The synoptic-scale surface wind climate regimes of the Mediterranean Sea according to the cluster analysis of ERA-40 wind fields, Theoretical and Applied Climatology, 96, 69–83 DOI 10.1007/s00704-00008-00033-00705.

Campbell, J. W. (1995), The Lognormal-Distribution as a Model for Biooptical Variability in the Sea, Journal of Geophysical Research-Oceans, 100, C7, 13237-13254.

Casotti, R., A. Landolfi, C. Brunet, F. D'Ortenzio, O. Mangoni, M. Ribera d'Alcala, and M. Denis (2003), Composition and dynamics of the phytoplankton of the Ionian Sea (eastern Mediterranean), Journal of Geophysical Research, 108, C9, 8116.

Civitrese, G., and M. Gacic (2001), Had the Eastern Mediterranean Transient an impact on the new production in the southern Adriatic? Geophysical Research Letters, 28, 8, 1627–1630.

Clark, D. K. (1997), Bio-optical algorithms-Case 1 waters. MODIS algorithm theoretical basis document 19.

Claustre, H., A. Morel, S. B. Hooker, M. Babin, D. Antoine, K. Oubelkheir, A. Bricaud, K. Leblanc, B. Queguiner, and S. Maritorena (2002), Is desert dust making oligotrophic waters greener? Geophysical Research Letters, 29, 10, art. no.-1469.

Cox, P. M., R. A. Betts, Jones C. D., Spall S. A., and T. I. J. (2000), Acceleration of global warming due to carbon-cycle feedbacks in a coupled climatemodel, Nature, 408, 184-187.

Crise, A., J. I. Allen, J. Baretta, G. Crispi, R. Mosetti, and C. Solidoro (1999), The Mediterranean pelagic ecosystem response to physical forcing, Progress in Oceanography, 44, 1-3, 219-243.

Cropp, R. A., A. J. Gabric, G. H. McTainsh, and R. D. Braddock (2005), Coupling between ocean biota and atmsopheric aerosols: Dust, dimethylsulphide, or artifact? Global Biogeochem. Cycles, 19, GB4002, doi:10.1029/2004GB002436.

Cushing, D. H. (1975), Marine ecology and Fisheries, 278 pp., Cambridge Univ. Press, London.

D'Ortenzio, F., D. Iudicone, C. de Boyer Montegut, P. Testor, D. Antoine, S. Marullo, R. Santoleri, and G. Madec (2005), Seasonal variability of the mixed layer depth

in the Mediterranean Sea as derived from in situ profiles, Geophysical Research Letters, 32, L12605, doi:10.1029/2005GL022463.

D'Ortenzio, F., S. Marullo, M. Ragni, M. R. d'Alcala, and R. Santoleri (2002), Validation of empirical SeaWiFS algorithms for chlorophyll- alpha retrieval in the Mediterranean Sea - A case study for oligotrophic seas, Remote Sensing of Environment, 82, 1, 79-94.

D'Ortenzio, F., M. Ragni, S. Marullo, and M. R. d'Alcala (2003), Did biological activity in the Ionian Sea change after the Eastern Mediterranean Transient? Results from analysis of remote sensing observations, Journal of Geophysical Research-Oceans, 108, C9, 8113, doi:8110.1029/2002JC001556.

D'Ortenzio, F., and M. Ribera d'Alcala (2009), On the trophic regimes of the Mediterranean Sea: a satellite analysis, Biogeosciences, 6, 139-148.

Dandonneau, Y., P. Y. Deschamps, E. Nicolas, H. Loisel, J. Blanchot, Y. Montel, F. Thieuleux, and G. Bécu (2004), Seasonal and interannual variability of ocean color and composition of phytoplankton communities in the North Atlantic, Equatorial Pacific and South Pacific, Deep-Sea Research Part II, 51, 303-318.

Darecki, M., and D. Stramski (2004), An evaluation of MODIS and SeaWiFS bio-optical algorithms in the Baltic Sea, Remote Sensing Of Environment, 89, 3, 326-350.

Doney, S. C. (2006), Plankton in a warmer world, Nature, 444, 695-696.

Ducet, N., P. Y. Le Traon, and G. Reverdin (2000), GLobal high-resolution mapping of ocean circulation from TOPEX/Poseidon and ERS-1 and -2, JOURNAL OF GEOPHYSICAL RESEARCH-OCEANS, 105, C8, 19477-19498.

Dulac, F., C. Moulin, C. E. Lambert, F. Guillard, J. Poitou, W. Guelle, C. R. Quetel, X. Schneider, and U. Ezat (1996), Quantitative remote sensing of African dust transport to the Mediterranean, in The Impact of Desert Dust across the Mediterranean, edited by S. Guerzoni and R. Chester, pp. 25-49, Kluwer Academic Publisher.

Eker-Develi, E., A. E. Kideys, and S. Tugrul (2006), Role of Saharan dust on phytoplankton dynamics in the northeastern Mediterranean, Marine Ecology-Progress Series, 314, 61-75.

Engelstaeter, S., I. Tegen, and R. Washington (2006), North African dust emissions and trasport, Earth Science Reviews, 79, 73-100.

Field, C. B., M. J. Behrenfeld, J. T. Randerson, and P. G. Falkowski (1998), Primary production of the biosphere: Integrating terrestrial and oceanic components., Science Of The Total Environment, 281, 237-240.

Follows, M., and S. Dutkiewicz (2001), Meteorological modulation of the North Atlantic spring bloom, Deep-Sea Research Part II, 49, doi:10.1016/S0967-0645(01)00105-9, 321-344.

Font, J., P. Puig, J. Salat, A. Palanques, and M. Emelianov (2007), Sequence of hydrographic changes in NW Mediterranean deep water due to the exceptional winter of 2005, Scientia Marina, 71, 2, 339-346.

Fougnie, B., P. Y. Deschamps, R. Frouin, and B. G. Mitchell (1998), Measuring water-leaving radiance with a polarization radiometer: Theory and experimental verification, EOS Transactions, 79, 1, 99.

Garcia, C. A. E., V. M. T. Garcia, and C. R. McClain (2005), Evaluation of SeaWiFS chlorophyll algorithms in the Southwestern Atlantic and Southern Oceans, Remote Sensing of Environment, 95, 125-137.

Gitelson, A., A. Karnieli, N. Goldman, Y. Z. Yacobi, and M. Mayo (1996), Chlorophyll estimation in the Southeastern Mediterranean using CZCS images: Adaptation of an algorithm and its validation, Journal of Marine Systems, 9, 3-4, 283-290.

Gordon, H. R. (1997), Atmospheric correction of ocean color imagery in the Earth Observing System era, Journal of Geophysical Research, 102, 17,081-017,106.

Gordon, H. R., and D. K. Clark (1981), Clear water radiances for atmospheric correction of coastal zone color scanner imagery, Applied Optics, 20, 4175-4180.

Gordon, H. R., T. Du, and T. Zhang (1997), Remote sensing of ocean color and aerosol properties: resolving the issue of aerosol absorption, Applied Optics, 36, 8670-8684.

Gordon, H. R., and M. Wang (1994), Retrieval of water leaving radiance and aerosol optical thickness over the oceans with seawifs: a preliminary algorithm., Applied optics, 33, 3, 443-458.

Goudie, A. S., and N. J. Middleton (2001), Saharan dust storms: nature and consequences, Earth-Science Reviews, 56, 179-204.

Gregg, W. W., and N. W. Casey (2004), Global and regional evaluation of the SeaWiFS chlorophyll data set, Remote Sensing Of Environment, 93, 4, 463-479.

Gregg, W. W., M. E. Conkright, P. Ginoux, J. E. O'Reilly, and N. W. Casey (2003), Ocean primary production and climate: Global decadal changes, Geophysical Research Letters, 30, 15, art. no.-1809.

Guerzoni, S., R. Chester, F. Dulac, B. Herut, M. D. Loye-Pilot, C. Measures, C. Migon, E. Molinaroli, C. Moulin, P. Rossini, C. Saydam, A. Soudine, and P. Ziveri (1999), The role of atmospheric deposition in the biogeochemistry of the Mediterranean Sea, Progress in Oceanography, 44, 147-190.

Guerzoni, S., E. Molinaroli, and R. Chester (1997), Saharan dust inputs to the western Mediterranean Sea: depositional patterns, geochemistry and sedimentological implications, Deep Sea Research II, 44, 3-4, 631-654.

Guieu, C., M. D. Loye-Pilot, C. Ridame, and C. Thomas (2002), Chemical characterization of the Saharan dust end-member: Some biogeochemical

implications for the western Mediterranean Sea, Journal of Geophysical Research-Atmospheres, 107, D15.

Henson, A. S., P. J. Dunne, and J. L. Sarmiento (2009), Decadal variability in North Atlantic phytoplankton blooms, Journal of Geophysical Research, 114, C04013, doi:10.1029/2008JC005139.

Herut, B., M. D. Krom, G. Pan, and R. Moritimer (1999), Atmospheric inputs of nitrogen and phosphorus to the SE Mediterranean: sources, fluxes and possible impact, Limnology and Oceanography, 44, 1683-1692.

Heussner, S., and ADIOS Partners (2003), Atmospheric Deposition and Impact of pollutants and key elements and nutrients on the Open Mediterranean Sea (ADIOS), Atmospheric deposition and impact of pollutants, key elements and nutrients on the open mediterranean sea (ADIOS), 99 pp, Centre National de la Recherche Scientifique, Perpignan, France.

Hooker, S. B., C. R. McClain, J. K. Firestone, T. L. Westphal, E.-n. Yeh, and Y. Ge (1994), The SeaWiFS Bio-optical Archive and Storage System, 40 pp, NASA Goddard Space Flight Center, Greenbelt, Maryland.

Hooker, S. B., and A. Morel (2003), Platform and environmental effects on above-water determinations of water-leaving radiances, Journal Of Atmospheric And Oceanic Technology, 20, 1, 187-205.

Howarth, R. W. (1988), Nutrient limitation of net primary production in marine ecosystems, Annu. Rev. Ecol. Syst., 19, 89-110.

IPCC (2001), Climate Change 2001: The Scientific Basis, 785 pp, Cambridge University Press, Geneva, Switzerland.

IPCC (2007), Climate Change 2007: Synthesis Report, 104 pp, Cambridge University Press, Geneva, Switzerland.

Israelevich, P. L., Z. Levin, J. H. Joseph, and E. Ganor (2002), Desert aerosol transport in the mediterranean region as inferred from the TOMS aerosol index, Journal of Geophysical Research, 107, D21, 4572doi:4510.1029/2001JD002011.

Krom, M. D., N. Kress, and S. Brenner (1991), Phosphorus limitation of primary productivity in the eastern Mediterranean Sea, Limnology and Oceanography, 36, 424-432.

Lacombe, H., J. C. Gascard, J. Gonella, and B. J. P. (1981), Response of the Mediterranean to the water and energy fluxes across its surface, on seasonal and interannual scales, Oceanologica Acta, 4, 2, 120-130.

Lacombe, H., and P. Tchernia (1972), Characteres hydrologiques et circulation des eaux en Mediterranee, in The Mediterranean Sea: a natural sedimentation ladoratory, edited by D. Stanley, Dowden Hutchinson and Ross, Strousberg.

Lalli, C. M., and T. R. Parsons (1997), Biological Oceanography, An Introduction, 314 pp., The Open University.

Lascaratos, A., W. Roether, K. Nittis, and B. Klein (1999), Recent changes in deep water formation and spreading in the eastern Mediterranean Sea: a review, Progress in Oceanography, 44, 5-36.

Le Traon, P. Y., and F. Ogor (1998), ERS-1/2 orbit improvement using TOPEX/POSEIDON: The 2cm challenge, JOURNAL OF GEOPHYSICAL RESEARCH-OCEANS, 103, C4, 8045-8057.

Levy, M., L. Memery, and G. Madec (1998), The onset of a bloom after deep winter convection in the northwestern Mediterranean sea: mesoscale process study with a primitive equation model, Journal Of Marine Systems, 16, 1-2, 7-21.

Levy, M., L. Memery, and G. Madec (1999), The onset of the Spring Bloom in the MEDOC area: mesoscale spatial variability, Deep-Sea Research Part I-Oceanographic Research Papers, 46, 7, 1137-1160.

Longhurst, A. R. (1998), Ecological Geography of the Sea, 398 pp., Academic Press, San Diego.

Lopez-Calderon, J., H. Manzo-Monroy, E. Santamaria-del-Angel, R. Castro, A. Gonzalez-Silvera, and R. Millan-Nunez (2006), Mesoscale variability of the Mexican tropical pacific using TOPEX and SeaWiFS data, Ciencias Marinas, 32, 539-549.

López-Jurado, J. L., C. González-Pola, and P. Vélez-Belchí (2005), Observation of an abrupt disruption of the long-term warming trend at the Balearic Sea, western Mediterranean Sea, in summer 2005, Geophysical Research Letters, 32, L24606, doi:10.1029/2005GRL024430.

Loye-Pilot, M. D., and J. M. Martin (1996), Saharan dust input to the western Mediterranean: An eleven years record in Corsica, in The Impact of Desert Dust Across the Mediterranean, edited by G. S. and R. Chester, pp. 191-200, Kluwer Academic Publisher.

Malanotte-Rizzoli, P. (2003), Introduction to special section: Physical and biochemical evolution of the eastern Mediterranean in the 1990s (PBE), Journal of Geophysical Research, 108, C9, 1.

Malanotte Rizzoli, P., B. Manca, M. Ribera dʹAlcalà, A. Theocharis, A. Bergamasco, D. Bregant, G. Budillon, G. Civitarese, D. Georgopoulos, A. Michelato, E. Sansone, P. Scarazzato, and E. Souvermezoglou (1997), A synthesis of the Ionian Sea hydrography, circulation and water mass pathways during POEM-Phase I, Progress in Oceanography, 39, 3, 153-204.

Malinverno, E., P. Ziveri, and C. Corselli (2003), Coccolithophorid distribution in the Ionian Sea and its relationship to eastern Mediterranean circulation during late fall to early winter 1997, Journal Of Geophysical Research-Oceans, 108, C9.

Manzella, G., G. Gasparini, and M. Astraldi (1988), Water exchange between the eastern and western Mediterranean through the strait of Sicily, Deep Sea Research, 35, 6.

Manzella, G. M. R., T. S. Hopkins, P. J. Minnett, and E. Nacini (1990), Atlantic water in the Strait of Sicily, Journal of Geophsical Research, 95, C2, 1569-1575.

Markaki, Z., K. Oikonomu, M. Kocak, G. Kouvarakis, A. Chaniotaki, N. Kubilay, and N. Mihalopoulos (2003), Atmospheric deposition of inorganic phosphorus in the Levantine Basin, eastern Mediterranenan: Spataial and temporal variability and its role in seawater productivity, Limnology and Oceanography, 48, 4, 1557-1568.

Martin, J. M. (1990), Glacial-interglacial CO2 change: The iron hypothesis, Paleoceanography, 5, 1-13.

Marty, J. C., J. Chiaverini, J. La Rosa, and J. C. Miquel (1995), Dyfamed, une station d'observation de l'environnement marin en Méditerranée., Met. Mar., 167, 33-36.

Marullo, S., B. Buongiorno Nardelli, M. Guarracino, and R. Santoleri (2007), Observing the Mediterranean Sea from space: 21 years of Pathfinder-AVHRR sea surface temperatures (1985 to 2005): re-analysis and validation, Ocean Science, 3, 299-310.

McClain, C. R., K. R. Arrigo, W. Esaias, M. Darzi, F. S. Patt, R. H. Evans, C. W. Brown, J. W. Brown, R. A. Barnes, and L. Kumar (1995), SeaWiFS Algorithms, Part 1, NASA Goddard Space Flight Center, Greenbelt, Maryland.

McClain, C. R., K. R. Arrigo, W. Esaias, M. Darzi, F. S. Patt, R. H. Evans, C. W. Brown, J. W. Brown, R. A. Barnes, and L. Kumar (1995), SeaWiFS Quality Control Masks and Flags: Initial Algorithms and Implementation Strategy, 3-7 pp, NASA Goddard Space Flight Center, Greenbelt, Maryland.

McClain, M. E., and G. S. Fargion (1999), Simbios project annual report., NASA Goddard Space Flight Center, Greenbelt, MD.

McClain, M. E., J. E. Richey, J. A. Brandes, and T. P. Pimentel (1997), Dissolved organic matter and terrestrial-lotic linkages in the central Amazon basin of Brazil, Global Biogeochemical Cycles, 11, 3, 295–312.

McGill, D. A. (1961), A preliminary study of the Oxygen and the Phosphate distribution in the Mediterranean Sea, Deep Sea Research, 8, 259-269.

MEDOC Group (1990), Observation of formation of deep water in the Mediterranean sea, Nature, 227, 1037-1040.

Meybeck, M. (1982), Carbon, nitrogen and phosphorus transport by world rivers, American Journal of Science, 282, 401-450.

Migon, C., and V. Sandroni (1999), Phosphorus in rainwater: Partitioning inputs and impact on the surface coastal ocean, 1160-1165 pp.

Morales-Baquero, R., E. Pulido-Villena, and I. Reche (2006), Atmospheric inputs of phosphorus and nitrogen to the southwest Mediterranean region: Biogeochemical responses of high mountain lakes, Limnology and Oceanography, 51, 2, 830-837.

Morel, A., and S. Maritorena (2001), Bio-optical properties of oceanic waters: A reappraisal, Journal of Geophysical Research-Oceans, 106, C4, 7163-7180.

Morel, A., and L. Prieur (1977), Analysis of variation in ocean color, Limnology and Oceanography, 22, 4, 709-722.

Moulin, C., H. R. Gordon, V. F. Banzon, and R. H. Evans (2001), Assessment of Saharan dust absorption in the visible from SeaWiFS imagery, Journal of Geophysical Research, 106, D16, 18239-18249.

Moulin, C., F. Guillard, F. Dulac, and C. E. Lambert (1997), Long-term daily monitoring of Saharan dust load over ocean using Meteosat ISCCP-B2 data; 1. Methodology and preliminary results for 1983-1994 in the Mediterranean, Journal of Geophysical Research, 102, D14, 16947-16958.

Moulin, C., C. E. Lambert, U. Dayan, V. Masson, M. Ramonet, P. Bousquet, M. Legrand, Y. J. Balkansky, W. Guelle, B. Marticorena, G. Bergametti, and F. Dulac (1998), Satellite climatology of dust transport in the Mediterranean atmosphere, Journal of Geophysical Research, 103, D11, 13137-13144.

Mueller, J. L. (2000), In-water radiometric profile measurements and data analysis protocols. NASA Tech. Memo. 2000-209966, Ocean Optics Protocols for Satellite Ocean Color Sensor Validation, Revision 2, 87-97 pp, NASA Goddard Space Flight Center, Greenbelt, Maryland.

Mueller, J. L., and R. W. Austin (1995), Ocean Optics Protocols for SeaWiFS Validation, Revision 1., 67 pp, NASA Goddard Space Flight Center, Greenbelt, Maryland.

Mueller, J. L., and G. S. Fargion (2002), Ocean Optics Protocols for SeaWiFS Validation, Revision 3. NASA Tech. Memo. 2002-210004, 308 pp pp, NASA Goddard Space Flight Center, Greenbelt, Maryland.

Neveux, J., and M. Panouse (1987), Spectrofluorometric determination of chlorophylls and pheophytins., Archive of Hydrobiology, 109, 561-567.

Nezlin, N. P., G. Lacroix, A. G. Kostianoy, and S. Djenidi (2004), Remotely sensed seasonal dynamics of phytoplankton in the Ligurian Sea in 1997-1999, Journal of Geophysical Research, 109, C7, 12 pp.

Nobileau, D., and D. Antoine (2005), Detection of blue-absorbing aerosols using near infrared and visible (ocean color) remote sensing observations, Remote Sensing Of Environment, 95, 3, 368-387.

O'Reilly, J. E., S. Maritorena, B. G. Mitchell, D. A. Siegel, K. L. Carder, S. A. Garver, M. Kahru, and C. McClain (1998), Ocean color chlorophyll algorithms for SeaWiFS, Journal of Geophysical Research-Oceans, 103, C11, 24937-24953.

O'Reilly, J. E., S. Maritorena, D. Siegel, M. C. O'Brien, D. Toole, B. G. Mitchell, M. Kahru, F. P. Chavez, P. Strutton, G. Cota, S. B. Hooker, C. R. McClain, K. L. Carder, F. Muller-Karger, L. Harding, A. Magnuson, D. Phinney, G. F. Moore, J. Aiken, K. R. Arrigo, R. Letelier, and M. Culver (2000), Ocean color chlorophyll a

algorithms for SeaWiFS, OC2, and OC4: version 4., in SeaWiFS Postlaunch Technical Report Series, vol.11. SeaWiFS postlaunch calibration and validation analyses: part 3, edited by S. B. Hooker and E. R. Firestone, pp. 9-23, NASA Goddard Space Flight Center., Greenbelt, MD.

Ouillon, S., and A. A. Petrenko (2005), Above-water measurements of reflectance and chlorophyll-a algorithms in the Gulf of Lions, NW Mediterranean Sea, Optics Express, 13, 7, 2531-2548.

Parsons, T., M. Takahashi, and B. Hargrave (1983), Biological Oceanographic Processes. Third edition, Pergamon Press, Oxford, UK.

Parsons, T., M. Takahashi, and B. Hargrave (1997), Biological Oceanographic Processes, Elsevier, New York.

Pinot, J.-M., J. L. Lopez-Jurado, and M. Riera (2002), The CANALES experiment (1996-1998). Interannual, seasonal, and mesoscale variability of the circulation in the Balearic Channels, Progress in Oceanography, 55, 335–370.

Prospero, J. M., P. Ginoux, O. Torres, S. E. Nicholson, and T. E. Gill (2002), Environmental characterization of global sources of atmospheric soil dust identified with the Nimbus 7 Total Ozone Mapping Spectrometer (TOMS) absorbing aerosol product, Reviews of Geophysics, 40, 1, 8755-1209.

Pujol, M. I., and G. Larnicol (2005), Mediterranean sea eddy kinetic energy variability from 11 years of altimetric data., Journal of Marine Systems, 58, 3-4, 121-142.

Rahmstorf, S. (2006), Thermohaline Ocean Circulation, in Encyclopedia of Quaternary Sciences, edited by Elsevier, Amsterdam.

Redfield, A. C., B. H. Ketchum, and F. A. Richards (1963), The influence of organisms on the composition of sea-water, in Composition of Sea-Water: Comparative and Descriptive Oceanography, edited by N. M. Hill, pp. 26-77, Wiley, J., New York.

Rio, M.-H., P. M. Poulain, A. Pascal, E. Mauri, G. Larnicol, and R. Santoleri (2007), A Mean Dynamic Topography of the Mediterranean Sea computed from altimetric data, in-situ measurements and a general circulation model, Journal of Marine Systems, 65, 1-4, 484-508.

Robinson, A. R., and M. Golnaraghi (1995), The Physical and dynamical oceanography of the Mediterranean sea, in In: Ocean Processes in Climate Dynamics: Global and Mediterranean Examples., edited by P. Malanotte-Rizzoli and A. R. Robinson, pp. 255-306, Kluwer Academic Publishers, Dordrecht, The Netherlands.

Robinson, A. R., J. Sellschopp, A. Warn-Varnas, W. G. Leslie, C. J. Lozano, P. J. Haley, L. A. Anderson, and P. F. J. Lermusiaux (1999), The Atlantic Ionian stream, Journal of Marine Systems, 20, 1-4, 129-156.

Robinson, I. S. (2005), Measuring the Oceans from Space, 669 pp., Springer-Paxis, Bath.

Roether, W., and R. Schlitzer (1991), Eastern Mediterranean deep water renewal on the basis of chlorofluoromethans and tritrium, Dynamics of Atmospheres and Oceans, 15, 333-354.

Salat, J., M. Emelianov, and J. L. Lopez-Jurado (2006), Unusual extension of Western Mediterranean deep water formation during winter 2005, paper presented at 5a Asamblea Hispano-Portuguesa de Geodesia y Geofísica, Comisión Española de Geodesia y Geofísica, Sevilla, Spain.

Santoleri, R., V. F. Banzon, S. Marullo, E. Napolitano, F. D'Ortenzio, and R. Evans (2003), Year-to-year variability of the phytoplankton bloom in southern Adriatic Sea (1998-2000): SeaWiFS observations and modelling study, JOURNAL OF GEOPHYSICAL RESEARCH, 108, C9, DOI:10.1029/2002JC001636.

Santoleri, R., G. Volpe, S. Marullo, and B. Buongiorno Nardelli (2008), Open Waters Optical Remote Sensing of the Mediterranean Sea, in Remote Sensing of the European Seas, edited by V. Barale and M. Gade, pp. 103-116, Springer.

Sarmiento, J., T. Herbert, and J. R. Toggweiler (1988), Mediterranean nutrient balance and episodes of anoxia. Global Biogeochemical Cycles 2, pp., Global Biogeochemical Cycles, 2, 4, 427-444.

Sarmiento, J. L., R. Slater, R. Barber, L. Bopp, S. C. Doney, A. C. Hirst, J. Kleypas, R. Matear, U. Mikolajewicz, P. Monfray, V. Soldatov, S. A. Spall, and R. Stouffer (2004), Response of ocean ecosystems to climate warming, Global Biogeochemical Cycles, 18, GB3003, doi:3010.1029/2003GB002134.

Schär, C., and G. Jendritzky (2004), Climate change: hot news from summer 2003, Nature, 432, 7017, 559-560.

Sciarra, R., G. Volpe, and R. Santoleri (2003), Complete catalogue of the Saharan dust events and polluted aerosols from historical SeaWiFS data. ADIOS Project, Deliverable n°32, 21 pp.

Siegel, D. A., M. Wang, S. Maritorena, and W. Robinson (2000), Atmospheric correction of satellite ocean color imagery: the black pixel assumption, Applied optics, 39, 21, 3582-3591.

Smith, R. O., H. L. Bryden, and K. Stansfield (2008), Observations of new western Mediterranean deep water formation using Argo floats 2004-2006, Ocean Science, 4, 2, 133-149.

Stommel, H. (1972), Deep winter-time convection in the western Mediterranean Sea, in Studies in physical oceanography, a tribute to Georg Wust on his 80th birthday, edited by A. L. Gordon, pp. 207-218, Gordon and Breach Science.

Stramska, M., and D. Stramski (2005), Effects of a nonuniform vertical profile of chlorophyll concentration on remote-sensing reflectance of the ocean, Applied Optics, 44, 9, 1735-1747.

Student (1908), Probable error of a correlation coefficient, Biometrika, 6, 302-310.

Sverdrup, H. U. (1953), On Conditions for the Vernal Blooming of Phytoplankton, ICES J. Mar. Sci., 18, 287-295.

Ternon, E., C. Guieu, M.-D. Loye-Pilot, N. Leblond, E. Bosc, B. Gasser, J.-C. Miquel, and J. Martın (2010), The impact of Saharan dust on the particulate export in the water column of the North Western Mediterranean Sea, Biogeosciences, 7, 809-826. www.biogeosciences.net/807/809/2010/.

Thingstad, T. F., M. D. Krom, R. F. C. Mantoura, G. A. F. Flaten, S. Groom, B. Herut, N. Kress, C. S. Law, A. Pasternak, P. Pitta, S. Psarra, F. Rassoulzadegan, T. Tanaka, A. Tselepides, P. Wassmann, E. M. S. Woodward, C. Wexels Riser, G. Zodiatis, and T. Zohary (2005), Nature of phosphorpus limitation in the ultraoligotrophic Eastern mediterranean, Science, 309, 1068-1071.

Thingstad, T. F., U. L. Zweifel, and F. Rassoulzadegan (1998), P limitation of heterotrophic bacteria and phytoplankton in the northwest Mediterranean, Limnology And Oceanography, 43, 1, 88-94.

Turner, S. M., P. D. Nightingale, L. J. Spokes, M. I. Liddicoat, and P. S. Liss (1996), Increased dimethylsulphide concentrations in sea water from in situ iron enrichment, Nature, 383, 513-517.

Vescovi, F. D., V. Marletto, and G. Montanari (2003), Osservazione delle mucillagini in Mare Adriatico con dati MODIS, paper presented at L'innovazione al servizio della conoscenza e della prevenzione, Milano, 24-25-26 Novembre.

Volpe, G., R. Santoleri, V. Vellucci, M. Ribera d'Alcala, S. Marullo, and F. D'Ortenzio (2007), The colour of the Mediterranean Sea: Global versus regional bio-optical algorithms evaluation and implication for satellite chlorophyll estimates, Remote Sensing of Environment, 107, 625-638.

Williams, N. (1998), The Mediterranean Beckons to Europe's oceanographers, Science, 279, 5350, 483-484.

Wilson, C., and D. Adamec (2001), Correlations between surface chlorophyll and sea surface height in the tropical Pacific during the 1997-1999 El Nino-Southern Oscillation event, Journal of Geophsical Research, 106, 31175-31188.

Wilson, C., and V. J. Coles (2005), Global climatological relationships between satellite biological and physical observations and upper ocean properties, JOURNAL OF GEOPHYSICAL RESEARCH, 110, C10001, doi:10.1029/2004JC002724.

Yoder, J. A., and M. A. Kennelly (2003), Seasonal and ENSO variability in global ocean phytoplankton chlorophyll derived from 4 years of SeaWiFS measurements, Global Biogeochemical Cycle, Global Biogeochemical Cycles, 17, 4, 1112, doi:1110.1029/2002GB001942.

Zecchetto, S., and F. De Biasio (2007), Sea surface winds over the Mediterranean basin from satellite data (2000-04): Meso- and local-scale features on annual and seasonal time scales, Journal of Applied Meteorology and Climatology, 46, 6, 814-827.

Zibordi, G., F. Melin, and J. F. Berthon (2006), Comparison of SeaWiFS, MODIS and MERIS radiometric products at a coastal site, Geophysical Research Letters, 33, 6.

Zingone, A., R. Casotti, M. R. D'Alcala, M. Scardi, and D. Marino (1995), ST-MARTINS SUMMER - THE CASE OF AN AUTUMN PHYTOPLANKTON BLOOM IN THE GULF OF NAPLES (MEDITERRANEAN-SEA), Journal of Plankton Research, 17, 3, 575-593.